AGU PUBLICATIONS

Reviews of Geophysics

REVIEW ARTICLE
10.1002/2015RG000495

Key Points:
- The Eurasian Arctic represents a data-rich and unique paleo-analogue for marine-based glaciation
- Interplay between the glacial, climate, and ocean systems drove complex and nonlinear deglaciation
- Well-constrained paleoreconstructions are fundamental for understanding future cryospheric change

Correspondence to:
H. Patton,
henry.patton@uit.no

Citation:
Patton, H., K. Andreassen, L. R. Bjarnadóttir, J. A. Dowdeswell, M. C. M. Winsborrow, R. Noormets, L. Polyak, A. Auriac, and A. Hubbard (2015), Geophysical constraints on the dynamics and retreat of the Barents Sea ice sheet as a paleobenchmark for models of marine ice sheet deglaciation, *Rev. Geophys.*, *53*, 1051–1098, doi:10.1002/2015RG000495.

Received 25 JUN 2015
Accepted 18 SEP 2015
Accepted article online 1 OCT 2015
Published online 14 NOV 2015

©2015. American Geophysical Union. All Rights Reserved.

Geophysical constraints on the dynamics and retreat of the Barents Sea ice sheet as a paleobenchmark for models of marine ice sheet deglaciation

Henry Patton[1], Karin Andreassen[1], Lilja R. Bjarnadóttir[2], Julian A. Dowdeswell[3], Monica C. M. Winsborrow[1], Riko Noormets[4], Leonid Polyak[1,5], Amandine Auriac[6], and Alun Hubbard[1]

[1]CAGE-Centre for Arctic Gas Hydrate, Environment and Climate, Department of Geology, UiT The Arctic University of Norway, Tromsø, Norway, [2]Geological Survey of Norway, Trondheim, Norway, [3]Scott Polar Research Institute, University of Cambridge, Cambridge, UK, [4]University Centre in Svalbard (UNIS), Longyearbyen, Norway, [5]Byrd Polar Research Center, Ohio State University, Columbus, Ohio, USA, [6]Department of Geography, Durham University, Durham, UK

Abstract Our understanding of processes relating to the retreat of marine-based ice sheets, such as the West Antarctic Ice Sheet and tidewater-terminating glaciers in Greenland today, is still limited. In particular, the role of ice stream instabilities and oceanographic dynamics in driving their collapse are poorly constrained beyond observational timescales. Over numerous glaciations during the Quaternary, a marine-based ice sheet has waxed and waned over the Barents Sea continental shelf, characterized by a number of ice streams that extended to the shelf edge and subsequently collapsed during periods of climate and ocean warming. Increasing availability of offshore and onshore geophysical data over the last decade has significantly enhanced our knowledge of the pattern and timing of retreat of this Barents Sea ice sheet (BSIS), particularly so from its Late Weichselian maximum extent. We present a review of existing geophysical constraints that detail the dynamic evolution of the BSIS through the last glacial cycle, providing numerical modelers and geophysical workers with a benchmark data set with which to tune ice sheet reconstructions and explore ice sheet sensitivities and drivers of dynamic behavior. Although constraining data are generally spatially sporadic across the Barents and Kara Seas, behaviors such as ice sheet thinning, major ice divide migration, asynchronous and rapid flow switching, and ice stream collapses are all evident. Further investigation into the drivers and mechanisms of such dynamics within this unique paleo-analogue is seen as a key priority for advancing our understanding of marine-based ice sheet deglaciations, both in the deep past and in the short-term future.

1. Introduction

At the continental scale, the morphology of terrestrially based ice is largely controlled by the specific surface distribution of accumulation and ablation [*Hindmarsh*, 1993]. However, the stability of marine-based ice sheets, defined as where the base of the ice sheet rests below sea level and where ice calving is the predominant mode of mass wasting, is usually considered to be influenced strongly by dynamics of the grounding line; that is, the junction between the grounded ice sheet and adjoining floating ice shelf [e.g., *Weertman*, 1974; *Thomas and Bentley*, 1978]. This is of particular relevance for West Antarctica, where the bed in the ice sheet interior is significantly deeper than at the present grounding line. However, limited process understanding related to grounding line motion and stability [*Schoof*, 2007; *Goldberg et al.*, 2009; *Gudmundsson et al.*, 2012], and deficiencies in grounding line treatment in ice sheet models [*Pattyn et al.*, 2012], still hinder predictions of marine ice sheet vulnerability.

Observations over the last decade have indicated that accelerated ice flow, driven by oceanographic and climatic changes, has intensified in unison along the oceanic margins of West Antarctica and Greenland [*Walker et al.*, 2007; *Holland et al.*, 2008; *Christoffersen et al.*, 2011; *Arneborg et al.*, 2012], with the ice dynamic effects spreading deep into the ice sheet interiors [*Krabill et al.*, 2004; *Pritchard et al.*, 2009; *Flament and Rémy*, 2012]. With compelling evidence that the West Antarctic ice sheet has previously undergone partial collapse during the Late Pleistocene [*Scherer*, 1998], there is a need to establish whether contemporary climatic and oceanographic changes could initiate a similar breakup, or if the hypothesized instability is an oversimplification resulting from inadequate understanding of the feedbacks that allow ice sheets to achieve equilibrium [*Vaughan*, 2008]. One approach to address this issue is to examine deglacial

reconstructions of paleo–ice sheets, where data are constrained on timescales much longer than the present-day record of satellite and airborne measurements.

The Barents and Kara Sea domain in the northern Eurasian Arctic provides a suitable and unique paleo–case study to explore the long-term growth and collapse of a marine-based ice sheet. As well as sharing several similarities with the West Antarctic Ice Sheet, including a bed predominantly below sea level, a largely sedimentary bedrock interface, and similar growth to the shelf break during the Last Glacial Maximum (LGM) [*Andreassen and Winsborrow*, 2009], increasing data confirm that the Barents Sea ice sheet (BSIS) was characterized by large and abrupt changes during its deglaciation [*Jakobsson et al*., 2014b]. A better comprehension of the mechanisms and drivers that forced unstable retreat and ice breakup in the Barents Sea over < 10 ka is therefore important in order to help predict future trajectories of modern marine-based ice sheet collapse.

As a result of the development of ideas and concepts over the past 150 years [*Ingólfsson and Landvik*, 2013], the timing and dimensions of former Barents Sea ice sheets have been much debated, particularly so for the LGM. Historic estimates for the extent of the BSIS during the last glacial cycle have ranged widely, from a minimalist model of glaciation restricted to present terrestrial areas [e.g., *Boulton*, 1979], to an enormous and long-lived ice sheet complex that dominated much of northern Eurasia [*Hughes et al*., 1977; *Grosswald*, 2001]. Much of this historical uncertainty stems from the then immature knowledge of the mechanics related to ice sheet inception, marine-based deglaciation, and the drivers that force dynamic ice sheet behavior, hindered ultimately by the relative dearth of geophysical constraints available. Following detailed and extensive geophysical data collection during recent decades from marine and terrestrial sectors across the Eurasian Arctic [e.g., *Landvik et al*., 1992; *Forman et al*., 1995; *Mangerud et al*., 1999; *Andreassen et al*., 2004; *Thiede et al*., 2004; *Polyak et al*., 2008; *Hormes et al*., 2013; *Möller et al*., 2015], substantiated against remotely sensed observations from the present-day ice sheets, consensus has harmonized toward the presence of a substantial grounded ice sheet centered over the Barents Sea during the LGM, with minimal incursion into mainland northern Russia [*Svendsen et al*., 2004a].

Dynamical understanding of the Late Weichselian ice sheet has progressed unevenly though, with data from eastern sectors of the Barents Sea and most of the Kara Sea particularly underrepresented in the scientific literature. Since the last major review detailing marginal limits of the Eurasian ice sheets by *Svendsen et al*. [2004a], a wealth of new information has arisen, with much focus placed on both terrestrial and marine sectors of Svalbard and the western Barents Sea region. While significant empirical knowledge gaps do remain across the ice sheet as a whole, circumstances are ripe for a fresh examination from ice sheet modelers to draw out well-constrained insights using numerical models.

The purpose of this study therefore is to draw together the various lines of geophysical evidence for glaciation in the Barents and Kara sea region, as well as inferred dynamics during the ice sheet's subsequent retreat, in order to provide a benchmark against which models reconstructing its marine-based deglaciation can be tested. The structure of the paper follows specific approaches that have been taken for reconstructing ice cover and dynamics, including geophysical and sedimentological observations, isostatic rebound modeling, geomorphological mapping, absolute dating, and the examination of proxy evidence such as ice-rafted debris (IRD) records from ocean cores. The paper concludes with a summary of the numerical ice sheet reconstructions to date, considerations for model-data integration, and also where new research is necessary in order to further constrain the dynamic evolution of the ice sheet.

2. Marginal Limits

During the last circa 160,000 years, as many as four major glaciations have been recorded in the Barents Sea region, including the extensive Late Saalian glacial maximum that occurred during marine isotope stage (MIS) 6 [*Mangerud et al*., 1998, 2001b; *Svendsen et al*., 2004a], and more limited ice cover during later (Weichselian) glacial events. Although subsequent glaciations tend to erode and "reset" the glacial record left by older ice sheets, the limits of past glaciations can be inferred from a variety of geological data sources. These sources include landform mapping (including buried features found within 3-D seismic data), sedimentological logging from cores, stratigraphic analyses from seismic records, and provenance analyses from ice-rafted debris deposits. Assignment of specific ages for glaciation is, to a large extent, based on the relative positioning of sediments within a known stratigraphic framework. Where available, a combination of optically stimulated luminescence and radiocarbon dating enables reliable chronologies of sediment successions. The following sections detail evidence for all the major

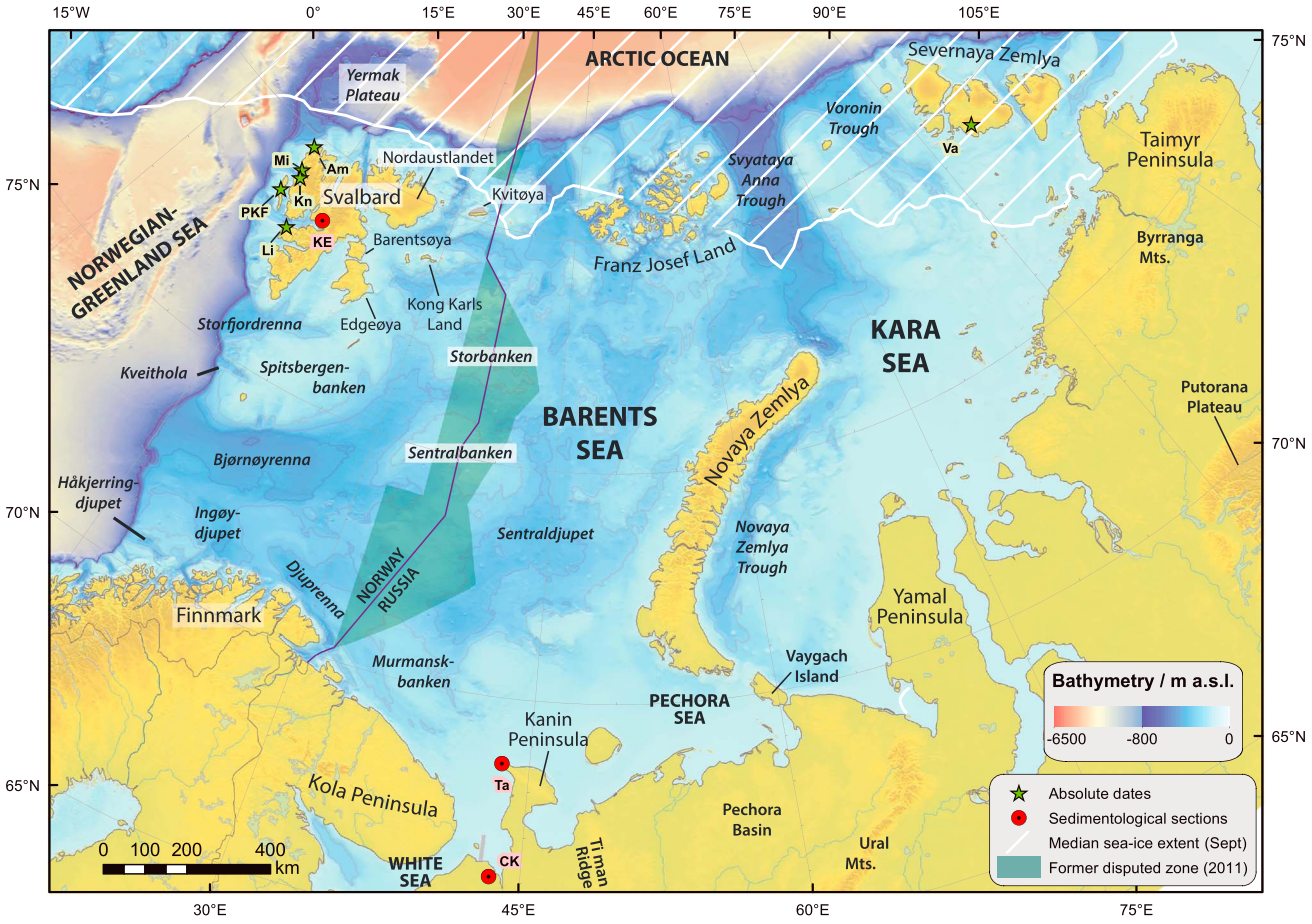

Figure 1. The Barents-Kara Sea shelf. Obstacles that have restricted comprehensive geophysical surveying of the shelf include disputed territorial claims and sea ice cover to the north. The median sea-ice margin drawn covers the September limit between 1981 and 2010 [*Fetterer et al.*, 2002]. Place names referred to in the text: Am = Amsterdamøya, CK = Cape Kargovsky, KE = Kapp Ekholm, Kn = Knølen, Li = Linnédalen, Mi = Mitrahalvøya, PKF = Prins Karls Forland, Ta = Tarkhanov, and Va = Vavilov Ice Cap. Bathymetric data source: IBCAO version 3.0 [*Jakobsson et al.*, 2012b].

Weichselian glaciations, with emphasis placed on the LGM for which empirical data are most abundant. It should be noted, however, that the maximum extent during the various glaciations was not necessarily attained at the same time in different regions. Place names and key sites referred to in the text are located in Figure 1. Relevant radiocarbon dates from previously published studies have been recalibrated in this study using Calib 7.1 [*Stuiver and Reimer*, 1993] and the IntCal13/MARINE13 calibration curves [*Reimer et al.*, 2013] and are thus presented in calendar years before present (cal ka B.P.) (Table 1). A ΔR value of 71 ± 21 (105 ± 24 north of 75°N) was used to account for local effects on the global reservoir correction [*Mangerud et al.*, 2006].

2.1. Early Weichselian (MIS 5d–5a/110–70 cal ka B.P.)

Based on the composite stratigraphical record of Kapp Ekholm, central Svalbard [*Mangerud and Svendsen*, 1992], three major ice stream pulses during the Weichselian have been proposed at circa 110 cal ka B.P. (MIS 5d), 60 cal ka B.P. (MIS 4), and 20 cal ka B.P. (MIS 2) [*Mangerud et al.*, 1998]. This lithostratigraphy and chronology is, however, not beyond doubt, in particular the dominance of the MIS 5d glaciation. Efforts to redate the sediments [*Forman*, 1999] using infrared- and red-stimulated luminescence dating failed to reproduce the chronology of *Mangerud et al.* [1998], and suggested the lowermost interglacial sediments were closer to 200 ka old rather than being of Early Weichselian age. The synthesis of terrestrial evidence with offshore data has also met with limited success; in sediment cores north of Svalbard, terrigenous input events were found only for the 60 ka and 20 ka pulses [*Winkelmann et al.*, 2008], suggesting the Early Weichselian glaciation might not have occurred on Svalbard as major glacial advances to the shelf break. These results are also in accordance with a core from the northern Barents Sea margin showing only moderate IRD input and low levels of coarse-grained material during MIS 5 [*Knies et al.*, 1999].

Table 1. Reported ^{14}C Ages Referred to in the Text [a]

Core/Location	Source	Latitude (N)	Longitude (E)	Uncorrected Age (^{14}C years B.P.)	Median Probability Age (years B.P.)	2σ Range (years B.P.)	Notes
Southern Barents Sea							
Dia 84-2	*Hald et al.* [1990]	73.28°	23.16°	27,760 ± 735	31,336	29,777–33,058	Reworked shells in marine sediments at base of glacigenic sediment unit "b4."
JM08-0309-GC	*Rüther et al.* [2011]	72.49°	17.01°	14,530 ± 65	17,082	16,808–17,375	AMS dating on bulk benthic foraminifera from the base of glacimarine sediments.
JM09-KA03-GC	*Rüther et al.* [2011]	72.74°	16.20°	13,835 ± 60	16,074	15,845–16,271	AMS dating on bulk benthic foraminifera from the base of glacimarine sediments.
F84	*Vorren et al.* [1978]	Tromsøflaket		13,960 ± 400	16,244	15,099–17,461	Macrofossils from upper part of a glaciomarine unit "Elphidium AZ.".
140	*Polyak et al.* [1995]	Sentraldjupet		13,175 ± 95	15,103	14,659–15,472	Foraminifera assemblage at base of glaciomarine unit "IIB."
JM05-085-GC	*Junttila et al.* [2010]	71.62°	22.93°	15,790 ± 80	18,587	18,361–18,765	Benthic foraminifera within laminated sediments containing clasts.
JM07-02-GC	*Junttila et al.* [2010]	71.16°	23.00°	13,110 ± 90	14,983	14,473–15,303	Middle of bioturbated mud horizon above diamicton.
MD 992295	*Vorren and Plassen* [2002]	69.55°	16.18°	14,760 ± 140	17,388	16,983–17,804	Mixed foraminifera from base of laminated muds above diamicton.
Lake 41	*Snyder et al.* [1997]	69.08°	36.05°	11,135 ± 80	12,991	12,792–13,136	Basal age from terrestrial plants above diamict.
Northern Barents Sea							
P1-91-AR-JPC5	*Lubinski et al.* [1996]	81.12°	43.43°	13,330 ± 80	15,291	15,049–15,623	Base of sediments overlying diamicton.
45	*Polyak and Solheim* [1994]	79.98°	41.95°	13,685 ± 150	15,809	15,318–16,226	Base of laminated glaciomarine deposits.
Hooker Island	*Forman et al.* [1996]	80.27°	52.34°	10,730 ± 115	11,937	11,394–12,428	Paired *Mya truncata* from marine sands 30 m asl.
Nansen Island	*Forman et al.* [1996]	80.58°	54.12°	10,360 ± 115	12,209	11,796–12,562	0.5 m long log from raised beach 27 m asl.
Bell Island	*Forman et al.* [1996]	80.01°	49.22°	9,705 ± 105	11,066	10,719–11,281	Driftwood embedded into raised beach 45 m asl.
Klagenfurt Island	*Forman et al.* [1997]	80.35°	60.23°	4,925 ± 160	5,673	5,302–6,004	1 m long log from raised beach 17 m asl.
Severnaya Zemlya	*Vasil'chuk et al.* [1997]	Vavilov Ice Cap		11,500 ± 60	13,348	13,219–13,462	Radiocarbon-dated mammoth remains indicate presence of ice-free conditions during the Late Weichselian.
				19,270 ± 110	23,215	22,907–23,533	

Table 1. (continued)

Core/Location	Source	Latitude (N)	Longitude (E)	Uncorrected Age (^{14}C years B.P.)	Median Probability Age (years B.P.)	2σ Range (years B.P.)	Notes
Svalbard							
Linnédalen	*Mangerud et al.* [1998]	78.05°	13.85°	36,100 ± 800	40,151	38,552–41,680	Paired shells beneath till and above sand and gravel foresets.
Amsterdamøya	*Salvigsen* [1977]	79.78°	10.80°	28,970 ± 430	32,424	31,425–33,491	*Mya Truncata/Hiatella arctica* shells from marine sediments within till.
JM02-460-PC	*Rasmussen et al.* [2007]	76.05°	15.73°	16,750 ± 110	19,608	19,278–19,938	*Neogloboquadrina pachyderma* in hemipelagic deposits above till.
JM09-020-GC	*Łącka et al.* [2015]	76.31°	19.70°	12,570 ± 60	13,947	13,780–14,114	Bivalvia shell beneath the upper surface of subglacial till horizon.
JM10-10-GC	*Rasmussen and Thomsen* [2014]	Inner Storfjorden		10,960 ± 44	12,375	12,121–12,562	Bivalve within mixture of glaciomarine and diamictic deposits.
Edgøya (Blåfjorddalen)	*Landvik et al.* [1992]	77.98°	22.98°	10,770 ± 110	12,025	11,535–12,489	*Mya truncata* within silty marine sands.
Barentsøya (Frankenhalvøya)	*Landvik et al.* [1992]	78.57°	21.33°	10,705 ± 95	11,886	11,376–12,316	*Nuculana pernula* within marine clayey silt above till
88-02	*Svendsen et al.* [1992]	78.05°	12.99°	12,985 ± 145	14,644	14,111–15,167	Base of marine muds overlying diamicton.
JM98-845-PC	*Forwick and Vorren* [2009]	78.34°	15.30°	10,310 ± 65	11,200	11,027–11,397	Above glaciomarine diamicton and a high IRD flux, related to final glacial withdrawal from Isfjorden to its tributaries.
NP90-9-PC3	*Landvik et al.* [2005]	79.02°	11.10°	13,960 ± 120	16,189	15,820–16,568	Base of laminated marine muds above glacial till.
NP94-51SC2	*Koç et al.* [2002]	80.36°	16.31°	14,162 ± 135	16,478	16,086–16,936	Benthic formaniniferal species including *Elphidium excavatum* and *Cassidulina reniforme*, typical of a glacier proximal environment. Above a strong IRD layer.
Kongsøya	*Salvigsen* [1981]	78.90°	29.08°	9,850 ± 40	11,247	11,199–11,324	Radiocarbon-dated driftwood log on raised beach 100 m asl.
NP05-71GC	Klitgaard *Kristensen et al.* [2013]	South of Kvitøya		12,760 ± 65	14,170	13,935–14,558	Formanifera within glaciomarine sediments. Imprecise age control at base of the core means precise timing of deglaciation is largely uncertain.
NP94-4	*Cadman* [1996]	77.30°	12.66°	14,770 ± 90	17,363	17,078–17,629	*Elphidium excavatum* forams in marine sediments above diamicton.

Table 1. (continued)

Core/Location	Source	Latitude (N)	Longitude (E)	Uncorrected Age (^{14}C years B.P.)	Median Probability Age (years B.P.)	2σ Range (years B.P.)	Notes
Agardhbukta	*Salvigsen and Mangerud* [1991]	78.09°	18.68°	9,870 ± 140	11,353	11,063–11,829	Mosses (*Polytrichum commune*) within raised beach foresets 50 m asl probably deposited from a living position further upstream.
Kara Sea							
Cape Oskar	*Bolshiyanov et al.* [2000]	Taimyr Peninsula		11,775 ± 110	13,607	13,365–13,826	Carex seeds within peat at the base of terrestrial section.
White Lake	*Alexanderson et al.* [2001]	Taimyr Peninsula		20,070 ± 270	23,550	22,890–24,185	Shell of *Astarte* sp. within "melt out" till on top of buried glacial ice (120 m asl).
Russkaya Gavan'	*Zeeberg et al.* [2001]	76.19°	62.58°	9,155 ± 70	9,696	9,501–9,937	*Hiatella arctica* fragments from the lateral moraine of the Shokal'ski Glacier.
7 - Svyataya Anna Trough	*Polyak et al.* [1997]	81.48°	67.55°	13,710 ± 130	15,850	15,393–16,227	Muds overlying stiff diamicton.
29	*Polyak et al.* [1997]	79.99°	69.95°	13,730 ± 110	15,884	15,509–16,234	Muds overlying stiff diamicton.
DM-4380	*Polyak et al.* [2000]	Novaya Zemlya Trough		12,170 ± 100	13,555	13,338–13,792	Base of core containing glaciomarine sediments.

[a]Dates were recalibrated using the program Calib 7.1 [*Stuiver and Reimer*, 1993] and the IntCal13/MARINE13 calibration curves [*Reimer et al.*, 2013]. A ΔR value of 71 ± 21 (105 ± 24 north of 75°N) was used to account for local effects on the global reservoir correction [*Mangerud et al.*, 2006].

A dominant Kara Sea-based glaciation during glacial events of MIS 5 is, however, less ambiguous. Within the central Russian sector, the outermost belt of moraines between southern Taimyr and the Pechora Lowland has been used to define the maximum extent of the Early Weichselian glaciation, merging with a large ice cap covering the Putorana Plateau in Siberia [*Svendsen et al.*, 2004a; *Astakhov*, 2006]. On the Taimyr Peninsula, an 850 km long zone of wide push moraines south of the Byrranga Mountains—the Jangoda-Syntabul-Baikuronyora Line—marks the Weichselian maximum limit here (Figure 2-JSB) [*Möller et al.*, 2015].

One of the most significant impacts of ice sheet expansion onto mainland Russia during the late Quaternary was the diversion and damming of northward flowing rivers in front of the ice margin. During the Early Weichselian, an ice sheet, documented as being the most extensive Weichselian ice sheet in Russia [*Svendsen et al.*, 2004a], dammed Lake Komi in the Pechora Lowland up to the elevation of the Tsilma Pass in the Timan Ridge (Figure 2) [*Mangerud et al.*, 2004]. Whether Lake Komi drained into another lake in the White Sea basin or via an ice-free corridor between the Scandinavian Ice Sheet and the Kara Sea Ice Sheet is still under debate [*Kjær et al.*, 2006; *Larsen et al.*, 2006]. Luminescence dating of beach and shoreface sediments of Lake Komi constrain the age of the maximum lake level to the range 80–100 cal ka B.P., with ice advance thus implied to correlate with MIS 5b [*Mangerud et al.*, 2001b]. The limited extent of the Scandinavian Ice Sheet at this time [*Baumann et al.*, 1995; *Sejrup et al.*, 2000; *Lundqvist*, 2004], and stratigraphic evidence from the White Sea area, suggest the two ice sheets did not merge [*Larsen et al.*, 2006]. However, currently available evidence appears unable to unambiguously associate this advance with either MIS 5d or MIS 5b [*Lambeck et al.*, 2006].

2.2. Middle Weichselian (MIS 4–3/70–40 cal ka B.P.)

Glacigenic sediments recovered in shallow cores from the western Svalbard continental slope reveal the Middle Weichselian to have been characterized by several phases of extensive iceberg production. The first phase (60–55 cal ka B.P.) correlates with a glacier advance recorded at the Kapp Ekholm section on Svalbard [*Mangerud and Svendsen*, 1992], with sedimentary clast provenances suggesting the main source was located

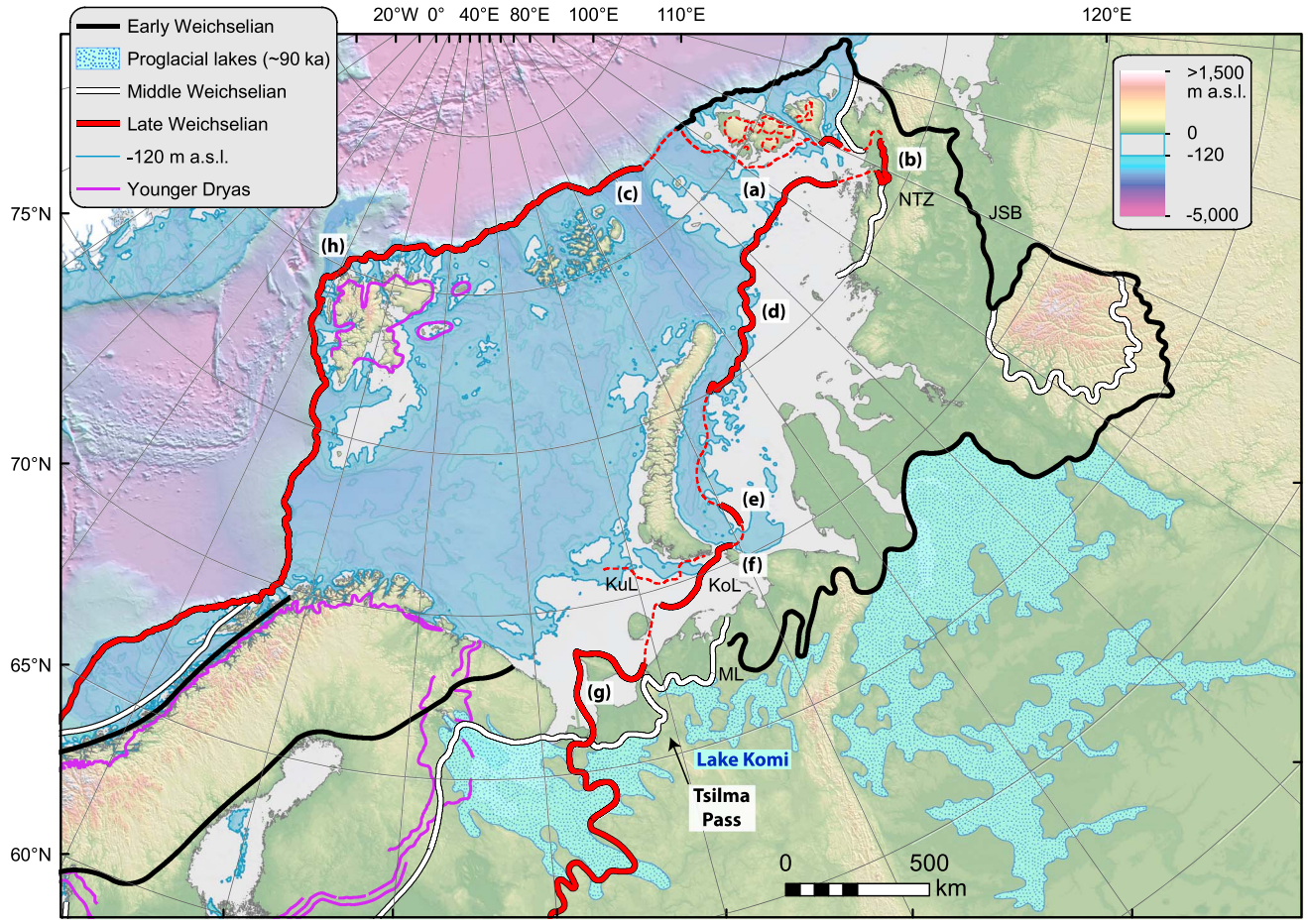

Figure 2. Grounded ice sheet limits from the Early and Middle Weichselian (as inferred by *Svendsen et al.* [2004a]) and the Late Weichselian ice sheet as identified by numerous workers (see section 2 for more details). A dashed line indicates the inferred margin where limits are still uncertain. Younger Dryas extents from *Mangerud* [2004] in Fennoscandia, and *Hormes et al.* [2013] in Svalbard. Acronyms referred to in the text: JSB = Jangoda-Syntabul-Baikuronyora Line, KoL = Kolguev Line, KuL = Kurentsovo Line, ML = Markhida Line, and NTZ = North Taimyr ice-marginal Zone. True-scale latitude: 75°N; elevation data: IBCAO version 3.0 [*Jakobsson et al.*, 2012b].

in the eastern Svalbard-Barents Sea area, and not in Fennoscandia or western Svalbard [*Andersen et al.*, 1996]. A similar IRD peak deposited along the outer shelf of the northern Kara Sea during MIS 4 provides further evidence for an extensive grounded ice sheet in this region prior to 50 cal ka B.P. [*Knies et al.*, 2001].

During the Weichselian glacial events, all three Eurasian ice sheets from the Barents Sea, Kara Sea, and Scandinavia terminated in the Arkhangelsk region of northwest Russia. Reconstruction of the glacial history in this region (synthesized by *Larsen et al.* [2006]) generally supports the east to west migration over time in major glacier activity [*Siegert et al.*, 2001; *Svendsen et al.*, 2004a] (e.g., Figure 3). However, extensive luminescence dating, supported by biostratigraphical evidence, indicates the separation of the Middle Weichselian Barents Sea and Kara Sea ice sheets into two shelf-based glaciations (70–65 and 55–45 cal ka B.P., respectively) separated by almost complete deglaciation [*Kjær et al.*, 2006; *Larsen et al.*, 2006]. Fluctuating dominance between the Barents and Kara seas at this time is suggested to be a result of oceanographic forcing (cf. section 7), specifically the ability of Atlantic moisture to penetrate into the Barents Sea.

The southern limit of the Middle Weichselian glacial maximum is now generally accepted to be the Markhida Line—an 800 km long ice-marginal belt trending east-west throughout northern Russia (Figure 2-ML) [*Astakhov et al.*, 1999; *Mangerud et al.*, 1999; *Svendsen et al.*, 2004a]. However, compelling evidence for two Middle Weichselian glaciations [e.g., *Larsen et al.*, 2006] separated by the widespread occurrence of marine tidal sediments deposited circa 65–60 cal ka B.P., led *Kjær et al.* [2006] to suggest that construction of the Markhida Line west of the Pechora valley was asynchronous, formed by these same two glaciations. The

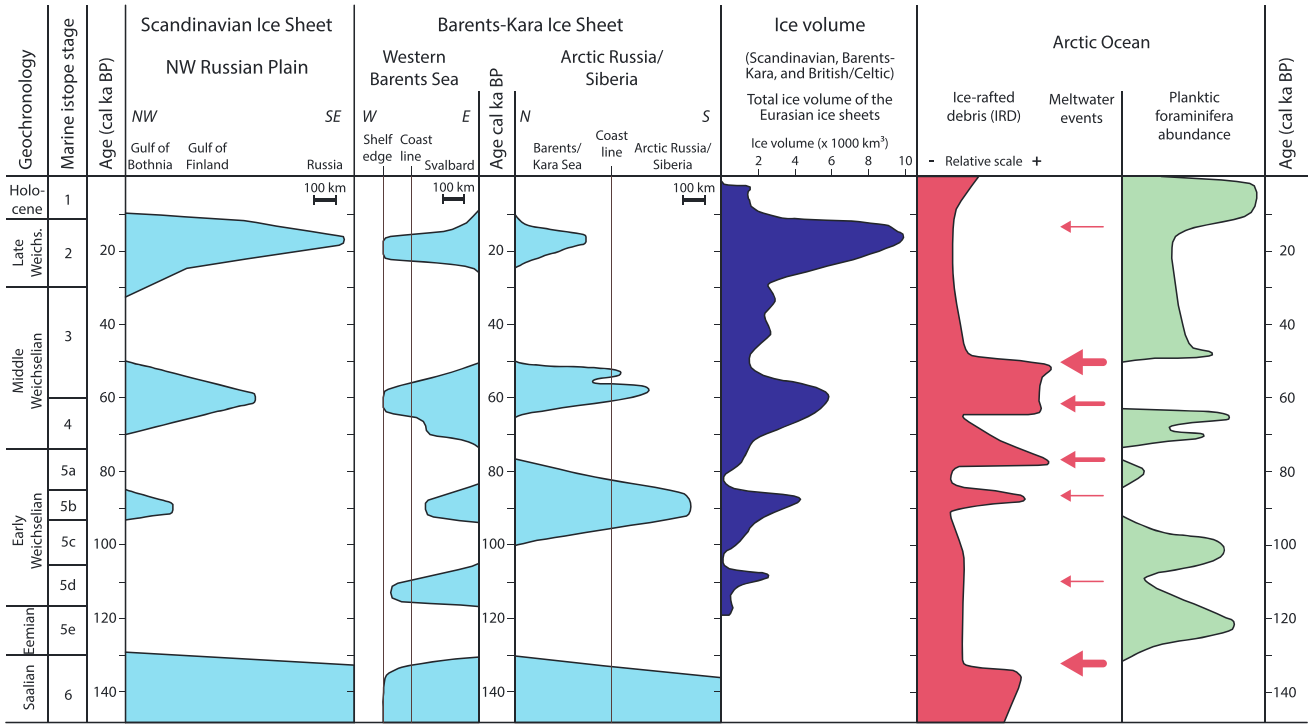

Figure 3. Time-distance diagram showing the asymmetric growth and decay of the Eurasian ice sheet through the Weichselian. Modified from *Svendsen et al*. [2004a].

composition of glacial erratics indicates that ice was moving from or across the southernmost Novaya Zemlya and Vaygach Island [*Polyak et al*., 2000].

East of the Kara Sea, mid-Weichselian ice cover is inferred to have been significantly smaller than ice cover during the previous Early Weichselian [*Svendsen et al*., 2004a]. For example, an inner system of moraine ridges encircling the Putorana Plateau (Norilsk Stage) suggests the presence of an extensive ice cap here at this time [*Hahne and Melles*, 1997], although not confluent with the larger Kara Sea ice sheet. To the south, a large mountain glacier complex existed in the Polar Urals (≥65 cal ka B.P.), which probably merged with the main ice sheet during peak glacial conditions [*Svendsen et al*., 2014]. North of the Byrranga Mountains, the North Taimyr ice-marginal zone (Figure 2—NTZ) marks a distinct belt of ice-marginal features 700–800 km long, containing thrust-block moraines up to 100 m high and 2–3 km wide [*Alexanderson et al*., 2001, 2002; *Möller et al*., 2015]. Mid-Weichselian ice incursion to this limit became too thin to maintain a deforming bed, subsequently froze, with further compressional flow resulting in the observed deformation of ice-cored sediments [*Alexanderson et al*., 2002]. Ice was thick enough, however, to dam a proglacial lake to circa 80 m above sea level (asl) in the Lower Taimyr River valley [*Mangerud et al*., 2004], dated to circa 60 ka [*Alexanderson et al*., 2001, 2002].

2.3. Middle-Late Weichselian Transition (MIS 3/2/40–30 cal ka B.P.)

The timing and location of ice sheet inception during the transition between MIS 3/2 in the Barents-Kara Sea region is still poorly constrained, with global sea level data suggesting that the global ice volume at this time was 60–65% of the LGM total [*Peltier and Fairbanks*, 2006]. However, a growing body of evidence, including radiocarbon-dated fauna and shorelines, as well as glacio-isostatic modeling, suggests that Fennoscandia and terrestrial areas in the Barents Sea hosted only limited remnants of the former Mid-Weichselian ice sheet during MIS 3 (i.e., the Ålesund interstadial) [*Ukkonen et al*., 1999, 2007; *Helmens*, 2000; *Arnold et al*., 2002; *Helmens and Engels*, 2010; *Lambeck et al*., 2010; *Olsen*, 2010; *Möller et al*., 2013; see also *Boreas*, 2010, vol. 39, issue 2, pp. 325–456]. Ice-free conditions have also been inferred on the outer coast of northern Norway (i.e., the Arnøy interstadial) [*Andreassen et al*., 1985], and on Novaya Zemlya as late as 30 cal ka B.P. [*Zeeberg et al*., 2001; *Mangerud et al*., 2008b].

While radiocarbon dates below till in Linnédalen, Spitsbergen, provide a minimum age of <40.1 cal ka B.P. for glaciation over west Svalbard [*Mangerud et al*., 1998], further maximum radiocarbon ages <32 cal ka suggest the BSIS responded faster and with a larger amplitude to global climate (and sea level) changes than other Northern Hemisphere ice sheets [*Landvik et al*., 1998]. For example, from Amsterdamøya, NW Svalbard, *Salvigsen* [1977] reported a maximum date for glaciation of circa 32 cal ka B.P., while *Hald et al*. [1990] reported a maximum age of circa 31 cal ka B.P. for southern Bjørnøyrenna. More recent data, including increasing IRD concentrations together with a decline in $\delta^{13}C$ values west of Svalbard, constrain ice advance to the western Barents shelf to circa 27 cal ka B.P. [*Jessen et al*., 2010], in accordance with earlier proposed reconstructions [*Elverhøi et al*., 1995; *Andersen et al*., 1996; *Mangerud et al*., 1998; *Vogt et al*., 2001].

2.4. Late Weichselian (MIS 2/30–13 cal ka B.P.)

2.4.1. Severnaya Zemlya and Taimyr Peninsula

A lack of glacigenic sedimentary successions suggest Severnaya Zemlya was either ice free during MIS 2, or that at least the ice caps were no larger than their present-day positions [*Raab*, 2003; *Möller et al*., 2006]. Mammoth finds next to the Vavilov Ice Cap dated to 24.9, 20.0, 19.3, and 11.5 cal ka B.P. support this interpretation [cf. *Vasil'chuk et al*., 1997]. South of the archipelago, a ubiquitous cover of Late Weichselian diamicton can be traced as far south as the 78th parallel (Figure 2a) [*Polyak et al*., 2008] coincident with a lobe that extended beyond the present coastline of the Taimyr Peninsula (Figure 2b) [*Alexanderson et al*., 2002; *Möller et al*., 2015]. The actual timing of their emplacement is uncertain, with tills on the northwestern Taimyr Peninsula dated to between circa 23.6 and 13.6 cal ka B.P. [*Alexanderson et al*., 2001]. However, ice was thin and unable to override any significant elevation rises. One suggested flow pattern of this ice is that local ice-spreading centers existed on the shallow banks west of the southern part of Severnaya Zemlya [*Polyak et al*., 2008]. Large, aligned erosional bedforms within the Voronin Trough, as well as diamicton similar to that found in the Svyataya (Saint) Anna and Franz-Victoria troughs, suggest that Late Weichselian ice probably drained to the shelf edge (Figure 2c) [*Polyak et al*., 2002, 2008]. Ice cover was thus likely continuous with the main Kara ice dome at the LGM. However, this diamicton is undated, and the proposed flow configuration here remains the least substantiated for the entire ice sheet.

2.4.2. Kara Sea

The existence for an LGM ice sheet advancing into the Kara Sea has been widely contested [*Arkhipov et al*., 1986; *Velichko et al*., 1997; *Mangerud et al*., 1999; *Grosswald and Hughes*, 2002], historically driven by a scarcity of geological data coming out of the Soviet Union during the Cold War [cf. *Ingólfsson and Landvik*, 2013]. Data from the Russian Arctic, in part coordinated by the QUEEN program (Quaternary Environment of the Eurasian North) [cf. *Svendsen et al*., 2004a], has since indicated that the Kara Sea was largely ice free during the LGM. North of ~75°N and east of ~60°E toward Novaya Zemlya, seismic profiling and sediment cores have identified a strongly furrowed facies associated with morainic features, bounded to the southeast by paleo–river channels and basin-fill deposits (Figure 2d) [*Polyak et al*., 2002; *Stein et al*., 2002]. The inferred ice sheet limit aligns with a well-defined moraine ridge southeast of the Novaya Zemlya Trough (Figure 2e) [*Svendsen et al*., 2004b]. Furthermore, a thin (<2 m) layer of diamict on Vaygach Island constrained by Middle Weichselian sublittoral deposits below and Holocene lacustrine sands above has been used to suggest Late Weichselian incursion here (Figure 2f) [*Zeeberg et al*., 2002].

Glacigenic diamicton found along the full axis of the Svyataya Anna Trough provides evidence for the extension of grounded ice to the shelf edge [*Polyak et al*., 1997]. Radiocarbon dates of circa 15.8 cal ka B.P. from deglacial sediments above also provide a minimum age for retreat from the deep, axial part of the trough. Abundant lineations and iceberg ploughmarks also indicate margin retreat within the Svyataya Anna Trough was rapid, and accompanied by readvances and extensive iceberg discharge (Figure 2c) [*Polyak et al*., 1997; *Jakobsson et al*., 2014a].

2.4.3. Southeastern Barents Sea

Sediment stratigraphy in the Pechora Sea substantiates land-based investigations that the LGM margin was located well off the present coastline in the Pechora Sea [*Astakhov et al*., 1999; *Mangerud et al*., 1999, 2002; *Polyak et al*., 2000], with the Kolguev Line (Figure 2-KoL) delimiting Late Weichselian tills offshore in this region (Figure 2g) [*Gataullin et al*., 2001]. Around 50–100 km further north of this the Kurentsovo Line marks a more distinct terminal position both morphologically and sedimentologically, probably resulting from a stable retreat stage [*Gataullin et al*., 2001]. This ice-marginal zone was tentatively correlated with the "Murmansk Bank Moraines," a 400 km long chain of ice-pushed ridges northeast of the Kola Trough [*Svendsen et al*., 2004b],

although the chain has more recently been reinterpreted as a possible inter ice-stream ridge between the Djuprenna and Nordkappbanken-east ice streams [*Winsborrow et al*., 2010]. Further geomorphological mapping from seismic data southeast of Sentraldjupet has revealed the Murmansk Bank line to extend northward, forming part of a grounding zone wedge deposited by late-phase ice flowing ENE [*Bjarnadóttir et al*., 2014].

The Arkhangelsk area, west of the Timan Ridge, serves as a key confluence zone for ice sourced from the Kara Sea, the Barents Sea, and Scandinavia. The encroachment of Scandinavian ice beyond the western Kanin Peninsula coastline is evidenced only by till deposits at Cape Kargovsky on the Kuloi coast [*Kjær et al*., 2003] and at Tarkhanov [*Demidov et al*., 2006] (Figure 2g). The maximum extent of this Scandinavian advance is placed between 20 and 17 cal ka B.P. [*Demidov et al*., 2006; *Linge et al*., 2006]. East of the Kanin Peninsula, Late Weichselian ice is assumed to have not reached the Russian mainland [*Larsen et al*., 1999; *Mangerud et al*., 1999]. The northern tip of the Kanin Peninsula is thus assumed to be the approximate coalescence zone between the Barents Sea and Scandinavian ice [*Svendsen et al*., 2004a].

2.4.4. Western Barents Sea

The presence of glacigenic debris flow deposits on trough mouth fans along the northern and western continental slope margins [*Laberg and Vorren*, 1995; *Dowdeswell et al*., 1996; *Kleiber et al*., 2000; *Dowdeswell and Elverhøi*, 2002; *Andreassen et al*., 2004] confirms a full glaciation of the western Barents Sea shelf during the LGM. Dating of these mass transport deposits west of Svalbard reveal ice reached the shelf break in a fairly uniform manner circa 24 cal ka B.P. [*Dowdeswell and Elverhøi*, 2002; *Jessen et al*., 2010]. North and west of Svalbard, sedimentation rates and IRD concentrations between 30 and 24 cal ka B.P. were relatively low [*Andersen et al*., 1996; *Mangerud et al*., 1998; *Knies et al*., 1999; *Kleiber et al*., 2000; *Vogt et al*., 2001; *Jessen et al*., 2010] suggesting that the last ice advance to the shelf break resulted in a relatively thin ice cover [*Andersen et al*., 1996]. The early discovery of iceberg ploughmarks on the Yermak Plateau in water depths of approximately 1000 m [*Vogt et al*., 1994; *Dowdeswell et al*., 2010a] has produced significant discussion on their origin [e.g., *Flower*, 1997; *Polyak et al*., 2001; *O'Regan et al*., 2010]. High-resolution multibeam bathymetry and sub-bottom acoustic profiling from the region reveal evidence for grounded ice on this relatively deep plateau [*Dowdeswell et al*., 2010a], possibly during MIS 6. However, a grounding line at the NW Spitsbergen shelf edge implies that ice from Svalbard did not flow across the Yermak Plateau during the Late Weichselian glacial maximum (Figure 2h) [*Ottesen and Dowdeswell*, 2009].

Glacial geomorphology of the seabed reveals that many of the sediments, IRD, and meltwater discharged at the shelf breaks were delivered by ice streams, occupying cross-shelf troughs [*Batchelor and Dowdeswell*, 2014], that were active during the glacial maximum and deglaciation of the ice sheet [*Ottesen et al*., 2002; *Andreassen et al*., 2008]. The retreat of these ice streams has since left a complex palimpsest of glacial landforms and sediments, characterized by patterns of nonlinear retreat, switching ice flow, and major readvances [*Ottesen et al*., 2005; *Dowdeswell et al*., 2006; *Winsborrow et al*., 2010, 2012; *Rüther et al*., 2012; *Bjarnadóttir et al*., 2013, 2014].

2.4.5. Northern Barents Sea

Difficulties associated with marine-based data collection from the northern Barents Sea, largely associated with perennial sea ice conditions (Figure 1), have so far hampered geomorphological reconstruction of LGM glaciation in this sector. However, evidence including emergence data from Franz Josef Land [*Forman et al*., 1996], IRD records from cores adjacent to the shelf break [*Knies et al*., 2000, 2001], as well as glacigenic diamicton found along the full axis of the Svyataya Anna Trough [*Polyak et al*., 1997] all indicate that grounded ice likely reached the shelf edge during the LGM.

2.5. Younger Dryas (MIS 1/13.1–11.5 cal ka B.P.)

The configuration of ice during the Younger Dryas stadial across the Barents-Kara Sea region is still largely uncertain, with little direct evidence found for an ice advance. Conversely, in western Europe, climate deterioration was accompanied by extensive glacier growth, and all glaciers were much larger than at any time during the Holocene [*Golledge et al*., 2008; *Ivy-Ochs et al*., 2009; *Nesje*, 2009]. Prominent end moraines have been mapped more or less continuously around Scandinavia, firmly placing ice in a terrestrial setting by this time [cf. *Mangerud*, 2004] (Figure 2). However, further north on western Spitsbergen, an opposite situation has been reported, with local glaciers significantly smaller than during the Little Ice Age [*Salvigsen*, 1979; *Mangerud and Svendsen*, 1990; *Svendsen and Mangerud*, 1992; *Mangerud and Landvik*, 2007]. In the absence of distinctly preserved geomorphology, defining marginal limits for the Younger Dryas ice sheet over

Svalbard has therefore become a task of probability based on the locations of deglaciation dates. The latest reconstruction produced by *Hormes et al*. [2013] (Figure 2) places ice cover over much of the terrestrial landscape of Svalbard, with only some coastal areas to the north and west ice free. The inner parts of Isfjorden, Storfjorden, and Wijdefjorden were also probably ice filled at this time.

While relatively little is known of the Younger Dryas ice sheet over Svalbard, even less is known of ice cover further east at this time. Similar negative glacier mass balance relationships have been inferred across Franz Josef Land during the Holocene, with radiocarbon dates indicating that glaciers were either near or behind present limits at the start of the Holocene circa 11.5 cal ka B.P. [*Lubinski et al*., 1999]. Elsewhere, pollen data indicate that some coastal areas of western Novaya Zemlya were probably ice free during the Younger Dryas [*Serebryanny et al*., 1998]. However, a set of moraine ridges off the west coast—the Admiralty Bank Moraines—have been speculated to represent a readvance position during this time, reflecting ice dispersal from an ice cap localized over Novaya Zemlya [*Gataullin and Polyak*, 1997; *Gataullin et al*., 2001]. Absolute chronologies are yet to confirm this, however.

3. Isostatic Loading

3.1. Maximum Late Weichselian Loading

The heights of past shorelines above present sea level provides an important constraint on the volumes of past ice sheets, with the pattern of postglacial emergence pivotal for constraining the location of maximum isostatic loading, as well as the relative timing of deglaciation. The isostatic fingerprint left by the former BSIS has long been recognized, with *Schytt et al*. [1968] first proposing a center of ice loading over the central Barents Sea. Increasing data relating to the age-height relation of shorelines in Svalbard, Kong Karls Land, Franz Josef Land and Novaya Zemlya [*Salvigsen*, 1981; *Forman*, 1990; *Mangerud and Svendsen*, 1992; *Mangerud et al*., 1992; *Forman et al*., 1995, 1996; *Zeeberg et al*., 2001; *Brückner and Schellmann*, 2003] have since refined constraints on the volume and postglacial emergence of the last ice sheet [*Lambeck*, 1995, 1996; *Peltier*, 2004]. Consensus on maximum Late Weichselian ice sheet loading is thus now placed over the northern Barents Sea and eastern Svalbard [cf. *Forman et al*., 2004] (Figure 4).

The highest raised beaches related to the last glaciation can be found on Kong Karls Land (>100 m on Kongsøya), Barentsøya (87 m), Edgeøya (89 m), and at Billefjorden (90 m) [*Salvigsen*, 1981; *Bondevik et al*., 1995; *Ingólfsson et al*., 1995; *Forman et al*., 2004]. Conversely, emergence data from Franz Josef Land indicate substantially less isostatic compensation than eastern Svalbard [*Salvigsen*, 1981; *Bondevik et al*., 1995]. Modest total emergence of 11–13 m asl on Novaya Zemlya also indicates only moderate glacial loading in the eastern Barents Sea (<1 km), early deglaciation, or both [*Forman et al*., 1995, 1999; *Zeeberg et al*., 2001; *Mangerud et al*., 2008b]. A lack of Late Weichselian or Holocene raised marine sediments along the coastlines of north Russia and southwest Yamal [*Forman et al*., 1999; *Mangerud et al*., 1999] implies the line of zero-emergence runs immediately south and east of Novaya Zemlya.

Minimum dates that constrain unloading of the crust after deglaciation can be obtained by radiocarbon dating organic material collected from raised marine sediments, such as driftwood, whalebones, or shells. By comparing the spatial distribution of many dates, a pattern of ice retreat and isostatic recovery can be built up [*Forman et al*., 2004; *Hormes et al*., 2013]. Despite the limited potential for finding raised beaches within the Barents Sea domain, data so far reveal that isostatic recovery commenced around western and northern Spitsbergen by circa 15.4–13.3 cal ka B.P. (13.4–12.0 ^{14}C ka) [e.g., *Forman et al*., 1987; *Brückner et al*., 2002], with whalebones dated between circa 15.4 and 13.6 cal ka B.P. (13.4 and 12.2 ^{14}C ka) indicating episodic open water conditions extending to near-shore areas of western Spitsbergen [*Forman et al*., 1987; *Forman*, 1990]. In contrast, coastal areas of eastern Svalbard, including Barentsøya, Edgeøya, and Kvitøya, did not become ice free until the beginning of the Holocene, < 12.0 cal ka B.P. [*Salvigsen and Mangerud*, 1991; *Landvik et al*., 1992]. Based on the lower emergence isobases around northern and western Spitsbergen, this region most likely experienced less loading and/or a shorter period of glaciation, suggesting proximity to the ice sheet margin [*Forman*, 1990; *Forman et al*., 1997] (Figure 4).

Further east, the oldest ^{14}C ages on driftage and shells of circa 12.2 cal ka B.P. from raised marine deposits on Franz Josef Land provide a similarly late minimum age on deglaciation here [*Forman et al*., 1996]. Maximum crustal compensation is found at Bell Island in the southwestern part of this island group, with a marine limit at 49 ± 1 m aht

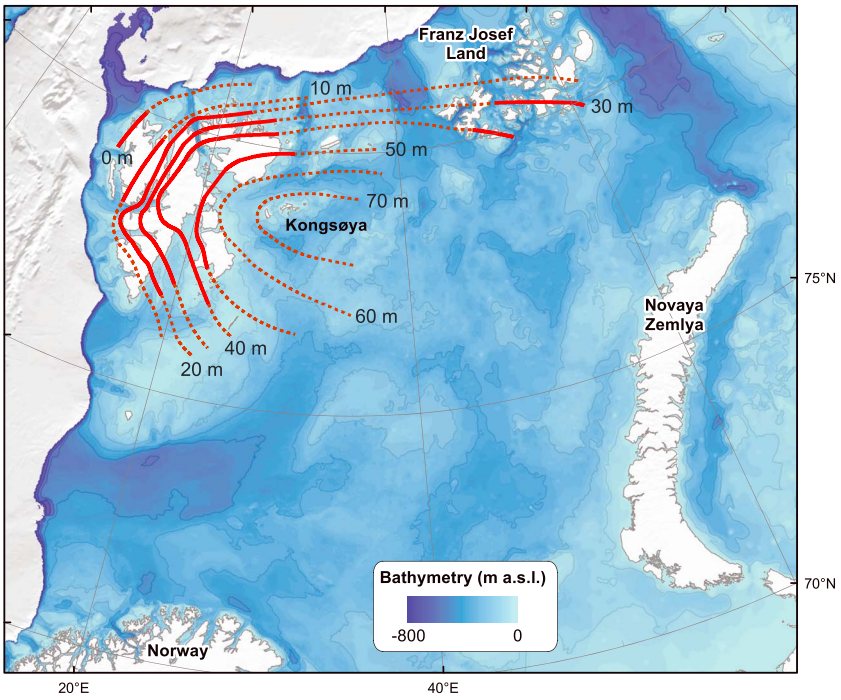

Figure 4. Estimated emergence isobases for the Barents Sea since 10.0 cal ka B.P. (9.0 ^{14}C ka). Modified from *Forman et al.* [2004].

(present mean high tide mark) [cf. *Forman et al.*, 2004] dated to 11 cal ka B.P. [*Forman et al.*, 1996]. The lowest compensation is found farthest east on Klagenfurt Island, with a marine limit of 20 ± 1 m a.h.t. dated to 5.7 cal ka B.P. [*Forman et al.*, 1997]. These data imply that Franz Josef Land probably sustained a modest Late Weichselian ice load (<1500 m), probably located within circa 200 km of the ice margin [*Emery and Aubrey*, 1991; *Fjeldskaar*, 1994].

With empirical evidence for past ice loading and deglacial rebound largely limited to shorelines bordering the northern Barents Sea region, the reconstruction of isobases has been continually hindered. Efforts to interpolate the distribution of isostatic loading into marine sectors using glacio isostatic adjustment models, such as ICE-5G and the more recent ICE-6G_C [*Peltier*, 2004; *Peltier et al.*, 2015], have tended to place the

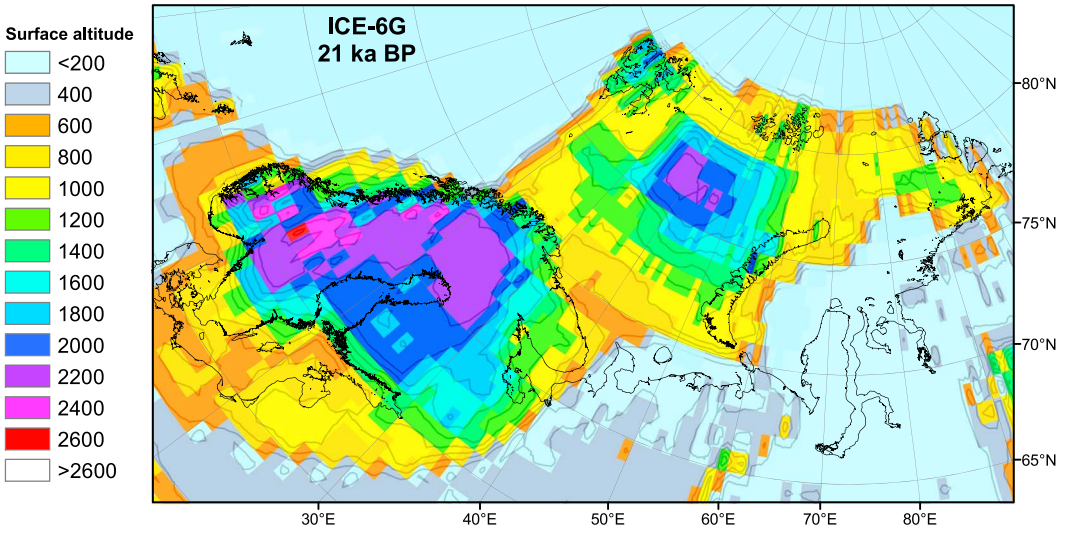

Figure 5. Surface altitudes (m asl) at 21 ka B.P. across Fennoscandia and the Eurasian Arctic according to the ICE-6G_C (VM5a) glacial-isostatic adjustment model [*Peltier et al.*, 2015].

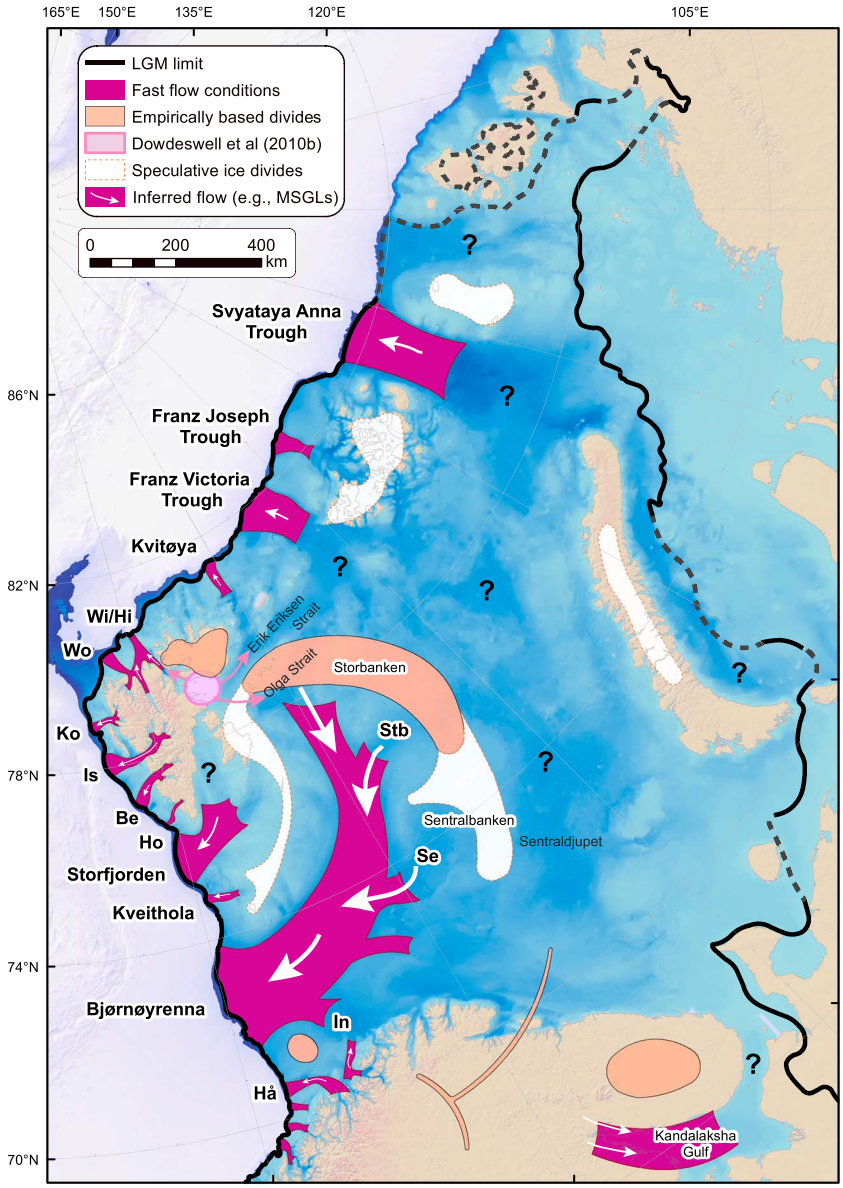

Figure 6. Inferred pattern of flow partitioning during deglaciation of the BSIS (although not necessarily contemporaneous), based on results from high-resolution geomorphological mapping (cf. section 5). Question marks indicate zones of significant uncertainty, including the positioning of a LGM ice dome over Hinlopenstretet (pink). Abbreviations referred to in the figure: Be = Bellsund, Hi = Hinlopen Trough, Ho = Hornsund, Hå = Håkjerringdjupet, In = Ingøydjupet, Is = Isfjorden, Ko = Kongsfjorden, Se = Sentralbankenna, Stb = Storbankenna, Wi = Wijdefjorden Trough, and Wo = Woodfjorden Trough. Elevation data source: IBCAO Version 3.0 [*Jakobsson et al.*, 2012b].

center of mass loading south east of Kongsøya, over Storbanken (Figure 5). However, the typically coarse resolution of such reconstructions, plus their lack of any inherent glaciological self-consistency, leaves their use as a geophysical constraint limited to broad spatial scales.

Reconstructions of former ice sheet drainage patterns using high-resolution maps of submarine geomorphology have been used to great effect to more tightly constrain the likely locations ice domes. East of Svalbard, streamlined landforms show ice drainage to have occurred eastward from Kong Karls Land into the Franz Victoria Trough [*Dowdeswell et al.*, 2010b; *Hogan et al.*, 2010a], indicating a major ice dome located on easternmost Spitsbergen around the southern entrance to Hinlopenstretet. However, geomorphological observations made farther south of Hinlopenstretet suggest that flow from this dome into

Bjørnøyrenna occurred only during the youngest deglaciation phase of the ice sheet, after a shift from its more central LGM position over Kong Karls Land and Storbanken [*Andreassen et al*., 2014] (Figure 6). Additional chronological information, along with the dating of high raised beaches on Kong Karls Land, would do much to resolve this issue. Further mapping of erratic boulders and cosmogenic radionuclide dating around Nordaustlandet have indicated the presence of additional smaller, cold-based LGM ice domes onshore [*Hormes et al*., 2011].

Significant centers of ice dispersal at the LGM also probably existed over currently glaciated topographic highs within the Barents and Kara seas, including Franz Josef Land, Novaya Zemlya, and Ushakov Island. However, streamlined and other submarine landforms of glacial origin relating to these suggested ice domes have yet to be discovered (Figure 6).

3.2. Constraining Late Weichselian Ice Thickness

Based on a combination of spatially heterogeneous empirical data documenting postglacial emergence, and an absence of terrestrial highlands suitable for cosmogenic-isotope exposure dating, estimates for a maximum ice thickness during the Late Weichselian have varied significantly. Early glacio-isostatic modeling by *Lambeck* [1996] suggested a maximum thickness of 3400 m over the central Barents Sea, with no substantial ice cover over the Kara Sea or West Siberia. However, based on similar present and postglacial emergence rates found between southwestern Norway, Franz Josef Land, and Novaya Zemlya, *Forman et al*. [1995] predicted an equivalent ice sheet loading between the two regions, thus inferring a maximum thickness of 2500 m over the northern Barents Sea, thinning to about 1500 m over Franz Josef Land and Novaya Zemlya. Further glaciological and isostatic modeling in a review by *Landvik et al*. [1998] has since supported this more modest estimation, with a value between 2000 and 3000 m.

Studies utilizing numerical ice sheet models (cf. section 8 for a more detailed discussion) have tended to reconstruct thinner ice sheets. In the seminal paper by *Svendsen et al*. [2004a], a "maximum-sized" modeled reconstruction for the Late Weichselian produced a maximum ice thickness between 1500 and 1800 m over the Barents Sea at 15 ka, reducing to 1200 m close to Novaya Zemlya [see also *Svendsen et al*., 1999]. Changes in ice thickness were also shown to be moderated by the development of ice streams within the bathymetric troughs on the western and northern shelves, draining ice from the Barents Sea interior [*Dowdeswell and Siegert*, 1999; *Siegert and Dowdeswell*, 2004]. Recent depictions of the ice configuration on Svalbard during peak glacial extent follow similar concepts of flow partitioning, often envisaged with individual ice domes and fast-flowing ice streams separated by slow flowing, cold-based inter ice stream areas [*Landvik et al*., 2005; *Ottesen and Dowdeswell*, 2009; *Alexanderson et al*., 2011]. Evidence for an internal warm-based/erosive boundary is limited to the fjords and lowlands, below circa 230 m asl in Nordaustlandet (NE Svalbard) [*Hormes et al*., 2011] and even lower in Krossfjorden (NW Svalbard) at 120 m asl [*Gjermundsen et al*., 2013].

Exposure age samples taken from western Svalbard and dated to pre-Late Weichselian (Table 2) reveal the possible presence of Late Weichselian nunataks >300 m asl on Amsterdamøya [*Landvik et al*., 2003], >470 m asl on Prins Karls Forland, and >313 m asl on Mitrahalvøya [*Landvik et al*., 2013], supporting numerical predictions of a generally low-aspect ice surface of approximately 1:67 for inter–ice stream areas [*Henriksen et al*., 2014] (Figure 7b). From LGM-age cosmogenic exposure age dating of erratic boulders on Knølen, the minimum ice surface elevation of the Kongsfjorden ice stream was >449 m asl [*Henriksen et al*., 2014], thus producing a much lower aspect surface gradient of approximately 1:125 (Figure 7b), in line with similar topographically constrained ice streams on Greenland [e.g., *Truffer and Echelmeyer*, 2003; *Thomas et al*., 2009].

A recent compilation of ^{10}Be ages of high-elevation erratic boulders from northwest Svalbard provides further constraints on the minimum ice thickness of the ice dome here during the Late Weichselian, with an erratic on Langskipet at 611 m asl suggesting an ice thickness of >900 m in Möllerfjorden and Lilliehöökfjorden [*Gjermundsen et al*., 2013]. The ^{10}Be ages from bedrock on summit peaks (including Kongen) all predate the Late Weichselian, although paired ^{10}Be and ^{26}Al data indicate summits here have all been covered by cold-based, nonerosive ice during the Quaternary, likely during all maximum glacial phases [*Hormes et al*., 2013]. The surface elevation of the ice dome over northwest Svalbard might thus have reached elevations of >1350 m asl [*Gjermundsen et al*., 2013]. In central Spitsbergen, one boulder sample at 1245 m asl, dated to 23.2 ± 1.3 ka, constrains ice surface elevation in Wijdefjorden (Figure 7a). By extrapolating these predicted minimum-surface profiles (Figure 7b) toward the center of isostatic loading east of Svalbard, it is conceivable

Table 2. Selected Exposure Ages Constraining Minimum Ice Surface Elevations and Ice-Free Areas on Svalbard

Source	Mountain/Area	Boulder/Bedrock	Elevation (m asl)	Latitude (N)	Longitude (E)	Exposure Age (^{10}Be)	Notes
Landvik et al. [2003]	Amsterdamøya	Boulder	293	79.77°	10.73°	73.9 ± 5.7	Perched boulders indicate no overriding ice since Early Weichselian. Both dates constrain ice surface gradient to between 1:25 and 1:50.
	Danskøya	Bedrock	74	79.72°	10.95°	18.0 ± 1.8	
Landvik et al. [2013]	Leefjellet	Boulder	473	78.75°	10.69°	20.7 ± 2.2	
	Mitrahalvøya	Boulder	166 (313)	79.18°	11.63°	13.5 ± 1.2	Glacial erratics (not sampled) were observed up to 313 m asl.
Gjermundsen et al. [2013]	Langskipet	Boulder	611	79.24°	11.81°	24.8 ± 1.8	Above 300 m deep fjords, implying a minimum ice thickness of >900 m.
	Aurivilliusfjellet	Boulder	730	79.60°	11.82°	18.3 ± 1.3	
		Boulder	687	79.60°	11.79°	20.1 ± 1.6	
	Reinsdyrflya	Boulder	97	79.84°	13.80°	14.8 ± 1.0	
	Kaffitoppen	Boulder	836	79.46°	11.39°	21.7 ± 1.4	LGM ice surface between 924 and 836 m or higher if summit date affected by nuclide inheritance.
	Kaffitoppen	Bedrock	924	79.47°	11.39°	41.3 ± 2.4	
	Kongen	Bedrock	1458	79.29°	12.48°	178.8 ± 10.6	Potentially ice covered if we assume a mean ice surface slope of 1:50 to the present coastline.
	Kongen	Bedrock	1457	79.29°	12.48°	182.8 ± 10.8	
Hormes et al. [2011]	Murchisonfjorden	Bedrock	231	80.06°	18.80°	33.3 ± 2.0	Positioning of boulder on bedrock with clear nuclide inheritance thus interpreted to be MIS 2 in age.
	Murchisonfjorden	Boulder	268	80.06°	18.75°	29.5 ± 2.0	
Hormes et al. [2013]	Wijdefjorden	Boulder	1245	79.17°	16.78°	23.2 ± 1.3	Granitic gneiss boulder
Henriksen et al. [2014]	Knølen	Boulder	406	79.04°	11.95°	20.0 ± 0.9	Quartz gneiss boulder. Signs of downslope movement by 10–15 m from solifluction.

that ice thickness may have reached values greater than 3000 m during phases of predominantly cold-based, high-aspect growth.

3.3. Prelate Weichselian Isostatic Effects

Observations required for successful inversion of rebound data for ice thickness during the early part of the Weichselian are few and less reliable, in part because later advances have frequently eroded or overprinted this older record. Raised beach features on western and northern Spitsbergen 40 m above the Late Weichselian marine limit indicate that the last glaciation was not the most extensive, nor resulted in the greatest ice sheet loads in the late Quaternary [*Forman and Miller*, 1984; *Mann et al.*, 1986; *Forman*, 1990]. Direct dating of subfossils place these high relative sea level events at about 80–60 ka and >140 ka ago [*Forman et al.*, 1987; *Miller et al.*, 1989; *Forman*, 1999]. Using isostatic rebound modeling and predictions of ice-dammed lake levels throughout the Early to Middle Weichselian, predictions of maximum ice loading during cold stadials (MIS 5d, 5b, 4) have been placed over the Kara-Barents Seas with an ice thickness not exceeding approximately 1200 m [*Lambeck et al.*, 2006]. While the Early Weichselian ice sheets were areally large, their volumes were relatively small when compared with the oscillations in global sea level at this time. Attribution of this imbalance is still unclear, but may reflect fluctuations of ice sheets in North America, or even Antarctica, during MIS 5–4 [*Lambeck et al.*, 2006].

4. Chronology

4.1. The Bjørnøya Trough Mouth Fan

Trough mouth fans (TMFs) are a common feature of high-latitude shelf margins, found seaward of glacially formed submarine troughs [*Vorren and Laberg*, 1997; *Ó Cofaigh et al.*, 2003]. These fans are fed primarily by glaciers and receive most of their sediments during relatively short periods associated with peak glacial conditions [*Dowdeswell and Siegert*, 1999]. TMFs are therefore excellent proxies for establishing paleo–environmental

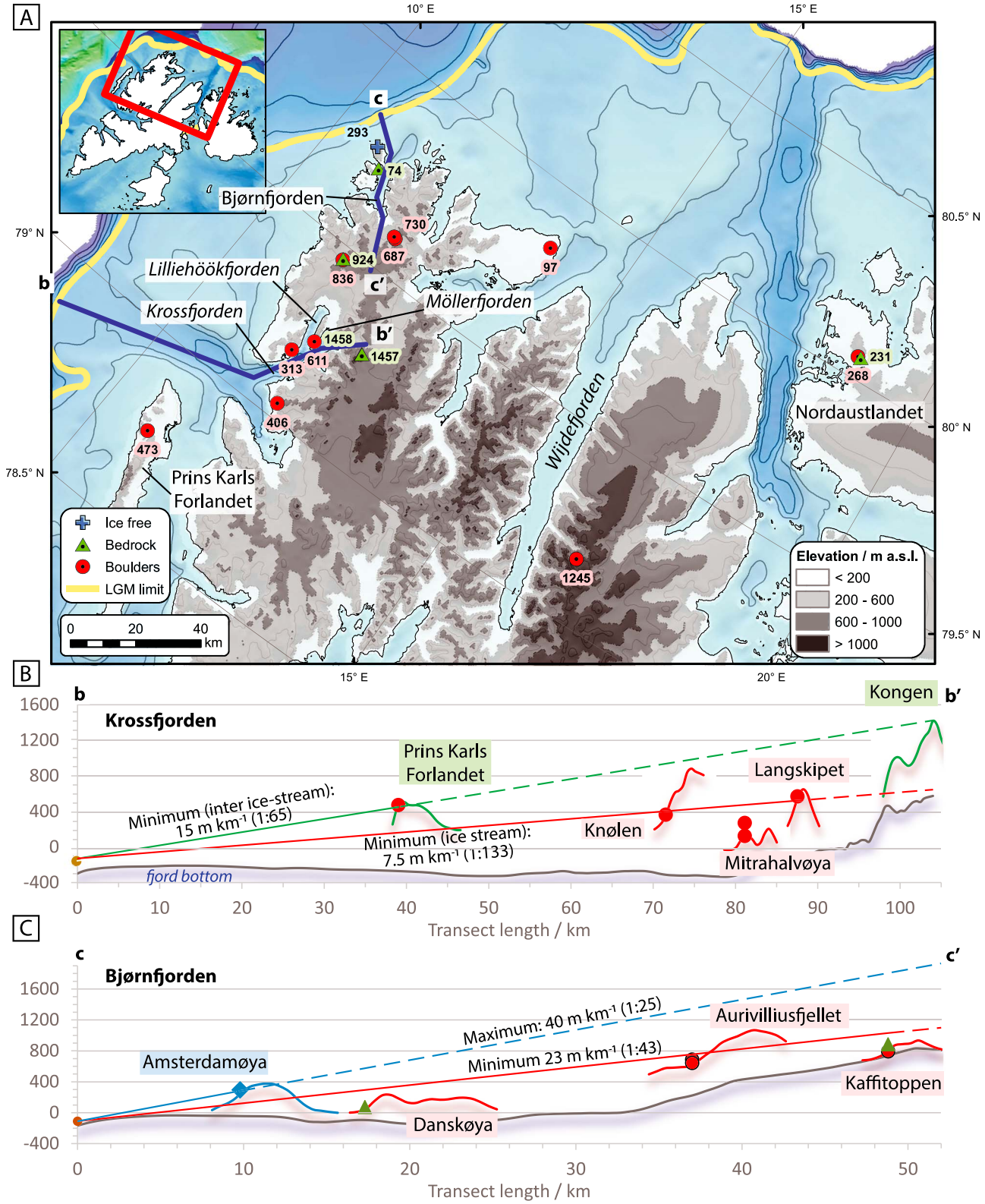

Figure 7. (a) Elevations of cosmogenic-exposure age dates constraining minimum and maximum LGM ice thicknesses across northern Svalbard. Data details are listed in Table 2. (b, c) Reconstructed Last Glacial Maximum mean ice surface profiles for ice streams exiting in Krossfjorden and Bjørnfjorden. Calculated gradients using boulder elevations on Spitsbergen mainland have been compensated for glacioisostatic uplift by 40 m [*Lehman and Forman*, 1992].

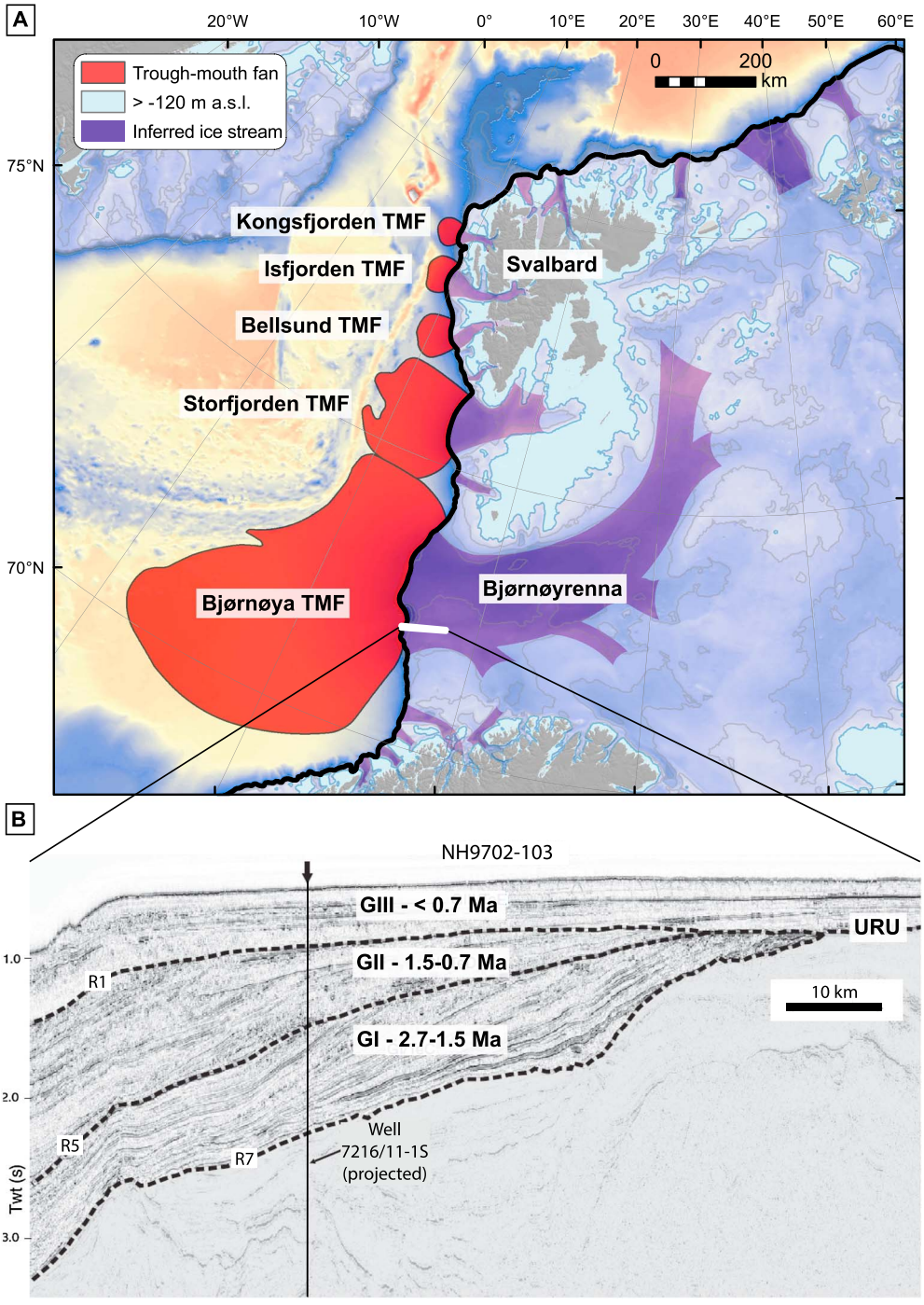

Figure 8. (a) Trough mouth fans along the western Barents Sea margin [cf. *Vorren et al.*, 1998]), (b) Downslope oriented seismic line NH9702-103 detailing sediment units GI-GIII and their bounding reflections R7, R5, and R1 [*Faleide et al.*, 1996] (modified from *Laberg et al.* [2010]).

conditions over timescales of up to a few millions of years, and a number can be found adjacent to the Norwegian shelf break (Figure 8a) [*Vorren et al.*, 1998; *Batchelor and Dowdeswell*, 2014].

The largest of these fans is the Bjørnøya (Bear Island) TMF, equivalent in areal extent to that of present-day Iceland, with a maximum thickness of approximately 3.5 km [*Vorren and Laberg*, 1997; *Andreassen and Winsborrow*, 2009]. Seismic profiles taken across the fan and the southwestern Barents Sea continental margin reveal a distinctive glacigenic stratigraphy (Figure 8b), separated from the stratified sedimentary bedrock

below by an upper regional unconformity (URU). Across the Barents Sea shelf this URU can be found at depths ranging from ~0 to 300 m [*Vorren et al*., 1989], with glacitectonic features within associated glacial sediments indicative of strong erosion of the bedrock [e.g., *Gataullin et al*., 1993]. Toward the shelf break, this URU splits into three major unconformities (R7, R5, and R1), which define the boundaries for three main seismic units, GI–GIII respectively [*Vorren et al*., 1991; *Faleide et al*., 1996] (Figure 8b). Based on a revised chronostratigraphy and compilation of borehole data (including StatoilHydro well 7216/11-1S) from this margin, *Knies et al*. [2009] proposed the base of the Pleistocene rests within seismic unit GI. Here slope sediments are inferred to be predominantly distal glacimarine [*Sættem et al*., 1992; *Laberg et al*., 2010], reflecting the inception of terrestrially restricted glaciation in Svalbard and the northern Barents Sea circa 2.7 Ma [*Butt et al*., 2000, 2002; *Jansen et al*., 2000; *Mattingsdal et al*., 2014]. A shift to more chaotic deposition occurs in GII, characterized by glacigenic debris flows, slide scars, and blocks of intact sediments originating from the outer shelf [*Andreassen et al*., 2004; *Laberg et al*., 2010]. This event coincides with the first documented shelf edge glaciations in the western Barents Sea during the Early-Middle Pleistocene (1.3–1.5 Ma) [*Faleide et al*., 1996; *Butt et al*., 2000; *Andreassen et al*., 2007b; *Rebesco et al*., 2014], as well as the first signs of extensive glacial erosion on the Yermak Plateau [*Mattingsdal et al*., 2014]. Unit GIII comprises mainly large debris flows deposited during full-glacial conditions, with sparse occurrence of glacimarine sediments [*Laberg et al*., 2010]. Eight distinct subunits within GIII indicate multiple periods where shelf sediments were eroded and transported subglacially as deformation till by ice streams to the shelf break [*Laberg and Vorren*, 1996b; *Andreassen et al*., 2004].

This change in sedimentation reflects a shift toward topographically focused ice streams becoming the dominant mechanism for erosion and deposition [*Knies et al*., 2009; *Laberg et al*., 2010]. During the last circa 0.7 Ma, ice streams in the southwest Barents Sea have had a profound effect, helping erode an estimated average of 440–530 m of bedrock, mainly from the cross-shelf troughs [*Siegert and Dowdeswell*, 1996; *Laberg et al*., 2012]. During the Late Weichselian glaciation alone, it is estimated that approximately 4600 km^3 of sediments were deposited on the Bjørnøya fan [*Dowdeswell and Siegert*, 1999]. This places the average linear erosion rate during the Late Pleistocene at 0.6–0.8 mm a^{-1} [*Laberg et al*., 2012]—significantly higher compared with estimates reported from the Fennoscandian ice sheet of approximately 0.38 mm a^{-1} [*Dowdeswell et al*., 2010c] and 0.13 mm a^{-1} from the southwestern Labrador Sea [*Hiscott and Aksu*, 1996]. First-order controls on the amount of erosion include the extent and duration of glacial activity, although other key factors include the weak composition of the sedimentary bedrock, the large drainage areas of the ice streams, and the basal thermal regime [*Laberg et al*., 2012].

4.2. Late Weichselian Ice Sheet Growth (MIS 2)

The preservation of IRD layers found in cores adjacent to the continental shelf break provides a rare and near continuous record of the waxing and waning of ice sheets during the most recent glacial cycles of the Quaternary. Through radiocarbon dating and provenance analyses of these IRD layers, alongside cross-correlation with glaciation curves from onshore sedimentary sections, major ice front fluctuations associated with the Late Weichselian ice sheet over the Barents Sea and Fennoscandia can be reconstructed with reasonable certainty [e.g., *Hebbeln*, 1992; *Baumann et al*., 1995; *Mangerud et al*., 1998; *Knies et al*., 2000]. The majority of data indicate that growth of the BSIS initiated circa 32.0 cal ka B.P. [*Andersen et al*., 1996; *Landvik et al*., 1998; *Siegert and Dowdeswell*, 2002], with advance onto the shelf tentatively suggested to have coincided with a decline in $\delta^{13}C$ values and IRD peak at circa 27.0 cal ka B.P. [*Jessen et al*., 2010]. Simultaneous advances of the British-Irish Ice Sheet [*Scourse et al*., 2009] and southern Fennoscandian Ice Sheet [*Sejrup et al*., 2000] also occurred at this time, in line with global sea level reaching its minimum at circa 26.0 cal ka B.P. [*Peltier and Fairbanks*, 2006].

A steep increase in bulk accumulation rates (deposition of debris flows) at circa 27.2 cal ka B.P. north of Kvitøya Trough [*Knies et al*., 2000, 2001], and hemipelagic sequences intercalated with glacial diamicton north of Franz Victoria Trough dated to 27.4 cal ka B.P. [*Kleiber et al*., 2000], imply a slightly earlier advance of grounded ice to the shelf edge along the northern Barents Sea margin. Early extension of the northern BSIS into these northern troughs was probably a result of close proximity to the hypothesized center of the ice sheet between Storbanken and Nordaustlandet [*Forman et al*., 1995]. Mass-transported sediments dated in cores along the western Svalbard shelf signify that full glaciation was achieved here by circa 24.0 cal ka B.P. [*Jessen et al*., 2010], also coinciding with maximum extension in the British sector of the Eurasian ice sheet complex [*Scourse et al*., 2009]. Further dates from debris flows within the Bjørnøyrenna

TMF and subglacial till in outer Bjørnøyrenna indicate that an ice stream reached the shelf edge twice during the Late Weichselian, first prior to 22 cal ka B.P. and second after 19 cal ka B.P. [*Sættem et al*., 1992; *Laberg and Vorren*, 1995].

While there is general agreement on the coverage of the northern and central Barents Sea by a major ice sheet (cf. section 2), earlier workers contested the scale of glaciation over the west coast of Spitsbergen. In contrast to the 800 m thick ice sheet over Prins Karls Forland predicted by *Landvik et al*. [1998], others have suggested that large sectors on the west coast of Svalbard remained ice free [e.g., *Salvigsen*, 1977; *Boulton*, 1979; *Miller et al*., 1989; *Forman*, 1990]. The most significant evidence for this is the preservation of old emerged beaches and associated organic materials dating to >36 ka B.P. [*Forman et al*., 1987]. Recent reports of well-preserved pre-Late Weichselian raised shorelines in northwest Spitsbergen [*Evans and Rea*, 2005] and Prins Karls Forland [*Andersson et al*., 1999, 2000] appear to add further support to this hypothesis. However, their presence could also be explained by their survival beneath cold-based ice, particularly in inter–ice stream areas [*Ottesen and Dowdeswell*, 2009]. Full preservation of former ground surfaces and delicate landforms, despite complete overriding by ice during several tens of millennia, has been previously suggested possible [*Kleman*, 1994; *Clark*, 1999] and found to be a common occurrence in other paleo–ice sheet domains [*Kleman and Hattestrand*, 1999; *Fabel et al*., 2002; *Briner et al*., 2006; *Davis et al*., 2006]. In a reevaluation of ice sheet growth on western Svalbard, *Landvik et al*. [2013] proposed an empirically based model of glaciation that involved major ice growth >470 m asl over Prins Karls Forland at the glacial maximum (cf. section 3). The identification of megascale glacial lineations in Forlandsundet [*Ottesen et al*., 2007] shows that wet-based conditions and tributary ice streams were subsequently established in the strait, probably in response to the reduction and deglaciation of the major ice streams in Isfjorden and Kongsfjorden [*Landvik et al*., 2013, 2014].

4.3. Constraining the Timing of Deglaciation (MIS 1)

For a marine-based ice sheet such as the BSIS, constraining the timing of deglaciation is typically carried out by radiocarbon dating of organic material found within cored deglacial sediments deposited above subglacial or ice-marginal tills. The most accurate deglaciation ages thus tend to be located as close to the upper till boundary as possible. However, radiocarbon age uncertainties are further affected by a number of factors, including poorly constrained variations in the marine radiocarbon reservoir effect (i.e., the delayed transfer of carbon-14 from the atmosphere to the deep ocean), sample contamination with older radiocarbon, and uncertainties associated with radiocarbon age calibration. Radiocarbon ages from early postglacial deposits thus usually represent a *minimum* age for deglaciation, with the true age of ice removal dependent on the rate of sedimentation up to the point that the dated material was deposited. Furthermore, the 2 sigma range provided with each calibrated date (Tables 1 and 3) represents a more "fuzzy" timeframe within which the probability that the sample date is correct remains equal.

Minimum ages constraining deglaciation across the Barents and Kara seas are sparsely distributed, particularly in central areas, resulting in poorly constrained retreat chronologies (Figure 10) [*Landvik et al*., 1998]. Early reconstructions along the western Svalbard margin generally agreed on an initial retreat in line with a distinct meltwater peak at circa 17.7 cal ka B.P. [*Elverhøi et al*., 1995; *Andersen et al*., 1996; *Landvik et al*., 1998; *Mangerud et al*., 1998], although *Vogt et al*. [2001] proposed a slightly earlier retreat circa 19.1 cal ka B.P.. More recently, deglaciation from the western Svalbard shelf break has been pushed back even further to circa 20.5 cal ka B.P., based on estimates for the onset of hemipelagic sedimentation in Storfjordrenna circa 19.6 cal ka B.P. [*Rasmussen et al*., 2007] and a nearby IRD concentration peak between 21.2 and 19.8 cal ka B.P. [*Jessen et al*., 2010] (cf. Table 3).

IRD fluctuations in cores north of Kvitøya Trough (PS2138-1) and Franz Victoria Trough (PS2446-4) between 22.8 and 19.5 cal ka B.P. suggest that further north and east the ice sheet experienced only marginal fluctuations on the outer shelf bordering the Arctic Ocean [*Knies et al*., 1999, 2000; *Kleiber et al*., 2000] (Figure 9). Two prominent IRD pulses at circa 18.6 and 16.3 cal ka B.P. at both sites indicate that abrupt, but stepwise, ice sheet disintegration in this sector followed at a later date [*Knies et al*., 2001] (Figure 10), contemporaneous with the inferred presence of surface meltwater in this region [*Chauhan et al*., 2015]. One suggested explanation for the two-stage collapse of this sector is that the armadas of icebergs released during initial collapse triggered positive ice-albedo feedback mechanisms, promoting sea ice formation and thus stabilizing the northern ice sheet margin [*Kleiber et al*., 2000; *Knies et al*., 2001].

Table 3. Dated Ice-Rafted Debris Peaks From the Barents Sea Continental Shelf Break [a]

Name	Source	Latitude (N)	Longitude (N)	Uncorrected ^{14}C Age	Median Probability Age (years B.P.)	2σ Range (years B.P.)	Notes
Norwegian Sea							
JM04-025PC	*Jessen et al.* [2010]	77.47°	9.50°		20.5–20.0[b]		High IRD flux signifies deglaciation from outer shelf.
JM03-373PC2		76.40°	13.10°		21.2–19.8[b]		
					15.70–14.65[b]		Very high IRD concentrations and sedimentation rates indicate increased calving, with retreat likely to the present Svalbard coastline.
23258	*Bischof* [1994]	74.99°	13.97°		circa 17.0[b]		Change from crystalline lithologies to almost exclusively clastic sedimentary rocks from Spitsbergenbanken/ Barents Sea.
Northern Barents Sea/Arctic Ocean							
PS2138-1	*Knies et al.* [2000]	81.54°	30.59°	20,480 ± 330	24,031	23,193–24,952	Peak release of kaolinite-rich sediments from the northern Barents Sea shelf, triggering extremely high bulk accumulation rates.
				circa 19,440[b]– 16,670 ± 210	22,785[b]–19,495	18,972–20,010	At least three IRD pulses reflect waxing and waning of the BSIS on the outer shelf.
				15,850 ± 130– 14,030 ± 80	18,604–16,283	18,311–18,870 16,017–16,578	Two major IRD pulse reflects rapid disintegration of the ice sheet from the shelf by rising summer insolation and sea level.
PS2446-4	*Kleiber et al.* [2000]	82.39°	40.91	23,580 ± 60	27,387	27,194–27,563	Hemipelagic sequences intercalated with glacial diamicton approximate the advance of grounded ice to the shelf break.
				21,550 ± 250– 19,730 ± 60	25,347–23,157	24,623–25,845 22,919–23,432	Temporary instability (increased calving) coincident with H2.
				15,870 ± 90– 12,860 ± 90	18,632–14,409	18,409–18,817 14,046–14,896	Two distinct IRD peaks (also evident in core PS2138-1 above) constrain the first phase of ice sheet disintegration.
PS2447-5		82.16°	42.03°	13,830 ± 80	16,021	15,761–16,261	Grounding line retreat approximated to 16.0 cal ka B.P. as indicated by a change in sedimentary pattern from stratified diamicton to massive, pebbly, silty clay.

[a]Reported ^{14}C ages were recalibrated using the program Calib 7.1 [*Stuiver and Reimer*, 1993] and the IntCal13/MARINE13 calibration curves [*Reimer et al.*, 2013]. A ΔR value of 71 ± 21 (105 ± 24 north of 75°N) was used to account for local effects on the global reservoir correction [*Mangerud et al.*, 2006].
[b]Not recalibrated.

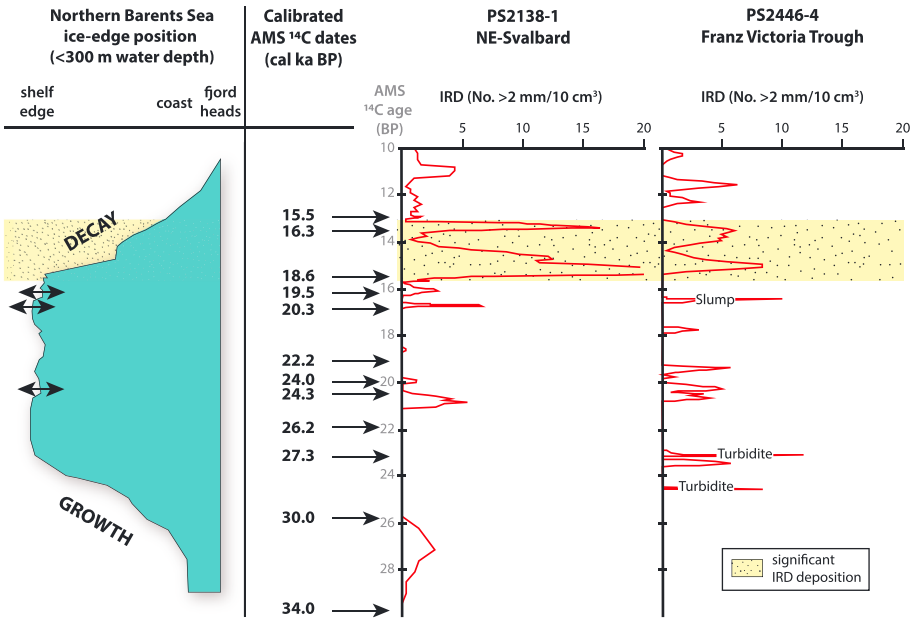

Figure 9. Extension of the BSIS on the northern Barents Sea margin during the last glacial/interglacial cycle with respect to ice-rafted debris peak values from the cores PS2138-1 and PS2446-4 (see Figure 10 for core locations). Original ^{14}C AMS dates have been recalibrated using a ΔR value of 105 ± 24 to account for local effects on the global reservoir correction [*Mangerud et al.*, 2006]. Modified from *Knies et al.* [2001].

The disintegration of long-term perennial sea ice coverage across the Polar North Atlantic after 17.6 cal ka B.P. likely impacted the stability of ice streams in this region [*Müller and Stein*, 2014]. At circa 17.0 cal ka B.P. the dropstone composition in cores west of Bjørnøyrenna switched from crystalline lithologies (sourced from western Norway) to clastic sedimentary rocks. *Bischof* [1994] suggested this represented undiluted material from the Barents Sea, in particular from Spitsbergenbanken. Radiocarbon dates from a 280 km wide grounding zone wedge in outer Bjørnøyrenna constrain a readvance of the Bjørnøyrenna Ice Stream to circa 17.1 cal ka B.P. [*Rüther et al.*, 2011], providing a possible source for the sharp change in IRD composition. Further dates from the wedge suggest that the ice front probably remained stable here for circa 500 years [*Rüther et al.*, 2011]. A contemporaneous advance of the Coast-parallel Trough Ice Stream off the Finnmark coast (Figure 12b) is supported by deglaciation ages presented by *Junttila et al.* [2010], who suggested open water downstream of the associated Ingøydjupet lobate sedimentary deposit from 18.6 cal ka B.P. and open water in the lobe area from circa 15.0 cal ka B.P. Similarly, radiocarbon dates from ice-proximal sediments within Franz Victoria Trough and Svyataya Anna Trough confirm that the deepest troughs along the northern Barents Sea were ice free by circa 16 cal ka B.P. (Figure 10) [*Polyak and Solheim*, 1994; *Polyak et al.*, 1997; *Kleiber et al.*, 2000; *Łącka et al.*, 2015].

While dated IRD pulses and ice-proximal sediments have provided reasonable constraints on retreat from the Barents-Kara shelf edge, such constraints are rare from the eastern sector. However, dated glacimarine deposits from the Taimyr Peninsula and Novaya Zemlya Trough indicate that deglaciation occurred significantly later from this margin. Further dates circa 14.7–15.5 cal ka B.P. from the southeast Barents Sea [*Polyak et al.*, 1995], as well as contemporaneous retreat of grounded ice from the deep, axial part of the Svyataya Anna Trough [*Polyak et al.*, 1997], indicate that large sectors of the Barents Sea (at least in the south) were becoming ice free by the Bølling interstadial [*Winsborrow et al.*, 2010]. Unfortunately, the configuration, timing and pace of retreat is still poorly constrained east of Storbanken, with retreat to ice domes over Novaya Zemlya and Franz Josef Land tentatively suggested by the alignment of the Admiralty Bank Moraines (Figure 11a).

Numerous sea level records indicate that deglaciation following the LGM was punctuated by a dramatic meltwater pulse (MWP-1A) between 14.1 and 13.6 cal ka B.P. that raised global sea level by approximately 20 m in less than 500 years [cf. *Deschamps et al.*, 2012]. A high-latitude signal of MWP-1a has been suggested to exist

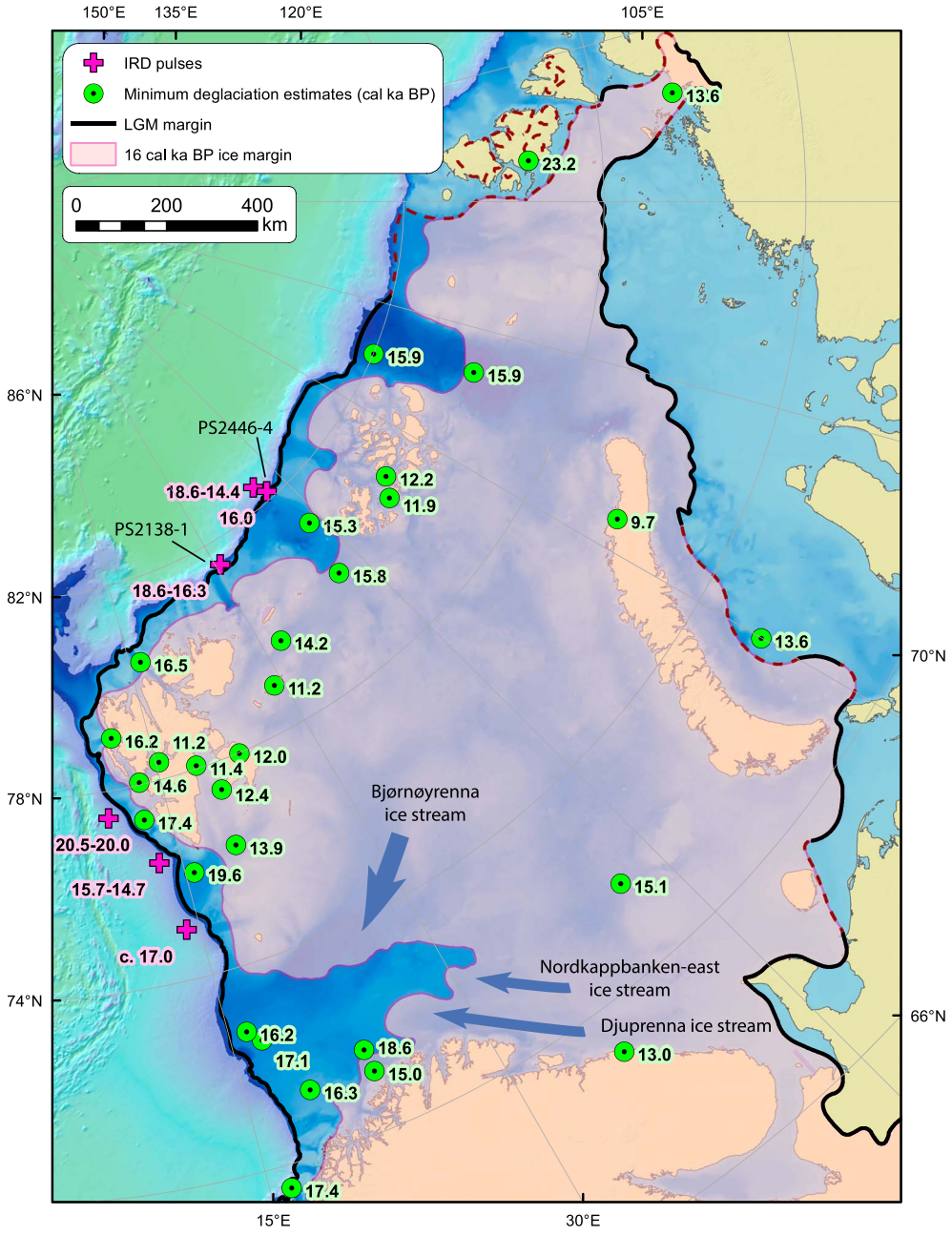

Figure 10. Selected minimum dates constraining retreat of the BSIS from the Last Glacial Maximum. Dates shown are median probability ages (cal ka B.P.) within ± 2σ. Core names and uncertainties ranges are listed in Table 1. The suggested ice sheet cover at ca. 16 cal ka B.P. is a coarse approximation based on an amalgamation of previously published interpretations [e.g., *Winsborrow et al.*, 2010; *Hormes et al.*, 2013].

in the in the near-synchronous deposition of interlaminated deposits along the western Barents Sea continental slope and outer shelf [cf. *Lucchi et al.*, 2013]. This regional stratigraphic event, indicating contemporaneous and further rapid retreat, can be found off West Svalbard and the Yermak Plateau [*Elverhøi et al.*, 1995; *Rasmussen et al.*, 2007; *Jessen et al.*, 2010], in Kveithola and Storfjorden troughs [*Rüther et al.*, 2012; *Lucchi et al.*, 2013] and in the southern Barents Sea [*Vorren et al.*, 1984]. According to the ICE-5G model of ice sheet deglaciation, the contribution of the Eurasian (and British-Irish) ice sheet to this event was in the region of 4.6 m of eustatic sea level rise [*Peltier*, 2004]. Implications of this breakup on the BSIS include major deglaciation of shelf edge troughs by the end of MWP-1A at 14.2 cal ka B.P., including the approximately 100 km long Kveithola trough [*Bjarnadóttir et al.*, 2013; *Rüther et al.*, 2013].

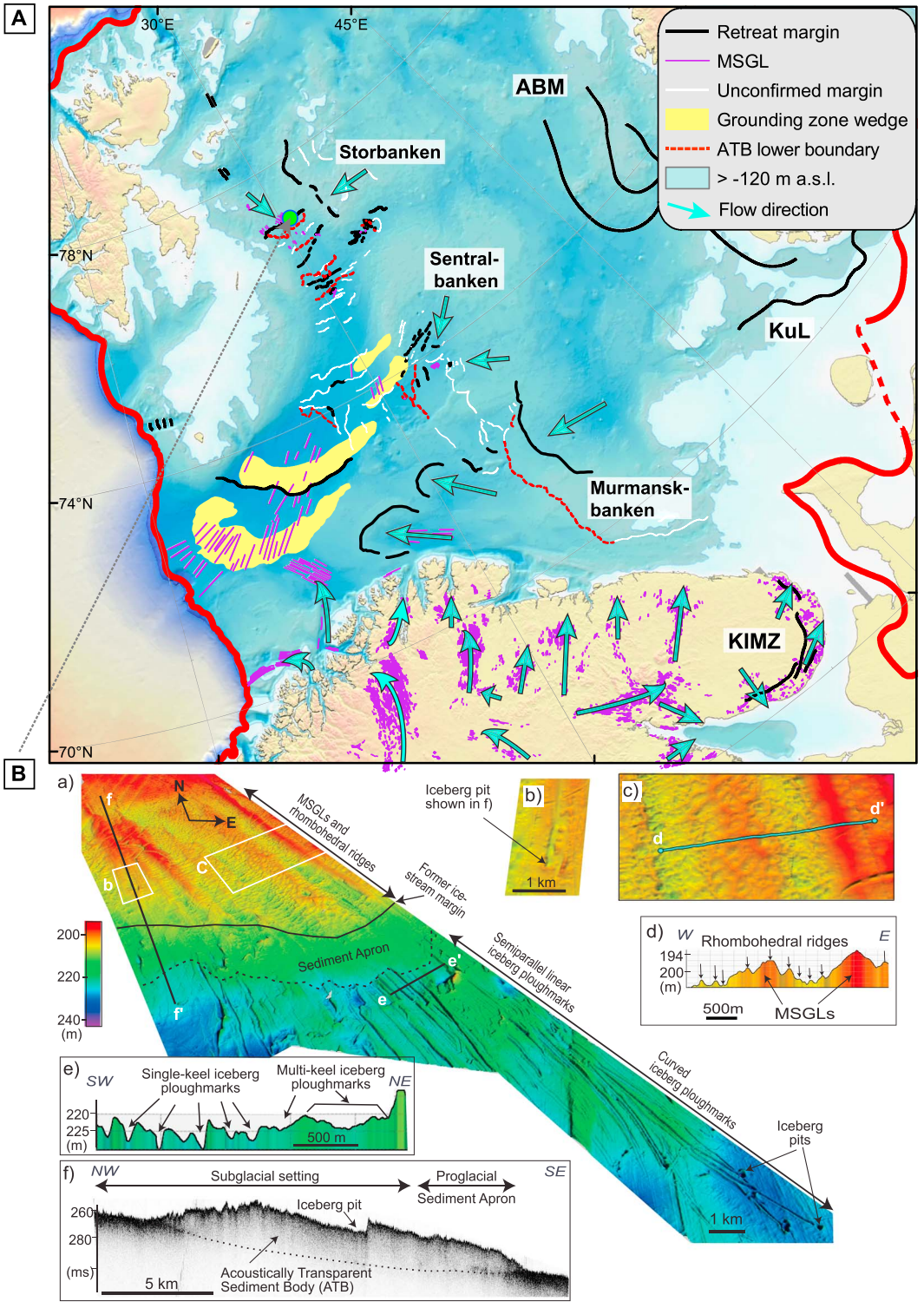

Figure 11. (a) Overview of ice margin positions and inferred flow directions through deglaciation of the western BSIS. Streamlined bedforms sourced from *Solheim et al.* [1990], *Hättestrand and Clark* [2006], *Winsborrow et al.* [2010], *Rüther et al.* [2013], *Andreassen et al.* [2014], and *Bjarnadóttir et al.* [2014]. Acoustically transparent sediment bodies (ATBs) have been previously interpreted to be grounding zone wedges [cf. *Bjarnadóttir et al.*, 2014]. Acronyms referred to in the text: ABM = Admiralty Bank Moraines, KIMZ = Keiva Ice Marginal Zone, KuL = Kurentsevo Line. (b) Multibeam echosounder bathymetry from northern Bjørnøyrenna. Landforms recognized include MSGL overprinted by crevasse squeeze ridges, multikeel iceberg ploughmarks, and iceberg pits. Modified from *Andreassen et al.* [2014].

The Younger Dryas terminated within less than a century at 11.5 cal ka B.P. north of Svalbard, marked by a sudden change in bottom water conditions and northward retreat of the Polar Front [*Ślubowska et al*., 2005]. Radiocarbon-dated flotsam found on raised beaches in Franz Josef Land and Kongsøya circa 12.2–11.3 cal ka B.P. indicate that the Barents Sea was largely ice free by the start of the Holocene (Figure 10). Withdrawal of ice from the major fjords of Svalbard was finally completed during the Early Holocene circa 11.2 cal ka B.P. [*Hormes et al*., 2013], including Isfjorden in central Spitsbergen [*Forwick and Vorren*, 2009]. Further transition toward the Holocene thermal maximum is reflected by the decreasing flux of IRD from 10.3 to 10.1 cal ka B.P. and contemporaneous deposition of diatom-rich sediments in cores west of Svalbard [*Jessen et al*., 2010; *Rasmussen et al*., 2014], reflecting a general northward and eastward retreat of the Polar Front [e.g., *Skirbekk et al*., 2010].

5. Flow Partitioning

The complex geomorphological footprint left by an ice sheet can provide excellent insights into temporal and spatial phases of former ice flow from the period of maximum glaciation through to deglaciation. A common method used to discern regions and trajectories of former ice streaming/fast flow is the grouping of elongated (megascale) glacial lineations (MSGLs) [cf. *Boulton and Clark*, 1990; *Clark*, 1993; *Stokes and Clark*, 2002]. In a more holistic sense, the glaciated landscape is represented by a palimpsest of changing ice dynamic and thermal regimes over many glacial cycles or phases of flow switching [e.g., *Kleman*, 1992].

A surge in the collection of high-resolution multibeam bathymetry and seismic data from the western Barents Sea during the previous decade has vastly improved our knowledge on the routing of ice flow and potential ice divides within the BSIS, as well as provided a more detailed understanding of the dynamics and interplay of the collapsing ice streams. The following section reviews these constraints and our current level of understanding of how flow regimes were partitioned within the Late Weichselian BSIS.

5.1. Svalbard

A major breakthrough in our understanding of the ice sheet flow regime over Svalbard came when *Landvik et al*. [2005] suggested that ice streams draining the major fjords and cross-shelf troughs of northwest Svalbard were interspersed with areas of dynamically less active ice on shallower intervening banks. Contemporaneous interpretations of geophysical data from the Barents Sea shelf identified numerous regions of former ice stream activity to further support this hypothesis [*Andreassen et al*., 2004; *Ottesen et al*., 2005]. Since then, MSGLs and marginal moraine systems have been extensively mapped from high-resolution bathymetric data around the archipelago, detailing a pattern of flow partitioning that is strongly influenced by the presence of deep troughs and fjords [*Ottesen et al*., 2007; *Ottesen and Dowdeswell*, 2009; *Dowdeswell et al*., 2010b; *Batchelor et al*., 2011]. All major troughs, including Kongsfjorden, Isfjorden, and Hinlopenstretet, show clear evidence for former ice streaming that would have extended deep into the ice sheet interior over Svalbard. However, direct geomorphological evidence from Storfjorden is still lacking, with limited detail on ice flow patterns between eastern Spitsbergen and the head of the more substantial Bjørnøyrenna Ice Stream. However, a sizeable trough mouth fan at the mouth of Storfjorden indicates this was probably a substantial route for ice sheet drainage [*Laberg and Vorren*, 1996a; *Rebesco et al*., 2014].

5.2. Northern Barents Sea

The pattern of Late Weichselian ice flow in the northern Barents Sea is not well known, mainly due to the lack of marine data collected from this region. Recent summers of seasonally low sea ice, however, have allowed for the acquisition of swath bathymetry data east of Svalbard, in Kvitøya Trough and around Kong Karls Land [*Dowdeswell et al*., 2010b]. Streamlined landforms found within Kvitøya Trough reveal ice flowed northward from an ice divide at the southern end of the trough, although modest elongation ratios suggest these were not formed by a major ice stream [*Hogan et al*., 2010b]. Further south, in Olga and Erik Eriksen straits, drumlins and hill-hole pairs confirm ice within these broad troughs flowed east-northeast toward the major ice stream occupying the Franz Victoria Trough from an ice dome occupying Hinlopenstretet [*Hogan et al*., 2010a]. However, this reconstruction differs from previous ones, which placed an ice dome further east over Kong Karls Land based on the identification of greatest uplift here from raised shorelines [e.g., *Forman et al*., 2004]. More recent cosmogenic-exposure dating from Nordaustlandet confirms this area was covered by local cold-based ice during MIS 2, which may well have been confluent with the proposed ice dome over southern Hinlopenstretet [*Hormes et al*., 2011].

Further east, a lack of detailed bathymetric data around Franz Josef Land and toward the Svyataya Anna and Voronin troughs presents a significant gap in our knowledge of ice sheet behavior along this margin. Limited side-scan sonar data from the Svyataya Anna Trough indicate the presence of De Geer moraines, flutes, and drumlin-like features eroded into bedrock or the till surface [*Polyak et al*., 1997]- indicative features of a marine-terminating ice stream. Furthermore, diamicton is recognized in sediment cores and on echo sounder records to at least 82°N and a water depth of 630 m, suggesting that grounded ice filled the entire trough to the shelf edge [*Polyak et al*., 1997].

5.3. Central Barents Sea

Since the resolution of a territorial boundary dispute between Russia and Norway in 2011 (Figure 1), new geophysical data from the former interior of the last BSIS has emerged, providing new insights into the configuration and dynamics of the BSIS during its retreat across this region. Through geomorphological mapping of multibeam swath bathymetry data and analyses of seismic and acoustic stratigraphy, ice flow indicators (e.g., MSGLs) show that during deglaciation the drainage basin for the Bjørnøyrenna ice stream included the topographic rises of Storbanken, Sentralbanken, and Kong Karls Land [*Andreassen et al*., 2014; *Bjarnadóttir et al*., 2014; Figure 6]. This configuration complements terrestrial observations of ice movement indicators [*Salvigsen et al*., 1995], as well as isostatic rebound modeling that suggests the maximum postglacial emergence (and thus greatest loading) occurred east of Kongsøya [*Forman et al*., 2004] (Figure 4). The orientation of MSGLs found south of Kongsøya and through Hinlopenstretet indicate a gradual shift of ice flow through the head of Bjørnøyrenna from a NE-SW direction to a NW-SE orientation [*Dowdeswell et al*., 2010b; *Andreassen et al*., 2014; *Bjarnadóttir et al*., 2014], suggestive of a reorganization of ice divides during deglaciation to a more dominant source area over northern Svalbard [*Bjarnadóttir et al*., 2014].

During the early phase of retreat across Sentralbanken and Murmanskbanken, ice flow was from the ENE, based largely on the orientation of inferred grounding line deposits (acoustically transparent sediment bodies–ATBs) (Figure 11a). As the ice sheet surface lowered during deglaciation, ice flow became increasingly topographically constrained over the shallower bank areas, with local ice divides over Sentralbanken and Sentraldjupet probably developing [*Bjarnadóttir et al*., 2014]. Further east, it has been speculated that the Admiralty Bank Moraines represent a readvance position during the Younger Dryas, reflecting ice dispersal from an ice cap localized over Novaya Zemlya [*Gataullin and Polyak*, 1997; *Gataullin et al*., 2001] (Figure 11a). However, absolute dating evidence has yet to confirm this hypothesis.

5.4. Southern Barents Sea

Separation and subsequent deglaciation of the Fennoscandian and Barents Sea ice sheets was characterized by large-scale reorganizations of ice flow, particularly with respect to both ice stream velocities and trajectories. These complex flow configurations, with ice streaming switching on and off over submillennial timescales, have been the subject of several studies utilizing high-resolution multibeam bathymetry and geomorphological mapping [*Andreassen et al*., 2008; *Andreassen and Winsborrow*, 2009; *Winsborrow et al*., 2012; *Bjarnadóttir et al*., 2013]. As an example, flow sets mapped at the local scale across the far southwest Barents Sea record the asynchronous and asymmetric readvance and retreat of Fennoscandian outlet ice streams on the outer shelf through Håkjerringdjupet and Ingøydjupet, despite catchment areas being topographically adjacent [*Winsborrow et al*., 2012; *Stokes et al*., 2014].

At the more regional scale, *Winsborrow et al*. [2010] used extensive marine and terrestrial data sets (Figure 11a) to provide a holistic overview of the flow dynamics of this region, including identifying major routes of ice stream discharge and readvance. Mapped flow sets were grouped into distinct timeslice reconstructions on the basis of relative ages assumed from ice flow overprinting, charting the changes in the location and extent of ice streams, areas of cold-based ice, and probable ice divide locations (Figure 12). During the LGM, the Bjørnøyrenna Ice Stream dominated drainage, fed by source areas throughout the western and central Barents Sea (Figure 12a) (the contribution of Fennoscandian ice exiting through the White Sea into this sector is, as yet, unknown). Following the early onset of deglaciation and retreat along the western Barents Sea shelf edge, outlet glaciers including the Bjørnøyrenna and Coast-parallel Trough ice streams experienced a phase of readvance, as evidenced by large grounding zone wedges (Figure 12b). At this point, a significant change in ice sheet dynamics occurred, with the center of maximum ice volume shifting eastward. The resulting ice divide migration brought about major readvances of the Djuprenna and Nordkappbanken-east Ice Streams, fed by

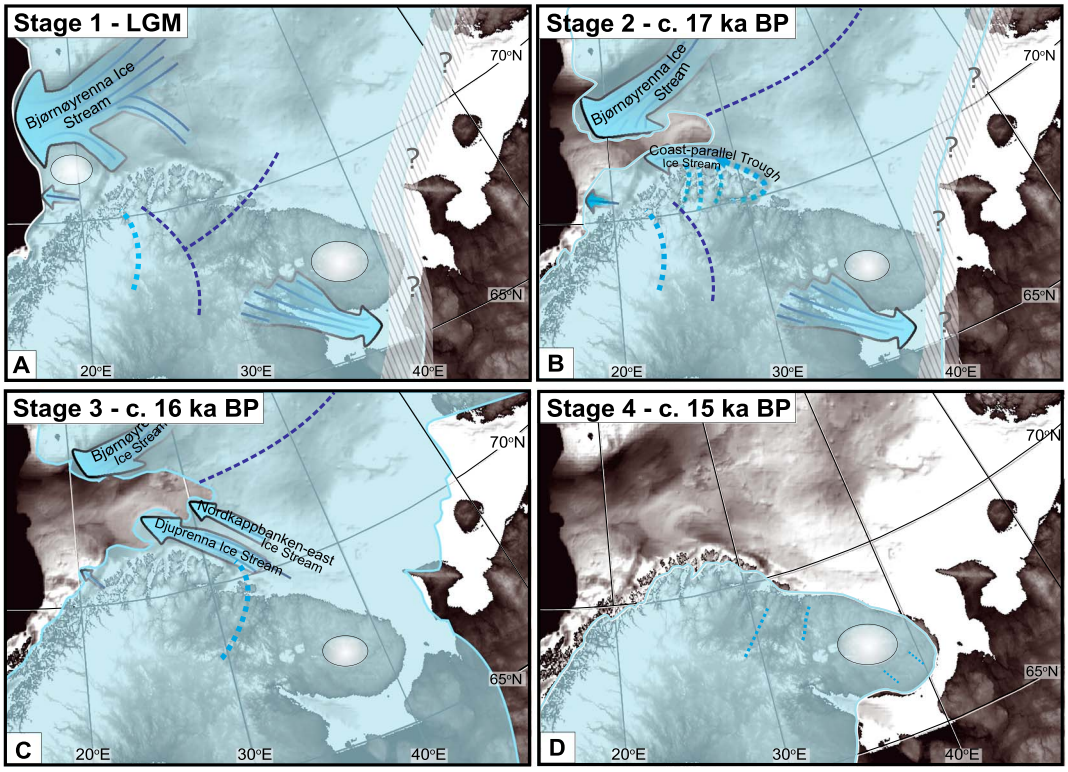

Figure 12. Reconstruction of the Late Weichselian maximum in the southern Barents Sea, and its subsequent deglaciation, based on onshore and offshore megascale geomorphic mapping (Figure 11a). Ice streams are shown as large blue arrows, warm-based ice as dashed blue arrows, cold-based ice as white discs, and possible ice divides as dashed dark blue lines. Modified from *Winsborrow et al.* [2010].

ice flowing north across the Kola Peninsula, meanwhile significant areas of the southwest Barents Sea remained ice free at this time (Figure 12c). From this stage, ice quickly retreated to its terrestrial source areas; in Fennoscandia, the ice margin within the outer fjord area in northern Norway corresponds approximately to the Outer Porsangen limit of *Sollid et al.* [1973] (Figure 12d).

The grouping of MSGLs into flow sets and their relative relationships described above are, however, associated with very time-specific phases of retreat. An alternative data set for validating modeled ice sheet output with over an entire glacial cycle is to examine the basal roughness of the subglacial bed, using, for example, a fast Fourier transform methodology [e.g., *Hubbard et al.*, 2000]. Subglacial abrasion is generally thought to reduce bedrock roughness parallel to the direction of ice flow. Therefore, by extracting minimum roughness values over broad spatial scales, the integrated effect of glacial erosion and deposition that represents bulk flow patterns over longer time periods can be reconstructed. An innovative study by *Gudlaugsson et al.* [2013] quantified, for the first time on a paleo–ice sheet bed, the subglacial roughness of southwestern Barents Sea. Their results showed similar roughness imprints to observations made from the Siple Coast region and Pine Island Glacier [*Bingham and Siegert*, 2009; *Rippin et al.*, 2011], indicating zones of former ice streaming, ice-marginal deposits, as well as an integrated flow direction signature (Figure 13). Although the data presented only highlight single roughness-minima directions, future work could build on this to include an analysis of multiple-roughness minima and extract potential cross-cutting flow patterns that dominate the geomorphological palimpsest.

6. Dynamics

Through the synthesis of vast quantities of geological data, the glacial reconstructions of *Svendsen et al.* [2004a] and the QUEEN (Quaternary Environment of the Eurasian North) community have provided a major benchmark for the interpretation of the timing and dimensions of late Quaternary glaciations affecting northern Eurasia. In short, the Svalbard-Barents Sea-Kara Sea ice sheet is depicted as an extensive and repeatedly

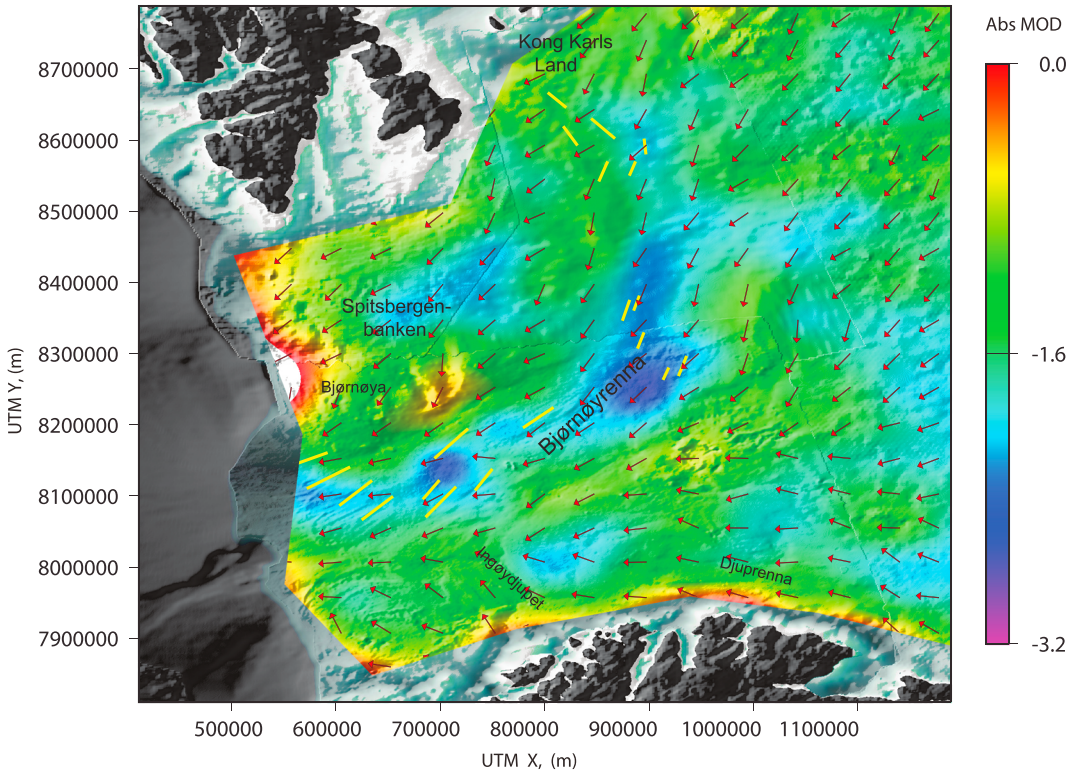

Figure 13. The spatial variation of the difference between the maximum and minimum basal roughness index, depending on orientation. The color range follows a logarithmic power scale. Arrows indicate the direction of the roughness minima compared with mapped MSGLs (yellow). Source: *Gudlaugsson et al.* [2013].

forming concentric dome, with buildup more extensive in the Kara Sea during the Early Weichselian but shifting toward the Barents Sea and Scandinavia during the Middle and Late Weichselian. Efforts to pinpoint internal and external drivers of dynamic glaciation, particularly across its marine sectors where technological advances have allowed for extensive collection of high-resolution geophysical data, have thus shifted emphasis within the scientific literature over the last decade toward more detailed and precise regional reconstructions [cf. *Ingólfsson and Landvik*, 2013]. Important dynamical insights for constraining transient reconstructions are presented in the following subsections.

6.1. Ice Stream Fluctuations and Stability

Extensive and high-resolution geophysical data collected from the Barents seafloor during the last decade [e.g., *Ottesen et al.*, 2005, 2007; *Andreassen et al.*, 2008; *Dowdeswell et al.*, 2010b; *Winsborrow et al.*, 2010; *Bjarnadóttir et al.*, 2014] has rapidly progressed insights into the behavior of the ice streams that forced the collapse and decay of this marine-based ice sheet. The largest and most extensively studied of these is the Bjørnøyrenna (Bear Island Trough) Ice Stream, with a catchment area in excess of 350,000 km^2 [*Winsborrow et al.*, 2010; *Batchelor and Dowdeswell*, 2014]. For comparison, this is larger than the combined basin area of ~325,000 km^2 for Pine Island and Thwaites glaciers, West Antarctica [*Rignot et al.*, 2002].

A series of grounding zone wedge deposits [*Batchelor and Dowdeswell*, 2015] and associated landforms in Bjørnøyrenna indicate that the retreat of this ice stream from the shelf break was punctuated by at least four cycles of streaming and stagnation [*Andreassen et al.*, 2008, 2014; *Winsborrow et al.*, 2010; *Bjarnadóttir et al.*, 2014], akin to the episodic retreat hypothesized in conceptual models for marine ice stream dynamics [*Dowdeswell et al.*, 2008; *Ó Cofaigh et al.*, 2008]. Furthermore, geomorphic features on buried surfaces found within seismic data indicate that the Bjørnøyrenna Ice Stream experienced similar oscillations between active and quiescent phases during pre-LGM glaciations [*Andreassen et al.*, 2004; *Andreassen and Winsborrow*, 2009]. Based on these and other landform assemblages described from Bjørnøyrenna (Figure 11b), a cyclical

landsystem model for retreat of the Bjørnøyrenna Ice Stream has been proposed [*Andreassen et al*., 2014; *Bjarnadóttir et al*., 2014], as follows:

1. Streamlined landforms (MSGLs) on the upper surface of the grounding zone wedge indicate the operation of a fast-flowing ice stream, providing a relatively high rate of sediment delivery to the ice margin [e.g., *Dowdeswell and Fugelli*, 2012].
2. Large, linear iceberg ploughmarks downstream of the former ice stream margin were formed during a period of fast flow and high calving rates, prior to termination of the ice stream advance and overprinting by a proglacial sediment apron. Their parallel nature indicate that these mega (multikeel) icebergs were transported within a densely pack matrix, with corrugation ridges formed by tidal action as the coherent mass drifted seaward [e.g., *Jakobsson et al*., 2011].
3. The superimposition and preservation of crevasse-squeeze (rhombohedral) ridges upon the MSGLs suggests that post–ice acceleration the ice stream floated completely free of its bed, forming an ice shelf at least temporarily [*Andreassen et al*., 2014; *Bjarnadóttir et al*., 2014].

This cyclic behavior, as documented by the deposition of multiple grounding zone wedges within Bjørnøyrenna, has been suggested to reflect multiple internal and external drivers. These include the availability of meltwater at the ice bed interface, the drainage capacity of the substrate, subglacial freezing, and the stabilizing forces acting on the ice (e.g., ice shelf buttressing) [*Andreassen and Winsborrow*, 2009; *Bjarnadóttir et al*., 2014]. Analogous and complex patterns of ice stream retreat have also been described from the nearby Kveithola Trough, with the formation of grounding zone systems characterized by high meltwater discharges [*Rebesco et al*., 2011; *Rüther et al*., 2012; *Bjarnadóttir et al*., 2013]. Further afield, in West Antarctica, similarly sized grounding zone wedges have been reported near stable grounding line positions of marine-based ice streams in Pine Island Trough [*Graham et al*., 2010; *Jakobsson et al*., 2012a; *Batchelor and Dowdeswell*, 2015] and beneath the Whillans Ice Stream [*Anandakrishnan et al*., 2007]. Cyclical "surge-like" activity during ice stream retreat has also been proposed for a number of contemporary Antarctic ice streams [*Bindschadler*, 1997; *De Angelis and Skvarca*, 2003; *Hughes*, 2011; *Engelhardt and Kamb*, 2013], as well as for paleo–ice streams [*Evans and Rea*, 1999; *Hubbard et al*., 2009]. In particular, relatively recent termination of fast flow of the Kamb Ice Stream has been associated with basal freeze-on [*Engelhardt*, 2004], with similar thermomechanical switching related to rapid climate fluctuations inferred from numerical modeling of the British-Irish Ice Sheet [*Hubbard et al*., 2009].

Chronological control on the deglaciation of the Bjørnøyrenna Ice Stream is limited, although retreat is assumed to have taken a maximum of 2000 years [*Winsborrow et al*., 2010]. Based on the succession of grounding zone wedges in Bjørnøyrenna, minimum rates of retreat have been estimated at approximately 0.275 km a^{-1} [*Winsborrow et al*., 2010], in line with observed rates of margin retreat of between 0.31 and 0.8 km a^{-1} along outlet glaciers in the Amundsen Sea sector, West Antarctica [*Shepherd et al*., 2002]. In Storfjordrenna, to the north of Bjørnøyrenna, two minimum dates for deglaciation indicate that the approximately 200 km long retreat of the grounding line from the shelf break occurred in approximately 7900 years [*Rasmussen et al*., 2007; *Rasmussen and Thomsen*, 2014] (Figure 10). The slower rate of retreat (approximately 0.025 km a^{-1}) here probably reflects the closer proximity of terrestrial ice centers to the trough mouth as well as a generally shallower bathymetry.

As evidenced by a shift in the orientation of MSGLs at the head of the Bjørnøyrenna Ice Stream (cf. section 5), the size and shape of its drainage basin changed significantly during deglaciation, with its main source area moving from Storbanken to northeast Svalbard [*Andreassen et al*., 2014]. A much reduced, and possibly isolated, ice dome may have persisted over Storbanken and Sentralbanken, as indicated by the distribution of recessional ridges [*Bjarnadóttir et al*., 2014] (Figure 11a). Further routes of ice stream drainage of the ice sheet during the LGM have been identified from geomorphological and sedimentological signatures found within cross-shelf troughs [e.g., *Ottesen et al*., 2005]. Notable examples include Franz Victoria Trough [*Lubinski et al*., 1996; *Kleiber et al*., 2000], Svyataya Anna Trough [*Polyak et al*., 1997], Kongsfjorden [*Landvik et al*., 2005], Isfjorden [*Forwick and Vorren*, 2009], Storfjorden [*Laberg and Vorren*, 1996a; *Lucchi et al*., 2013], and Kveithola [*Rebesco et al*., 2011; *Bjarnadóttir et al*., 2013] (Figure 6). Geomorphic mapping from within these troughs suggest a complex/episodic retreat history, with variations in the number and spacing of grounding zone wedges [*Batchelor and Dowdeswell*, 2015] indicating that different ice streams behaved independently during deglaciation from the shelf. Further, the excellent preservation of megascale lineations suggests ice streams retreated rapidly with mass loss dominated by calving [*Ottesen et al*., 2007].

Patterns of ice flow in the northern Barents Sea are still largely unknown due to a lack of detailed bathymetry data collection. Recent surveying east of Svalbard has indicated, however, significant differences from previous reconstructions. In particular, it has been proposed that ice flowed *east* from Nordaustlandet along the Erik Eriksen and Olga straits toward the Franz Victoria Trough [*Dowdeswell et al*., 2010b; *Hogan et al*., 2010a]. The newly realized catchment size of this ice stream places increased significance on the Franz Victoria Trough as an important drainage pathway for the northern sector of the ice sheet, with full-glacial balance flux now estimated to be $>40\,km^3\,a^{-1}$. More detailed surveying of the seabed east of Storbanken and the accurate positioning of ice divides between Novaya Zemlya and the Svyataya Anna Ice Stream will likely see this value rise substantially.

Given the relatively large scale and depth of the Svyataya Anna Trough, its influence on ice sheet stability in the eastern sector would have been considerable. For example, the current depth of the trough approximately 650 m at the shelf break suggests it must have hosted a significant flux of ice to remain grounded throughout its length [*Polyak et al*., 1997]. Numerical modeling has shown that the Svyataya Anna Trough ice stream had an ice flux equal to about half that in Bjørnøyrenna at 15 ka, placing it as the second largest within the BSIS during the Late Weichselian [*Dowdeswell and Siegert*, 1999]. During more eastern-dominated glaciations of the Early-Middle Weichselian, its significance would undoubtedly have been even greater. It has thus been cited as a possible source for the "megabergs" that produced ploughmarks at >850 m below present sea level on the Yermak Plateau [*Vogt et al*., 1994].

6.2. Flow Switching

The overprinting of numerous flow sets provides a clear indication that some ice stream activity was asynchronous through deglaciation of the BSIS, probably influenced by migrating ice divides and catchment areas through time. Complex patterns of ice stream flow switching—as evidenced by abrupt changes in velocity [e.g., *Nygård et al*., 2007] and/or flow direction [e.g., *Dowdeswell et al*., 2006; *Ó Cofaigh et al*., 2010]—have been identified at the confluence zone between the Barents Sea and Fennoscandian ice sheets [*Andreassen et al*., 2007b; *Winsborrow et al*., 2010, 2012]. Following retreat of the Bjørnøyrenna Ice Stream, a shift in both ice volume and dynamic behavior to the eastern sector of the Barents Sea and Fennoscandian ice sheets occurred (Figure 12).

Based on observations of similar patterns of flow switching, *Winsborrow et al*. [2012] identified five possible hypotheses for this behavior: infilling of accommodation space, thus changing regional bathymetry [*Dowdeswell et al*., 2006], variations in ice stream grounding line bathymetry [*Stokes et al*., 2009, 2014], variations in the basal thermal regime [*Ó Cofaigh et al*., 2010], variations in the routing of subglacial meltwater [*Conway et al*., 2002; *Vaughan et al*., 2008], and competition for ice discharge [*Payne and Dongelmans*, 1997; *Greenwood and Clark*, 2009]. Of these, variation in grounding line bathymetry is identified as the most influential factor on ice stream behavior in this region and at the millennial timescale of deglaciation. Eustatic sea level effects probably drove initial margin retreat from the shelf edge [*Lambeck*, 1995; *Winsborrow et al*., 2010], and thus, landscape controls would have played an important role in determining the punctuated retreat of the grounding line [cf. *Jamieson et al*., 2014]. Similar dynamics are reflected in the retreat of marine-terminating glaciers from the Finnmark coast, where the complex interplay between topographic (e.g., width and depth) and glaciological factors (e.g., catchment size) evolving through time forced phases of asynchronous and rapid retreat regardless of any external climate forcing [*Stokes et al*., 2014]. Collecting accurate bathymetry of bed topographies (and potential sediment thickness through seismic data), alongside models of isostatic rebound through time, is thus seen as essential for reconstructing the timing and pace of retreating ice streams that once occupied the numerous troughs that dissect the Barents and Kara seas.

6.3. Dynamic Thinning

Pre-LGM exposure age dates from high-elevation erratics on northwest Svalbard appear to indicate an early onset of ice sheet thinning prior to marginal retreat from the shelf edge [*Gjermundsen et al*., 2013]. Boulders on Langskipet (24.8 ± 1.6 ka), Kaffitopen (21.7 ± 1.4), and Aurivilliusfjellet (20.1 ± 1.6) collectively predate the suggested ice margin retreat from the outer shelf circa 20.5 cal ka B.P. west of Svalbard [*Jessen et al*., 2010] and disintegration circa 18.6 cal ka B.P. farther northeast [*Knies et al*., 2001] (Figure 10). Although gradual warming of the northern middle-to-high latitudes initiated between 21.5 and 19 cal ka B.P. (followed by a

somewhat steeper increase until 17.5 cal ka B.P.) [*Shakun et al*., 2012], it does not fully explain why the ice sheet would have thinned before significantly retreating.

Recent observations of extensive dynamic thinning on the margins of the Greenland and Antarctic ice sheets [*Wingham et al*., 1998; *Shepherd et al*., 2002; *Thomas et al*., 2003; *Rignot*, 2008; *Pritchard et al*., 2009; *Flament and Rémy*, 2012], and associated speedups of ice flow that extend far inland [*Rignot et al*., 2011], point toward internal changes in ice flow such as the removal of ice shelf buttressing through oceanic warming [*Scambos et al*., 2004; *Shepherd et al*., 2004; *Dupont and Alley*, 2005]. Possible factors to explain the relatively early thinning on Svalbard post-LGM thus include a shift toward a more arid climatic regime [*Pausata et al*., 2011; *Hormes et al*., 2013] (accumulation variability over a wide range of timescales has been shown to have a large influence on ice sheet elevation changes [*Helsen et al*., 2008]), ice piracy associated with migrating ice divides, or changes in basal thermal and/or hydrological conditions [e.g., *Pattyn et al*., 2006].

7. Climatic and Ocean Forcings

7.1. Spatial Shifts in Ice Sheet Development

The availability of geological data from the Russian sector of the Barents Sea, associated with work carried out by QUEEN project members [cf. *Svendsen et al*., 2004a], helped reveal a discordant pattern of ice sheet development during the Weichselian between ice covering the eastern Eurasian Arctic and over Fennoscandia. In essence, the Barents-Kara Ice Sheets became progressively smaller during each successive glaciation, whereas the dimensions of the Scandinavian Ice Sheets increased through time (Figures 2 and 3).

This east-west migration can be best explained by variations in feedbacks associated with climatic and oceanographic forcings during the initiation phases of each glaciation. For example, atmospheric general circulation modeling (AGCM) by *Marsiat and Valdes* [2001] has revealed potential far-field controls on the styles of glaciation possible in the Eurasian Arctic, related to sea surface temperature (SST) gradients between the North Atlantic and North Pacific and its effect on atmospheric circulation patterns. Under very warm North Pacific SSTs and cold North Atlantic SSTs, warm and moist air is transported from the midlatitude Atlantic Ocean across the European continent. The moist air is, in turn, deflected northward by a very stable anticyclonic cell centered over eastern Europe. Such conditions are considered necessary to build a "maximum" style ice sheet [*Siegert and Marsiat*, 2001]. By contrast, under warm North Atlantic SSTs and cold North Pacific SSTs, warm air is instead split into two branches. The majority is directed toward the northern part of the oceanic basin, while a much weaker flux of heat enters Central Europe. No deflection occurs, with the Kara Sea region instead dominated by a stable anticyclonic flow of air that acts to isolate the region climatically. Cold dry winds coming off the Fennoscandian Ice Sheet would further exacerbate a situation of long-term cold, dry air in this region [*Marsiat and Valdes*, 2001]. This predicted effect on the distribution of precipitation (and consequently the distribution of ice sheet mass balance) during the LGM is further supported by reconstructions through ice sheet modeling [e.g., *Siegert and Marsiat*, 2001; *Siegert and Dowdeswell*, 2004] and independent geological evidence [*Tarasov et al*., 1999; *Hubberten et al*., 2004; *Mangerud et al*., 2008a].

7.2. Late Weichselian Ice Sheet Initiation

Geological records infer that the continental shelves in the Eurasian Arctic were free of ice at the end of the Middle Weichselian [*Mangerud et al*., 1998; *Kleiber et al*., 2000; *Knies et al*., 2001; *Stein et al*., 2001] (section 2), indicating that ice sheet growth at the onset of the Late Weichselian was rapid. Ice sheet and climate modeling have further implied that growth was driven by a maritime type of climate that produced relatively high precipitation rates along the western flanks [e.g., *Hubberten et al*., 2004]. Relatively warm waters advected into the Norwegian Sea as far north as Spitsbergen between 27 and 22.5 cal ka B.P., resulting in seasonally ice-free waters [*Müller and Stein*, 2014], therefore providing a crucial regional moisture source during initial buildup of ice [*Hebbeln et al*., 1994; *Knies et al*., 1999]. However, the mechanisms that describe the onset of glaciation in the Barents Sea have so far remained equivocal.

The growth of marine ice sheets such as the BSIS represents a significant glaciological problem, for which varying theories have been proposed. An early hypothesis suggested that, in combination with sea level lowering, sea ice gradually thickened to considerable depths, eventually becoming grounded and forming initial loci for further ice buildup [*Denton and Hughes*, 1981; *Hughes*, 1987]. A less contentious proposal by *Kvasov* [1978] and *Elverhøi et al*. [1993], supported by modeling work by *Howell et al*. [2000], suggested that ice

growth occurred in response to falling sea level and the concurrent expansion of ice caps located on subaerially exposed islands and banks surrounding the Barents Sea. These ice caps continued to grow until they joined to form a continuous ice sheet. *Möller et al*. [2006] and *Ingólfsson et al*. [2008] argued for a similar model of buildup for the Kara Sea ice sheet, with islands and highlands in the periphery of the Kara Sea critical as nucleation areas for ice caps that later merged on the shallow shelf areas. Numerical work by *Peyaud et al*. [2007] proposed a modified model for ice sheet inception, suggesting fringing ice shelves converged and eventually thickened across marine sectors in response to widespread buttressing against localized zones of grounding.

Beyond the primary oceanic and atmospheric drivers of mass balance distribution, the influence of terrestrial water bodies on Eurasian ice sheet growth has also been described using AGCMs. During the Early and Middle Weichselian, ice centered over the Barents and Kara seas was large enough to block a number of northbound Russian rivers, forming large ice-dammed lakes with a combined area twice that of the Caspian Sea [cf. *Mangerud et al*., 2001a, 2004] (Figure 2). Based on their large heat capacity, *Krinner et al*. [2004] proposed that the lakes forced a strong summer cooling effect, resulting in reduced summer ablation along the southern margins of the ice sheet. Numerical ice sheet modeling suggests that the effect may have accounted for up to 50% of the maximum ice volume during the Early Weichselian [*Peyaud et al*., 2007]. Similar mesoscale atmospheric feedbacks have also been suggested for Lake Agassiz and the Laurentide Ice Sheet [*Hostetler et al*., 2000].

7.3. Late Weichselian Deglaciation

The global sea level lowstand from 26.5 to 19 ka [*Peltier and Fairbanks*, 2006] coincides well with the duration of maximum extent of most global ice sheets [*Clark et al*., 2009]. Widespread deglaciation within the Northern Hemisphere followed circa 21–19 cal ka B.P., marked by an abrupt 10–15 m rise in sea level [*Clark et al*., 2004] which was probably triggered by increases in summer insolation [*Clark et al*., 2009]. However, mass loss for marine-based ice sheets is primarily conducted via calving margins, and, as such, rising sea levels have been historically cited as the trigger for deglaciation of the BSIS [e.g., *Forman et al*., 1995; *Lambeck*, 1995; *Landvik et al*., 1998]. In contrast, *Jones and Keigwin* [1988] proposed a self-destructive view where deglaciation was not initiated by external factors, but instead a consequence of isostatic depression of the ice sheet bed triggering marine drawdown through the major cross-shelf troughs. As with the marine-based sections of the Late Weichselian British-Irish Ice Sheet [*Bradwell et al*., 2008] and the Atlantic and Arctic margins of the Laurentide Ice Sheet [*Shaw et al*., 2006; *Stokes et al*., 2009], deglaciation was dominated by large ice streams that showed considerable variation in their flow. In all cases, rising sea level is identified as the initial trigger for deglaciation, followed by stepwise but rapid retreat and large calving fluxes.

The complex interplay between eustatic sea level rise and isostatic uplift through space and time presents a significant challenge to isolate precise drivers of glacial retreat. Postglacial emergence curves derived from islands around the margins of the Barents Sea indicate very rapid glacio-isostatic uplift, with half of the emergence occurring within 2000 years of the onset of deglaciation [*Landvik et al*., 1998]. Within the ice sheet interior, it could thus be expected that isostatic rebound periodically exceeded eustatic sea level rise and has been suggested as a possible mechanism for intermittent grounding of the retreating ice margin [*Winsborrow et al*., 2010]. Reconstructions of paleobathymetry during deglaciation are needed to test this hypothesis.

Eustatic sea level effects alone, however, present an incomplete picture. Paleo-oceanographic studies confirm the dynamic interplay between ice sheet stability and oceanographic conditions in this region of the Polar North Atlantic [e.g., *Martrat et al*., 2003; *Rasmussen et al*., 2007; *Jessen et al*., 2010; *Lucchi et al*., 2013]. In particular, the reconstruction of recurrent phases of sea ice advance and retreat in the Fram Strait since the LGM reveals the significant role of discontinuous (or pulse-like) flow of heat along the eastern Nordic Seas on the region. For example, rapid sea surface warming preceded the collapse of perennial sea ice in the Fram Strait after the LGM, coincident with the onset of Heinrich Event 1 at 17.5 cal ka B.P. [*Müller and Stein*, 2014]. This breakup accompanied (or amplified) the subsequent breakdown of the Atlantic meridional overturning circulation (AMOC) and widespread destabilization of tidewater glacier fronts across European sectors [e.g., *Grousset et al*., 2001].

Through albedo feedbacks and moisture insulation effects, the growth or melting of sea ice can also rapidly switch the regional climate system between phases of positive and negative glacier mass balance

[e.g., *Gildor and Tziperman*, 2000; *Bintanja and Selten*, 2014], while simultaneously dictating rates of mass loss and margin retreat at marine-terminating margins [e.g., *Reeh et al*., 2001; *Andreassen et al*., 2014]. It has been suggested that the input of freshwater into the Arctic Ocean through the Fram Strait from Lake Agassiz [*Murton et al*., 2010] may have instigated the increased sea ice formation in the Arctic at the beginning of the Younger Dryas [*Fahl and Stein*, 2012]. The subsequent capping of the ocean as a moisture source in this region could thus explain the limited regrowth of glaciers observed on Svalbard [e.g., *Mangerud and Landvik*, 2007], but also for the repeated weakening of the AMOC between 12.8 and 11.8 cal ka B.P. [*Müller and Stein*, 2014]. Meltwater freshening during MWP-1A induced a similar, although smaller, reexpansion of sea ice until 14.5 cal ka B.P. [*Müller and Stein*, 2014].

Conversely, it has been suggested that warming surface water temperatures in the North Atlantic prior to Heinrich events HE3 and HE2 (circa 31.7 cal ka B.P. and 26.3–23.8 cal ka B.P., respectively) caused rapid destabilization of marine ice shelves around the Nordic seas [*Rasmussen and Thomsen*, 2008]. Similar effects of enhanced ocean-driven melting have also been observed in present-day Antarctica [*Shepherd et al*., 2004; *Pritchard et al*., 2012] and Greenland [*Holland et al*., 2008; *Christoffersen et al*., 2011; *Kjær et al*., 2012] and are now recognized as a primary driver for mass loss from marine-terminating glaciers [e.g., *Bartholomaus et al*., 2013; *Chauché et al*., 2014].

7.4. A Younger Dryas Readvance?

Prominent moraines constraining the limits of the Younger Dryas ice sheet have not been found on Svalbard, most likely because ice in this region did not readvance. Relatively low IRD concentrations on the Yermak Plateau [*Birgel and Hass*, 2004; *Chauhan et al*., 2014], and at the western [*Ślubowska-Woldengen et al*., 2007] and northern [*Koç et al*., 2002] Svalbard shelf indicate that ice rafting was reduced at this time even though waters were seasonally open. Furthermore, reports that glaciers west of the main ice sheet on Spitsbergen were smaller during the Younger Dryas than the Little Ice Age (circa A.D. 1900) appear to corroborate overall minimal glacier advance during this cold interval [*Mangerud and Svendsen*, 1990; *Mangerud and Landvik*, 2007; *Reusche et al*., 2014]. This finding is at odds with widespread observations of significant glacier growth around much of Scandinavia and western Europe [*Golledge et al*., 2008; *Ivy-Ochs et al*., 2009; *Nesje*, 2009].

The limited empirical evidence available appears to suggest that the subdued Younger Dryas ice growth was climatically controlled. A nondepositional event corresponding to the Younger Dryas in the southeast Barents Sea may indicate a halt in deglaciation and/or a spread of perennial sea ice [*Polyak et al*., 1995]. East of Svalbard the Younger Dryas cold interval was also characterized by a switch to near-perennial sea ice, implying climate gradients in this region had shifted strongly [*Kristensen et al*., 2013; *Müller and Stein*, 2014]. The sea ice insulation of a large moisture source here under prevailing easterly winds [*Renssen et al*., 2001; *Birgel and Hass*, 2004] would thus have created a significant rain shadow over Svalbard [*Mangerud and Landvik*, 2007]. Modeled data indicate that present Svalbard glaciers are particularly sensitive to increases in precipitation associated with sea ice decline [*Day et al*., 2012]. The starvation of precipitation was likely exacerbated by relatively high summer insolation, with values at this latitude about 10% higher than today [*Berger and Loutre*, 1991].

8. Numerical Modeling

8.1. Previous Modeling Synopsis

The first systematic efforts to model numerically the Eurasian ice sheet (including the Eurasian Arctic) were undertaken as part of the international QUEEN collaboration [cf. *Siegert and Dowdeswell*, 2004], building effectively upon the vast acquisition of geological data from Russian sectors at the time. The modeling approach adopted by Siegert and coworkers was an inverse one, with climatic inputs varied to yield a simulated ice sheet growth consistent with predicted Eurasian ice extents [cf. *Svendsen et al*., 2004a]. Although a relatively basic model was used, centered around the continuity equation for ice [*Mahaffy*, 1976], results indicated that at its maximum extent the ice sheet occupied the entire Barents Sea and much of the Kara Sea (Figure 14a). Climate forcings required by the model supported earlier suggestions that precipitation and temperature patterns were dictated by strong eastward and northward gradients. Specifically, rates of ice accumulation in excess of 300 mm a^{-1} and a MAAT (mean annual air temperature) of approximately −12°C were calculated in northwest Norway, while on Severnaya Zemlya accumulation rates were effectively zero with MAATs well below −20°C [*Siegert et al*., 1999]. Further comparison of the predicted LGM paleoclimate with results from an

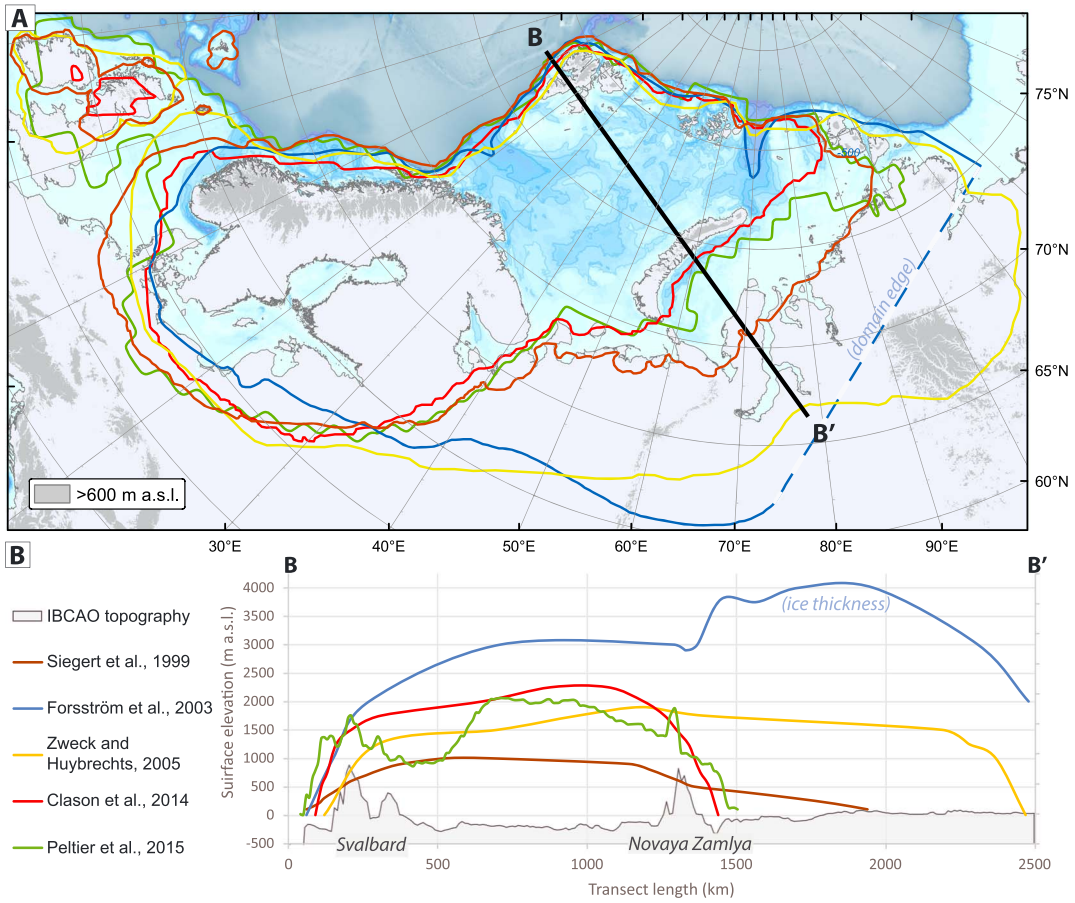

Figure 14. Evolution of numerical reconstructions of the Eurasian ice sheet (circa 20 ka B.P.): (a) Lateral extents and (b) variations in modeled surface elevation (except for *Forsström et al.* [2003] indicating ice thickness) across the central Barents Sea. Present-day topography used is from IBCAO v.3 [*Jakobsson et al.*, 2012b].

atmospheric general circulation model revealed similar findings [*Siegert and Marsiat*, 2001]. In this case, a warm, maritime climate across the west of Scandinavia was suggested to be caused by the local availability of a moisture source, while extreme polar desert conditions to the east across the Taimyr Peninsula were shown to be related to the weakening of the anticyclonic cell system over eastern Europe [*Marsiat and Valdes*, 2001].

Deglaciation of this modeled ice sheet occurred primarily as a response to sea level rise and increased mean annual temperatures [*Siegert and Dowdeswell*, 2002]. Marine sectors decayed first, with increased water depths at the ice margin amplifying calving rates. Meanwhile rising surface temperatures caused the elevation of the ELA to rise along the southern margins of the ice sheet, with strong north-south temperature gradients from mainland Russia to the Arctic implied [*Siegert and Marsiat*, 2001].

Since the conclusion of modeling efforts within the QUEEN collaboration over a decade ago, new attempts at simulating Barents Sea glaciation have been few and far between [e.g., *Zwech and Huybrechts*, 2005; *Clason et al.*, 2014], with studies largely reconfirming dynamical and climatological insights from the late 1990s. The relatively limited focus given by numerical modelers to the region reflects two broad challenges: (1) the ability (and computational efficiency) of common SIA-based ice sheet models (i.e., simple, zero order models that follow the Shallow Ice Approximation, whereby normal stress deviators and shear stresses in vertical planes are neglected) to reconstruct feedbacks associated with marine ice sheet deglaciation and ice streaming across such a large domain and (2) rationalizing the poor coverage and sometimes conflicting nature of temporal and physical constraints, as well as the highly heterogeneous climatic and oceanographic boundary conditions.

However, notable modeling insights include those from the SICOPOLIS (SImulation COde for POLythermal Ice Sheets) ice sheet model [cf. *Greve*, 1997] – a more sophisticated model than that previously used by *Dowdeswell and Siegert* [1999], incorporating thermomechanical coupling, isostatic effects and a time-evolving

climatology. *Forsström et al*. [2003] and *Forsström and Greve* [2004] found freshwater fluxes from melting and calving events were in phase with Heinrich events H3-H1, corresponding with a northward shift of fast ice flow activity from the LGM through to the Holocene. Furthermore, *Peyaud et al*. [2007] using the GRISLI (Grenoble Ice Shelf and Land Ice) ice sheet model found the summer cooling effect from large ice-dammed lakes bordering the Eurasian southern margins [cf. *Krinner et al*., 2004] appears to exert significant influence on ice sheet inception (section 7.2).

8.2. Model-Data Integration

The empirical data presented in this review provides an up-to-date and holistic benchmark for marine-based glaciation of the Barents Sea continental shelf. However, a key perspective on the reconstruction of paleo–ice sheets that is often overlooked is the importance of data-model integration, i.e., how modelers and those collecting empirical data can collaborate better together to help improve the accuracy of reconstructions.

The detailed nature of the empirical data sets presented as well as the increasing sophistication of ice sheet models have developed to a stage now where detailed and direct comparison between the two disciplines should be encouraged. That is, to go beyond the cursory model validation of "margin-matching" and to use more quantitative-based tools that can measure the adherence, or uncertainty, of model output to empirical data. At the simplest level, automated Geographic Information System (GIS) tools already exist that can assess and score the level of correspondence between modeled ice extent and ice-marginal features such as end moraines, as well as between modeled basal flow directions and paleo–flow direction indicators such as glacial lineations [*Napieralski et al*., 2007; *Li et al*., 2008].

More sophisticated and integrative methods include treating the determination of past ice sheet evolution as a Bayesian statistical inference problem. For example, through the incorporation of large data sets of relative sea level and ice margin chronologies, *Tarasov et al*. [2012] used a Bayesian framework for model calibration to statistically emulate model response to parameter variation, thus providing posterior probability distributions for modeled glacial histories of the North American ice complex—essentially establishing an ice sheet reconstruction with objective confidence intervals. More recent work on the Antarctic ice sheet has followed this ensemble method for deriving quantitative uncertainty estimates, using model-to-observation misfit scores from constraints such as former ice sheet elevations, extents, and relative sea level indicators [*Briggs and Tarasov*, 2013; *Briggs et al*., 2014]. However, a key challenge in this respect is the ability to quantify effectively the structural uncertainties within numerical models, such as grid dependencies that underestimate dynamic effects [e.g., *Hulton and Mineter*, 2000; *Golledge et al*., 2012]. While several approaches exist to resolve this issue [cf. *Stokes et al*., 2015], increasing model complexity and degrees of freedom offers the most obvious route. Though given the nonlinearity and computational inefficiency of such higher-order models, the challenge of finding accurate model configurations over paleotimescales become considerable.

Alongside model improvements for data integration and analysis, a number of key considerations can help guide empirical workers to present their data in a form suitable for model evaluation, thus ensuring maximum constraint value can be extracted [*Briggs and Tarasov*, 2013; *Stokes et al*., 2015]: (i) explicitly outlining assumptions of data interpretation and the quantification of uncertainties associated with raw observations and introduced postcollection; (ii) the emphasis of data quality versus quantity, few data points with tight error bars are generally more valuable than abundant, low-quality data; (iii) the provision of raw data for recalibration; and (iv) accessibility via a centralized online database.

A recent example database specifically compiled for model-data integration is DATED-1, a chronological database spanning the last glacial cycle of the Eurasian ice sheet complex, alongside interpreted timeslice maps every 1 ka that depict margin evolution [*Gyllencreutz et al*., 2007; *Hughes et al*., 2015]. As part of their interpretations, each timeslice reconstruction includes maximum, minimum and "probable" ice sheet bounds that represent all lines of geological uncertainty. Such limits give modelers a practical empirical envelope from which simulated reconstructions can be compared or validated.

8.3. Future Modeling

Since the last focused attempts to numerically model the dynamic evolution of the BSIS [*Forsström and Greve*, 2004; *Siegert and Dowdeswell*, 2004], considerable empirical advances have been made in our understanding of why, when and how the last BSIS grew and retreated from the shelf edge. Circumstances are thus ripe for a fresh examination from ice sheet modelers, integrating recent empirical insights into the next generation of

marine ice sheet models. As evidenced by previous attempts, accurately modeling the dynamic evolution of the BSIS is a challenging task, hampered by several particular difficulties:

1. The Late Weichselian BSIS was large, with an areal extent equivalent to approximately 2.4×10^6 km^2 (~20% larger than West Antarctica) and covering 14° of latitude and 90° of longitude. If the entire Eurasian ice sheet complex is taken into account, the required domain roughly doubles in size. Aside from the problems in incorporating the numerous Earth system feedbacks present over such an extensive domain, transient modeling at a grid resolution that sufficiently captures realistic ice flow and mass balance requires significant computational resources.
2. Marine-based ice sheets are inherently complicated ice masses to reconstruct accurately and are host to a number of numerical challenges that require dynamic coupling, including ice streaming, grounding line dynamics, ice shelf flow, and iceberg calving. The continued development of ice sheet models during the last decade [*Blatter et al*., 2011; *Kirchner et al*., 2011] has led to the implementation of more sophisticated physics beyond the SIA into so-called "higher-order" and "full Stokes" models [*Pattyn*, 2003; *Pattyn et al*., 2008; *Bueler and Brown*, 2009; *Larour et al*., 2012; *Gagliardini et al*., 2013]. However, the computational limitation of current full Stokes models in transient experiments to centennial timeframes still precludes their useful application in modeling paleo–ice sheet dynamics, at least beyond steady state solutions. Until higher-order and full Stokes models become more accessible, such paleo-studies will still rely heavily upon the use of first-order/SIA-based models. A possible way forward, within the near future at least, is the adaptive coupling of the full Stokes and SIA stress solutions, such as the ISCAL method (Ice Sheet Coupled Approximation Levels), currently in development for the Elmer/ICE code (J. Ahlkrona et al., Dynamically coupling the nonlinear Stokes equations with the Shallow Ice Approximation in glaciology: Description and first applications of the ISCAL method, *Journal of Computational Physics*, in review, 2015).
3. The Eurasian High Arctic is characterized by strong temperature and precipitation gradients, which were further strengthened during the Late Weichselian to produce an extreme polar desert environment across the Kara Sea [*Marsiat and Valdes*, 2001; *Siegert and Marsiat*, 2001]. The distributions of modern air temperature and precipitation is linked strongly to distance from the relatively warm ocean currents and storm tracks moving up the Norwegian-Greenland Sea from the North Atlantic. However, factors such as the influence of sea ice trapping potential moisture sources, the cooling effect of large proglacial lakes, shifting rain shadows forced by prevailing winds over the ice sheet itself, and changes in the position of the Polar Front and oceanic circulation combine to create a complex and widely variable climate and oceanographic system throughout each glacial cycle. To account for such complexities, previous ice sheet reconstructions have incorporated results from atmospheric general circulation modeling (though not directly coupled) to achieve steady state solutions [*Siegert and Dowdeswell*, 2004] and a time-evolving simulation of deglaciation with mixed success [*Charbit et al*., 2002]. Future modeling should therefore look to build on these results to explore the interactive links between lithospheric, oceanic, atmospheric, and cryospheric processes.
4. Important geological constraints that describe ice sheet flow partitioning, chronology, and general patterns of retreat are still missing for some sectors, particularly the eastern and central Barents Sea, and northern Kara Sea. The problem of output validation is therefore spatially dissonant, leading to a potentially varied suite of reconstructions that could be treated as plausible end members.
5. The isostatic footprint left by the Late Weichselian ice sheet is primarily constrained by data restricted to peripheral areas (Figure 4). This resulting ambiguity has led to widely differing reconstructions in terms of overall ice thickness during the LGM (cf. section 3). Glacial isostatic adjustment modeling that is able to utilize accurately determined ice sheet model output is therefore imperative in order to confirm the thickness and duration of the former ice sheet [e.g., A. Auriac et al., Glacial isostatic adjustment associated with the Barents Sea ice sheet: A modeling inter-comparison, *Quaternary Science Reviews*, in review, 2015]. Furthermore, future glacial isostatic adjustment (GIA) modeling should aim to take into account the east-west variations in the densities of the crust and lithospheric mantle [*Ebbing et al*., 2007; *Ritzmann et al*., 2007] in order to better reconstruct the complex rebound signals observed.

9. Outlook and Conclusions

The wealth of geophysical data documenting the dynamic interplay between the glacial, climate, and ocean systems of the former Barents Sea ice sheet (BSIS) is the best data set for constraining models of marine-based glaciation currently available [*Ingólfsson and Landvik,* 2013*; Jakobsson et al*., 2014b]. Implications for studying

the BSIS therefore have relevance far beyond the regional scale, particularly when considering the present-day concerns regarding instabilities of marine-terminating ice margins in West Antarctica and parts of Greenland [e.g., *Fastook*, 1984; *Reeh et al*., 2001; *Howat and Eddy*, 2011; *Joughin and Alley*, 2011] and the implications such rapid collapse would have globally [*Intergovernmental Panel on Climate Change*, 2013].

Continued geophysical data collection onshore and offshore around the Barents Sea over the last century has revealed that characteristics of the last BSIS share many similarities with observations made from the present-day ice sheets. These include a flow partitioning marked by large, topographically constrained ice streams interspersed with areas of dynamically less active ice, complex patterns of flow switching and ice divide migration, and asynchronous and asymmetric ice stream retreat driven by a combination of external and internal feedback mechanisms. However, a common hindrance of paleo-studies is that the glacial landform and chronological record is strongly biased toward extreme events and stable phases of retreat, while records of ice sheet dynamics during their growth phase are poorly preserved or not preserved at all [*Jakobsson et al*., 2014b]. Questions therefore still remain regarding the dynamic evolution of the BSIS, including the following:

1. In terms of the basic ice sheet flow configuration, the eastern sectors of the BSIS remain a large unknown, with even the extent of the last ice sheet still unclear in some far northeastern areas. Further knowledge on the positioning of ice domes and divides, as well as flow trajectories, is urgently required.
2. Furthermore, understanding how Kara Sea-based ice coalesced and interacted with Fennoscandian and Barents Sea ice will be vital for determining patterns of retreat across the region.
3. Ice stream behavior is crucial to the understanding of long-term ice sheet stability. More detailed knowledge on the absolute rate of retreat of ice streams, such as in Bjørnøyrenna, is not only a crucial constraint for numerical models of deglaciation but also for determining the influence of external and internal factors that drove the collapse of the ice sheet.
4. The evolution and distribution of conditions at the ice-bed interface, including thermal, hydrological, and rheological properties are also still largely unknown. Understanding such attributes is vital for inferring properties of flow, patterns of ice erosion and deposition, and also ice sheet stability. In the case of the western Barents Sea, an understanding of the interaction between buried gas hydrate deposits and overriding ice is an important aspect to reconstructing the complex retreat patterns and geomorphological footprints observed [*Solheim and Elverhøi*, 1993; *Andreassen et al*., 2007a; *Wadham et al*., 2012].
5. Absolute dates detailing the timing of deglaciation in central and eastern sectors of the domain are extremely sparse. Although relative flow patterns tend to show a general eastward migration of the ice sheet complex during deglaciation, further data collection from these sectors will significantly reduce uncertainties in future reconstructions.

Continuing collection of geophysical data from the Barents and Kara seas, as well as adopting novel, state-of-the-art techniques such as 3-D seismics, will help to resolve these questions. Nevertheless, with capabilities of numerical ice sheet models ever increasing, and a rapidly growing database of empirical constraints on glacial events emerging from the Eurasian Arctic, there exists abundant scope for the next generation of ice sheet models to examine more precisely the mechanisms and drivers that forced this polar, marine-based ice sheet to grow and eventually collapse. Such investigations are seen as a priority not only for reconstructing paleo–environmental conditions in the dynamic Arctic but also for advancing our understanding of deglaciation trajectories with respect to both future and paleo–climate changes.

Glossary

AGCM	atmospheric general circulation model.
AMOC	Atlantic meridional overturning cell, a major current in the Atlantic Ocean, characterized by a northward flow of warm, salty water in the upper layers of the Atlantic.
BSIS	Barents Sea ice sheet. Also commonly referred to as the Svalbard-Barents Sea ice sheet or the Barents-Kara ice sheet.
Cal ka B.P.	calendar thousand years before present (1950).

Cold based	ice which is below the pressure melting point and thus frozen to its bed.
Cosmogenic-isotope exposure dating	a geochronological technique for measuring the length of time rock has been exposed at the Earth's surface.
De Geer moraines	occur as closely spaced ridges in association with subaqueous sediments, and mark the intermittent retreat of water-terminating glaciers.
Drumlin	an oval or elongated, streamlined hill of glacial sediments formed beneath an ice sheet and aligned in the direction of ice flow.
Flute	elongate streamlined ridges of sediment aligned parallel to former ice flow.
Grounding line	the point at which non-floating glacier margins terminate or transition into floating ice shelves.
GRISLI	GRenoble Ice Shelf and Land Ice (ice sheet model).
Heinrich Event	a climatic event that triggered the release of large armadas of icebergs across the North Atlantic and the subsequent deposition of a significant IRD layer.
ICE-5G/6G	versions of an Earth model that mathematically analyses glacio-isostatic adjustment processes
Ice piracy	the adjustment of adjacent outlet glacier catchments driven by changes in the drawdown of ice flow. The most obvious effect of this is ice divide migrations.
IRD	ice-rafted debris, commonly associated with debris-rich icebergs that subsequently melt and release sediments into the water column.
Isostasy	the effects of depression and rebound of the Earth's crust from changes in the loading of ice mass.
LGM	Last Glacial Maximum, with nearly all ice sheets at their maximum position between 26.5 and 19 cal ka B.P.
Luminescence dating	a geochronological technique for measuring the time elapsed since crystalline materials in sediments have been exposed to sunlight or intense heat by measuring the accumulated radiation dose.
m aht	meters above present mean high tide mark
m asl	meters above present mean sea level
Marine-based ice sheet	an ice sheet whose bed is predominantly grounded below sea level.
MIS	marine oxygen isotope stage, numbered alternating warm and cold periods in the Earth's paleoclimate starting from present.
MSGL	megascale glacial lineation, an extremely elongated corrugations in sediment (6–70 km), aligned parallel to former ice flow. Indicative of former ice streaming.
MWP-1A	a dramatic postglacial meltwater pulse, that raised global sea level by approximately 20 m in less than 500 years.
Palimpsest	overprinted glacial flow indicators that usually indicate switching patterns of ice flow direction.
Proglacial lake	water ponded between frontal glacier margins and topographic high points.
QUEEN	Quaternary Environment of the Eurasian North (research program).
Radiocarbon dating	a method for dating organic material by measuring the amount of radiocarbon (^{14}C), a radioactive isotope of carbon that starts decaying upon the death of the animal or plant.
Saalian	the glacial period prior to the Weichselian in Northern and Central Europe, spanning from 200 to 130 ka B.P. Equivalent to the Illinoian glaciation in North America.

SIA	the shallow ice approximation, a widely used and computationally efficient set of equations used for modeling "sheet" flow. The approximation assumes basal shear is completely balanced by the gravitational driving stress, and thus ignores longitudinal and transverse stresses.
SICOPOLIS	SImulation COde for POLythermal Ice Sheets (ice sheet model).
SST	sea surface temperature.
Subaerial	exposed to the atmosphere.
Subglacial	at the boundary between glacier ice and the underlying bed.
TMF	trough mouth fan, a sediment deposit found at the mouth of transverse troughs on glaciated continental shelves.
URU	upper regional unconformity, a geological boundary between (glacially eroded) bedrock and overlying sediments.
Weichselian	the last glacial period in Northern and Central Europe, spanning from 115 to 11.7 ka B.P. Equivalent to the Wisconsin glaciation in North America.
Warm based	ice which is at the pressure melting point and thus wet at its bed.
Younger Dryas	an abrupt and short-lived return to glacial-like conditions at the end of the last glacial period that affected the entire Northern Hemisphere.

Acknowledgments

Funding for this work was supported by the Research Council of Norway (RCN) through the PetroMaks project "Glaciations in the Barents Sea area" (GlaciBar) (grant 200672) and its Centres of Excellence funding scheme to the Centre for Arctic Gas Hydrate, Environment and Climate (CAGE), (grant 223259). This is also a contribution to the European Commission Initial Training Network (ITN) project "*Glaciated North Atlantic Margins*" *(GLANAM)* (grant 317217) as well as the RCN funded project "*Research Centre for Arctic Petroleum Exploration*" *(ARCEx)* (grant 228107). We thank Editor-in-Chief Mark Moldwin, Renata Lucchi, and another anonymous reviewer for their constructive comments that helped improve the quality of this paper. Sources for the recalibrated absolute dates used in this review can be found in Tables 1–3. Mapped geomorphological data used are listed in the references. Paleotopography data associated with the ICE-6G_C model were obtained from the project website (http://www.atmosp.physics.utoronto.ca/~peltier/data.php).

The Editor on this paper was Fabio Florindo. He thanks Renata G. Lucchi and two anonymous reviewers.

References

Alexanderson, H., C. Hjort, P. Möller, O. Antonov, and M. Pavlov (2001), The North Taymyr ice-marginal zone, Arctic Siberia—A preliminary overview and dating, *Global Planet. Change*, *31*(1–4), 427–445, doi:10.1016/S0921-8181(01)00133-3.

Alexanderson, H., L. Adrielsson, C. Hjort, P. Möller, O. Antonov, S. Eriksson, and M. Pavlov (2002), Depositional history of the North Taymyr ice-marginal zone, Siberia-a landsystem approach, *J. Quat. Sci.*, *17*(4), 361–382, doi:10.1002/jqs.677.

Alexanderson, H., J. Y. Landvik, and H. T. Ryen (2011), Chronology and styles of glaciation in an inter-fjord setting, northwestern Svalbard, *Boreas*, *40*(1), 175–197, doi:10.1111/j.1502-3885.2010.00175.x.

Anandakrishnan, S., G. A. Catania, R. B. Alley, and H. J. Horgan (2007), Discovery of till deposition at the grounding line of Whillans Ice Stream, *Science*, *315*(5820), 1835–1838, doi:10.1126/science.1138393.

Andersen, E. S., T. M. Dokken, A. Elverhøi, A. Solheim, and I. Fossen (1996), Late Quaternary sedimentation and glacial history of the western Svalbard continental margin, *Mar. Geol.*, *133*(3–4), 123–156, doi:10.1016/0025-3227(96)00022-9.

Andersson, T., S. L. Forman, Ó. Ingólfsson, and W. F. Manley (1999), Late Quaternary environmental history of central Prins Karls Forland, western Svalbard, *Boreas*, *28*(2), 292–307, doi:10.1111/j.1502-3885.1999.tb00221.x.

Andersson, T., S. L. Forman, Ó. Ingólfsson, and W. F. Manley (2000), Stratigraphic and morphologic constraints on the Weichselian glacial history of Northern Prins Karls Forland, Western Svalbard, *Geogr. Ann. Ser. A*, *82*(4), 455–470, doi:10.1111/j.0435-3676.2000.00134.x.

Andreassen, K., and M. Winsborrow (2009), Signature of ice streaming in Bjørnøyrenna, Polar North Atlantic, through the Pleistocene and implications for ice-stream dynamics, *Ann. Glaciol.*, *50*(52), 17–26, doi:10.3189/172756409789624238.

Andreassen, K., T. O. Vorren, and K. B. Johansen (1985), Pre-Late Weichselian glacimarine sediments at Arnøy, North Norway, *Geol. Föreningen i Stock. Förhandlingar*, *107*(1), 63–70, doi:10.1080/11035898509452615.

Andreassen, K., L. C. Nilssen, B. Rafaelsen, and L. Kuilman (2004), Three-dimensional seismic data from the Barents Sea margin reveal evidence of past ice streams and their dynamics, *Geology*, *32*(8), 729–732, doi:10.1130/G20497.1.

Andreassen, K., E. G. Nilssen, and C. M. Ødegaard (2007a), Analysis of shallow gas and fluid migration within the Plio-Pleistocene sedimentary succession of the SW Barents Sea continental margin using 3D seismic data, *Geo-Mar. Lett.*, *27*(2–4), 155–171, doi:10.1007/s00367-007-0071-5.

Andreassen, K., C. M. Odegaard, and B. Rafaelsen (2007b), Imprints of former ice streams, imaged and interpreted using industry three-dimensional seismic data from the south-western Barents Sea, *Geol. Soc. London, Spec. Publ.*, *277*(1), 151–169, doi:10.1144/GSL.SP.2007.277.01.09.

Andreassen, K., J. S. Laberg, and T. O. Vorren (2008), Seafloor geomorphology of the SW Barents Sea and its glaci-dynamic implications, *Geomorphology*, *97*(1–2), 157–177, doi:10.1016/j.geomorph.2007.02.050.

Andreassen, K., M. C. M. Winsborrow, L. R. Bjarnadóttir, and D. C. Rüther (2014), Ice stream retreat dynamics inferred from an assemblage of landforms in the northern Barents Sea, *Quat. Sci. Rev.*, *92*, 246–257, doi:10.1016/j.quascirev.2013.09.015.

Arkhipov, S., L. Isayeva, V. G. Bespaly, and O. Glushkova (1986), Glaciation of Siberia and north-east USSR, *Quat. Sci. Rev.*, *5*, 463–474.

Arneborg, L., A. K. Wåhlin, G. Björk, B. Liljebladh, and A. H. Orsi (2012), Persistent inflow of warm water onto the central Amundsen shelf, *Nat. Geosci.*, *5*(12), 876–880, doi:10.1038/ngeo1644.

Arnold, N. S., T. H. van Andel, and V. Valen (2002), Extent and dynamics of the Scandinavian ice sheet during oxygen isotope stage 3 (65,000–25,000 yr B.P.), *Quat. Res.*, *57*(1), 38–48, doi:10.1006/qres.2001.2298.

Astakhov, V. I. (2006), Evidence of Late Pleistocene ice-dammed lakes in West Siberia, *Boreas*, *35*(4), 607–621, doi:10.1111/j.1502-3885.2006.tb01167.x.

Astakhov, V. I., J. I. Svendsen, A. Matiouchkov, J. Mangerud, O. Maslenikova, and J. Tveranger (1999), Marginal formations of the last Kara and Barents ice sheets in northern European Russia, *Boreas*, *28*(1), 23–45, doi:10.1111/j.1502-3885.1999.tb00205.x.

Bartholomaus, T. C., C. F. Larsen, and S. O'Neel (2013), Does calving matter? Evidence for significant submarine melt, *Earth Planet. Sci. Lett.*, *380*, 21–30, doi:10.1016/j.epsl.2013.08.014.

Batchelor, C. L., and J. A. Dowdeswell (2014), The physiography of High Arctic cross-shelf troughs, *Quat. Sci. Rev.*, *92*, 68–96, doi:10.1016/j.quascirev.2013.05.025.

Batchelor, C. L., and J. A. Dowdeswell (2015), Ice-sheet grounding-zone wedges (GZWs) on high-latitude continental margins, *Mar. Geol.*, *363*, 65–92, doi:10.1016/j.margeo.2015.02.001.

Batchelor, C. L., J. A. Dowdeswell, and K. A. Hogan (2011), Late Quaternary ice flow and sediment delivery through Hinlopen Trough, Northern Svalbard margin: Submarine landforms and depositional fan, *Mar. Geol.*, *284*(1–4), 13–27, doi:10.1016/j.margeo.2011.03.005.

Baumann, K.-H., K. S. Lackschewitz, J. Mangerud, R. F. Spielhagen, T. C. W. Wolf-Welling, R. Henrich, and H. Kassens (1995), Reflection of Scandinavian ice sheet fluctuations in Norwegian Sea sediments during the past 150,000 years, *Quat. Res.*, *43*(2), 185–197, doi:10.1006/qres.1995.1019.

Berger, A., and M. F. Loutre (1991), Insolation values for the climate of the last 10 million years, *Quat. Sci. Rev.*, *10*(4), 297–317, doi:10.1016/0277-3791(91)90033-Q.

Bindschadler, R. (1997), Actively surging West Antarctic ice streams and their response characteristics, *Ann. Glaciol.*, *24*, 409–414.

Bingham, R. G., and M. J. Siegert (2009), Quantifying subglacial bed roughness in Antarctica: Implications for ice-sheet dynamics and history, *Quat. Sci. Rev.*, *28*(3–4), 223–236, doi:10.1016/j.quascirev.2008.10.014.

Bintanja, R., and F. M. Selten (2014), Future increases in Arctic precipitation linked to local evaporation and sea-ice retreat, *Nature*, *509*(7501), 479–82, doi:10.1038/nature13259.

Birgel, D., and H. Hass (2004), Oceanic and atmospheric variations during the last deglaciation in the Fram Strait (Arctic Ocean): A coupled high-resolution organic-geochemical and sedimentological study, *Quat. Sci. Rev.*, *23*(1–2), 29–47, doi:10.1016/j.quascirev.2003.10.001.

Bischof, J. F. (1994), The decay of the Barents ice sheet as documented in nordic seas ice-rafted debris, *Mar. Geol.*, *117*(1–4), 35–55, doi:10.1016/0025-3227(94)90005-1.

Bjarnadóttir, L. R., D. C. Rüther, M. C. M. Winsborrow, and K. Andreassen (2013), Grounding-line dynamics during the last deglaciation of Kveithola, W Barents Sea, as revealed by seabed geomorphology and shallow seismic stratigraphy, *Boreas*, *42*(1), 84–107, doi:10.1111/j.1502-3885.2012.00273.x.

Bjarnadóttir, L. R., M. C. M. Winsborrow, and K. Andreassen (2014), Deglaciation of the central Barents Sea, *Quat. Sci. Rev.*, *92*, 208–226, doi:10.1016/j.quascirev.2013.09.012.

Blatter, H., R. Greve, and A. Abe-Ouchi (2011), Present state and prospects of ice sheet and glacier modelling, *Surv. Geophys.*, *32*(4–5), 555–583, doi:10.1007/s10712-011-9128-0.

Bolshiyanov, D. Y., M. Ryazanova, L. Savilieva, and Z. Pushina (2000), Peatbog at the shoreline of Cape Oskar (Taymyr Peninsula), in *Quaternary Environments of the Eurasian North (QUEEN)*, fourth workshop, Lund, Sweden, p. 9, European Science Foundation.

Bondevik, S., J. Mangerud, L. Ronnert, and O. Salvigsen (1995), Postglacial sea-level history of Edgeøya and Barentsøya, eastern Svalbard, *Polar Res.*, *14*(2), 153–180, doi:10.1111/j.1751-8369.1995.tb00687.x.

Boulton, G. S. (1979), Glacial history of the Spitsbergen archipelago and the problem of a Barents Shelf ice sheet, *Boreas*, *8*(1), 31–57, doi:10.1111/j.1502-3885.1979.tb00429.x.

Boulton, G. S., and C. D. Clark (1990), The Laurentide ice sheet through the last glacial cycle: The topology of drift lineations as a key to the dynamic behaviour of former ice sheets, *Trans. R. Soc. Edinburgh: Earth Sci.*, *81*(04), 327–347, doi:10.1017/S0263593300020836.

Bradwell, T., et al. (2008), The northern sector of the last British Ice Sheet: Maximum extent and demise, *Earth Sci. Rev.*, *88*(3–4), 207–226, doi:10.1016/j.earscirev.2008.01.008.

Briggs, R. D., and L. Tarasov (2013), How to evaluate model-derived deglaciation chronologies: A case study using Antarctica, *Quat. Sci. Rev.*, *63*, 109–127, doi:10.1016/j.quascirev.2012.11.021.

Briggs, R. D., D. Pollard, and L. Tarasov (2014), A data-constrained large ensemble analysis of Antarctic evolution since the Eemian, *Quat. Sci. Rev.*, *103*, 91–115, doi:10.1016/j.quascirev.2014.09.003.

Briner, J. P., G. H. Miller, P. T. Davis, and R. C. Finkel (2006), Cosmogenic radionuclides from fiord landscapes support differential erosion by overriding ice sheets, *Geol. Soc. Am. Bull.*, *118*(3–4), 406–420, doi:10.1130/B25716.1.

Brückner, H., and G. Schellmann (2003), Late Pleistocene and Holocene shorelines of Andréeland, Spitsbergen (Svalbard): Geomorphological evidence and palaeo-oceanographic significance, *J. Coast. Res.*, *19*(4), 971–982.

Brückner, H., G. Schellmann, and K. van der Borg (2002), Uplifted beach ridges in northern Spitsbergen as indicators for glacio-isostasy and palaeo-oceanography, *Z. Geomorphol.*, *46*(3), 309–336.

Bueler, E., and J. Brown (2009), Shallow shelf approximation as a "sliding law" in a thermomechanically coupled ice sheet model, *J. Geophys. Res.*, *114*, F03008, doi:10.1029/2008JF001179.

Butt, F. A., A. Elverhøi, A. Solheim, and C. F. Forsberg (2000), Deciphering Late Cenozoic development of the western Svalbard Margin from ODP Site 986 results, *Mar. Geol.*, *169*(3–4), 373–390, doi:10.1016/S0025-3227(00)00088-8.

Butt, F. A., H. Drange, A. Elverhøi, O. H. Otterå, and A. Solheim (2002), Modelling Late Cenozoic isostatic elevation changes in the Barents Sea and their implications for oceanic and climatic regimes: Preliminary results, *Quat. Sci. Rev.*, *21*(14–15), 1643–1660, doi:10.1016/S0277-3791(02)00018-5.

Cadman, V. (1996), Glacimarine Sedimentation and Environments during the Late Weichselian and Holocene in the Bellsund Trough and Van Keulenfjorden, Svalbard, PhD thesis, p. 250, Univ. of Cambridge.

Charbit, S., C. Ritz, and G. Ramstein (2002), Simulations of Northern Hemisphere ice-sheet retreat: Sensitivity to physical mechanisms involved during the last deglaciation, *Quat. Sci. Rev.*, *21*(1–3), 243–265.

Chauché, N., A. Hubbard, J.-C. Gascard, J. E. Box, R. Bates, M. Koppes, A. Sole, P. Christoffersen, and H. Patton (2014), Ice-ocean interaction and calving front morphology at two west Greenland tidewater outlet glaciers, *Cryosphere*, *8*(4), 1457–1468, doi:10.5194/tc-8-1457-2014.

Chauhan, T., T. L. Rasmussen, R. Noormets, M. Jakobsson, and K. A. Hogan (2014), Glacial history and paleoceanography of the southern Yermak Plateau since 132 ka BP, *Quat. Sci. Rev.*, *92*, 155–169, doi:10.1016/j.quascirev.2013.10.023.

Chauhan, T., T. L. Rasmussen, and R. Noormets (2015), Palaeoceanography of the Barents Sea continental margin, north of Nordaustlandet, Svalbard, during the last 74 ka, *Boreas*, doi:10.1111/bor.12135, early view.

Christoffersen, P., R. I. Mugford, K. J. Heywood, I. Joughin, J. A. Dowdeswell, J. P. M. Syvitski, A. Luckman, and T. J. Benham (2011), Warming of waters in an East Greenland fjord prior to glacier retreat: Mechanisms and connection to large-scale atmospheric conditions, *Cryosphere*, *5*(3), 701–714, doi:10.5194/tc-5-701-2011.

Clark, C. D. (1993), Mega-scale glacial lineations and cross-cutting ice-flow landforms, *Earth Surf. Processes Landforms*, *18*(1), 1–29.

Clark, C. D. (1999), Glaciodynamic context of subglacial bedform generation and preservation, *Ann. Glaciol.*, *28*(1), 23–32, doi:10.3189/172756499781821832.

Clark, P. U., A. M. McCabe, A. C. Mix, and A. J. Weaver (2004), Rapid rise of sea level 19,000 years ago and its global implications, *Science*, *304*(5674), 1141–1144, doi:10.1126/science.1094449.

Clark, P. U., A. S. Dyke, J. D. Shakun, A. E. Carlson, J. Clark, B. Wohlfarth, J. X. Mitrovica, S. W. Hostetler, and A. M. McCabe (2009), The Last Glacial Maximum, *Science*, *325*(5941), 710–714, doi:10.1126/science.1172873.

Clason, C., P. Applegate, and P. Holmlund (2014), Modelling Late Weichselian evolution of the Eurasian ice sheets forced by surface meltwater-enhanced basal sliding, *J. Glaciol.*, *60*(219), 29–40.
Conway, H., G. Catania, C. F. Raymond, A. M. Gades, T. A. Scambos, and H. Engelhardt (2002), Switch of flow direction in an Antarctic ice stream, *Nature*, *419*(6906), 465–467.
Davis, P. T., J. P. Briner, R. D. Coulthard, R. W. Finkel, and G. H. Miller (2006), Preservation of Arctic landscapes overridden by cold-based ice sheets, *Quat. Res.*, *65*(1), 156–163, doi:10.1016/j.yqres.2005.08.019.
Day, J. J., J. L. Bamber, R. J. Valdes, and J. Kohler (2012), The impact of a seasonally ice free Arctic Ocean on the temperature, precipitation and surface mass balance of Svalbard, *Cryosphere*, *6*, 35–50, doi:10.5194/tc-6-35-2012.
De Angelis, H., and P. Skvarca (2003), Glacier surge after ice shelf collapse, *Science*, *299*(5612), 1560–1562, doi:10.1126/science.1077987.
Demidov, I., M. Houmark-Nielsen, K. Kjær, and E. Larsen (2006), The last Scandinavian Ice Sheet in northwestern Russia: Ice flow patterns and decay dynamics, *Boreas*, *35*(3), 425–443, doi:10.1080/03009480600781883.
Denton, G. H., and T. J. Hughes (Eds.) (1981), *The Last Great Ice Sheets*, John Wiley, New York.
Deschamps, P., N. Durand, E. Bard, B. Hamelin, G. Camoin, A. L. Thomas, G. M. Henderson, J. Okuno, and Y. Yokoyama (2012), Ice-sheet collapse and sea-level rise at the Bølling warming 14,600 years ago, *Nature*, *483*(7391), 559–564, doi:10.1038/nature10902.
Dowdeswell, J. A., and A. Elverhøi (2002), The timing of initiation of fast-flowing ice streams during a glacial cycle inferred from glacimarine sedimentation, *Mar. Geol.*, *188*(1–2), 3–14, doi:10.1016/S0025-3227(02)00272-4.
Dowdeswell, J. A., and E. M. G. Fugelli (2012), The seismic architecture and geometry of grounding-zone wedges formed at the marine margins of past ice sheets, *Geol. Soc. Am. Bull.*, *124*(11–12), 1750–1761, doi:10.1130/B30628.1.
Dowdeswell, J. A., and M. J. Siegert (1999), Ice-sheet numerical modeling and marine geophysical measurements of glacier-derived sedimentation on the Eurasian Arctic continental margins, *Geol. Soc. Am. Bull.*, *111*(7), 1080–1097.
Dowdeswell, J. A., N. H. Kenyon, A. Elverhøi, J. S. Laberg, F.-J. Hollender, J. Mienert, and M. J. Siegert (1996), Large-scale sedimentation on the glacier-influenced polar North Atlantic Margins: Long-range side-scan sonar evidence, *Geophys. Res. Lett.*, *23*(24), 3535–3538, doi:10.1029/96GL03484.
Dowdeswell, J. A., D. Ottesen, and L. Rise (2006), Flow switching and large-scale deposition by ice streams draining former ice sheets, *Geology*, *34*(4), 313–316, doi:10.1130/G22253.1.
Dowdeswell, J. A., D. Ottesen, J. Evans, C. Ó. Cofaigh, and J. B. Anderson (2008), Submarine glacial landforms and rates of ice-stream collapse, *Geology*, *36*(10), 819–822, doi:10.1130/G24808A.1.
Dowdeswell, J. A., et al. (2010a), High-resolution geophysical observations of the Yermak Plateau and northern Svalbard margin: Implications for ice-sheet grounding and deep-keeled icebergs, *Quat. Sci. Rev.*, *29*(25–26), 3518–3531, doi:10.1016/j.quascirev.2010.06.002.
Dowdeswell, J. A., K. A. Hogan, J. Evans, R. Noormets, C. O. Cofaigh, and D. Ottesen (2010b), Past ice-sheet flow east of Svalbard inferred from streamlined subglacial landforms, *Geology*, *38*(2), 163–166, doi:10.1130/G30621.1.
Dowdeswell, J. A., D. Ottesen, and L. Rise (2010c), Rates of sediment delivery from the Fennoscandian Ice Sheet through an ice age, *Geology*, *38*(1), 3–6, doi:10.1130/G25523.1.
Dupont, T. K., and R. B. Alley (2005), Assessment of the importance of ice-shelf buttressing to ice-sheet flow, *Geophys. Res. Lett.*, *32*, L04503, doi:10.1029/2004GL022024.
Ebbing, J., C. Braitenberg, and S. Wienecke (2007), Insights into the lithospheric structure and tectonic setting of the Barents Sea region from isostatic considerations, *Geophys. J. Int.*, *171*(3), 1390–1403, doi:10.1111/j.1365-246X.2007.03602.x.
Elverhøi, A., W. Fjeldskaar, A. Solheim, M. Nyland-Berg, and L. Russwurm (1993), The Barents Sea ice sheet—A model of its growth and decay during the last ice maximum, *Quat. Sci. Rev.*, *12*(10), 863–873, doi:10.1016/0277-3791(93)90025-H.
Elverhøi, A., E. S. Andersen, T. Dokken, D. Hebbeln, R. Spielhagen, J. I. Svendsen, M. Sørflaten, A. Rørnes, M. Hald, and C. F. Forsberg (1995), The growth and decay of the Late Weichselian Ice Sheet in Western Svalbard and adjacent areas based on provenance studies of marine sediments, *Quat. Res.*, *44*(3), 303–316, doi:10.1006/qres.1995.1076.
Emery, K. O., and D. G. Aubrey (1991), *Sea Levels, Land Levels and Tide Gauges*, Springer, New York.
Engelhardt, H. (2004), Thermal regime and dynamics of the West Antarctic ice sheet, *Ann. Glaciol.*, *39*(1), 85–92, doi:10.3189/172756404781814203.
Engelhardt, H., and B. Kamb (2013), Kamb Ice Stream flow history and surge potential, *Ann. Glaciol.*, *54*(63), 287–298, doi:10.3189/2013AoG63A535.
Evans, D. J. A., and B. R. Rea (1999), Geomorphology and sedimentology of surging glaciers: A land-systems approach, *Ann. Glaciol.*, *28*(1), 75–82, doi:10.3189/172756499781821823.
Evans, D. J. A., and B. R. Rea (2005), Late Weichselian deglaciation and sea level history of St Jonsfjorden, Spitsbergen: A contribution to ice sheet reconstruction, *Scott. Geogr. J.*, *121*(2), 175–201, doi:10.1080/00369220518737230.
Fabel, D., A. P. Stroeven, J. Harbor, J. Kleman, D. Elmore, and D. Fink (2002), Landscape preservation under Fennoscandian ice sheets determined from in situ produced ^{10}Be and ^{26}Al, *Earth Planet. Sci. Lett.*, *201*(2), 397–406, doi:10.1016/S0012-821X(02)00714-8.
Fahl, K., and R. Stein (2012), Modern seasonal variability and deglacial/Holocene change of central Arctic Ocean sea-ice cover: New insights from biomarker proxy records, *Earth Planet. Sci. Lett.*, *351–352*, 123–133, doi:10.1016/j.epsl.2012.07.009.
Faleide, J. I., A. Solheim, A. Fiedler, B. O. Hjelstuen, E. S. Andersen, and K. Vanneste (1996), Late Cenozoic evolution of the western Barents Sea-Svalbard continental margin, *Global Planet. Change*, *12*(1–4), 53–74, doi:10.1016/0921-8181(95)00012-7.
Fastook, J. L. (1984), West Antarctica, the sea-level controlled marine instability: Past and future, in *Climate Processes and Climate Sensitivity*, vol. 29, edited by J. E. Hansen and T. Takahashi, pp. 275–287, AGU, Washington, D. C.
Fetterer, F., K. Knowles, W. Meier, and M. Savoie (2002), *Sea Ice Index. Arctic Median September 1981–2010*, National Snow and Ice Data Center, Boulder, Colo., doi:10.7265/N5QJ7F7W.
Fjeldskaar, W. (1994), Viscosity and thickness of the asthenosphere detected from the Fennoscandian uplift, *Earth Planet. Sci. Lett.*, *126*(4), 399–410, doi:10.1016/0012-821X(94)90120-1.
Flament, T., and F. Rémy (2012), Dynamic thinning of Antarctic glaciers from along-track repeat radar altimetry, *J. Glaciol.*, *58*(211), 830–840, doi:10.3189/2012JoG11J118.
Flower, B. P. (1997), Overconsolidated section on the Yermak Plateau, Arctic Ocean: Ice sheet grounding prior to ca. 660 ka?, *Geology*, *25*(2), 147–150, doi:10.1130/0091-7613(1997)025.
Forman, S. L. (1999), Infrared and red stimulated luminescence dating of late Quaternary near-shore sediments from Spitsbergen, Svalbard, *Arct. Antarct. Alp. Res.*, *31*(1), 34–49.
Forman, S. L., and G. H. Miller (1984), Time-dependent soil morphologies and pedogenic processes on raised beaches, Bröggerhalvöya, Spitsbergen, Svalbard Archipelago, *Arct. Alp. Res.*, *16*(4), 381–394.

Forman, S. L. (1990), Post-glacial relative sea-level history of northwestern Spitsbergen, Svalbard, *Geol. Soc. Am. Bull.*, *102*(11), 1580–1590, doi:10.1130/0016-7606(1990)102.
Forman, S. L., D. Lubinski, G. H. Miller, J. Snyder, G. Matishov, S. Korsun, and V. Myslivets (1995), Postglacial emergence and distribution of late Weichselian ice-sheet loads in the northern Barents and Kara seas, Russia, *Geology*, *23*(2), 113–116, doi:10.1130/0091-7613(1995)023.
Forman, S. L., D. Lubinski, G. H. Miller, G. G. Matishov, S. Korsun, J. Snyder, F. Herlihy, R. Weihe, and V. Myslivets (1996), Postglacial emergence of western Franz Josef Land, Russian, and retreat of the Barents Sea ice sheet, *Quat. Sci. Rev.*, *15*(1), 77–90.
Forman, S. L., R. Weihe, D. Lubinski, G. Tarasov, S. Korsun, and G. Matishov (1997), Holocene relative sea-level history of Franz Josef Land, Russia, *Geol. Soc. Am. Bull.*, *109*(9), 1116–1133, doi:10.1130/0016-7606(1997)109.
Forman, S. L., D. J. Lubinski, J. J. Zeeberg, L. Polyak, G. H. Miller, G. Matishov, and G. Tarasov (1999), Postglacial emergence and late Quaternary glaciation on northern Novaya Zemlya, Arctic Russia, *Boreas*, *28*(1), 133–145, doi:10.1111/j.1502-3885.1999.tb00210.x.
Forman, S. L., D. J. Lubinski, Ó. Ingólfsson, J. J. Zeeberg, J. A. Snyder, M. J. Siegert, and G. G. Matishov (2004), A review of postglacial emergence on Svalbard, Franz Josef Land and Novaya Zemlya, northern Eurasia, *Quat. Sci. Rev.*, *23*(11–13), 1391–1434, doi:10.1016/j.quascirev.2003.12.007.
Forman, S., D. Mann, and G. H. Miller (1987), Late Weichselian and Holocene relative sea-level history of Bröggerhalvöya, Spitsbergen, *Quat. Res.*, *27*, 41–50.
Forsström, P.-L., and R. Greve (2004), Simulation of the Eurasian ice sheet dynamics during the last glaciation, *Global Planet. Change*, *42*(1–4), 59–81, doi:10.1016/j.gloplacha.2003.11.003.
Forsström, P.-L., O. Sallasmaa, R. Greve, and T. Zwinger (2003), Simulation of fast-flow features of the Fennoscandian ice sheet during the Last Glacial Maximum, *Ann. Glaciol.*, *37*, 383–389.
Forwick, M., and T. O. Vorren (2009), Late Weichselian and Holocene sedimentary environments and ice rafting in Isfjorden, Spitsbergen, *Palaeogeogr. Palaeoclimatol. Palaeoecol.*, *280*(1–2), 258–274, doi:10.1016/j.palaeo.2009.06.026.
Gagliardini, O., et al. (2013), Capabilities and performance of Elmer/Ice, a new-generation ice sheet model, *Geosci. Model Dev.*, *6*(4), 1299–1318, doi:10.5194/gmd-6-1299-2013.
Gataullin, V., and L. Polyak (1997), Morainic Ridge Complex, Eastern Barents Sea, in *Glaciated Continental Margins: An Atlas of Acoustic Images*, edited by T. A. Davis et al., pp. 82–83, Chapman and Hall, London.
Gataullin, V., L. Polyak, O. Epstein, and B. Romanyuk (1993), Glacigenic deposits of the Central Deep: A key to the late Quaternary evolution of the eastern Barents Sea, *Boreas*, *22*(1), 47–58, doi:10.1111/j.1502-3885.1993.tb00163.x.
Gataullin, V., J. Mangerud, and J. I. Svendsen (2001), The extent of the Late Weichselian ice sheet in the southeastern Barents Sea, *Global Planet. Change*, *31*(1–4), 453–474, doi:10.1016/S0921-8181(01)00135-7.
Gildor, H., and E. Tziperman (2000), Sea ice as the glacial cycles' climate switch: Role of seasonal and orbital forcing, *Paleoceanography*, *15*(6), 605–615, doi:10.1029/1999PA000461.
Gjermundsen, E. F., J. P. Briner, N. Akçar, O. Salvigsen, P. Kubik, N. Gantert, and A. Hormes (2013), Late Weichselian local ice dome configuration and chronology in Northwestern Svalbard: Early thinning, late retreat, *Quat. Sci. Rev.*, *72*, 112–127, doi:10.1016/j.quascirev.2013.04.006.
Goldberg, D., D. M. Holland, and C. Schoof (2009), Grounding line movement and ice shelf buttressing in marine ice sheets, *J. Geophys. Res.*, *114*, F04026, doi:10.1029/2008JF001227.
Golledge, N. R., A. Hubbard, and D. E. Sugden (2008), High-resolution numerical simulation of Younger Dryas glaciation in Scotland, *Quat. Sci. Rev.*, *27*(9–10), 888–904, doi:10.1016/j.quascirev.2008.01.019.
Golledge, N. R., A. N. Mackintosh, B. M. Anderson, K. M. Buckley, A. M. Doughty, D. J. A. A. Barrell, G. H. Denton, M. J. Vandergoes, B. G. Andersen, and J. M. Schaefer (2012), Last Glacial Maximum climate in New Zealand inferred from a modelled Southern Alps icefield, *Quat. Sci. Rev.*, *46*, 30–45, doi:10.1016/j.quascirev.2012.05.004.
Graham, A. G. C., R. D. Larter, K. Gohl, J. A. Dowdeswell, C.-D. Hillenbrand, J. A. Smith, J. Evans, G. Kuhn, and T. Deen (2010), Flow and retreat of the late Quaternary Pine Island-Thwaites palaeo-ice stream, West Antarctica, *J. Geophys. Res.*, *115*, F03025, doi:10.1029/2009JF001482.
Greenwood, S. L., and C. D. Clark (2009), Reconstructing the last Irish Ice Sheet 2: A geomorphologically-driven model of ice sheet growth, retreat and dynamics, *Quat. Sci. Rev.*, *28*(27–28), 3101–3123, doi:10.1016/j.quascirev.2009.09.014.
Greve, R. (1997), A continuum-mechanical formulation for shallow polythermal ice sheets, *Philos. Trans. R. Soc., A*, *355*(1726), 921–974, doi:10.1098/rsta.1997.0050.
Grosswald, M. G. (2001), The late Weichselian Barents-Kara ice sheet: In defense of a maximum reconstruction, *Russ. J. Earth Sci.*, *3*(6), 427–452.
Grosswald, M. G., and T. J. Hughes (2002), The Russian component of an Arctic Ice Sheet during the Last Glacial Maximum, *Quat. Sci. Rev.*, *21*(1–3), 121–146, doi:10.1016/S0277-3791(01)00078-6.
Grousset, F. E., E. Cortijo, S. Huon, L. Hervé, T. Richter, D. Burdloff, J. Duprat, and O. Weber (2001), Zooming in on Heinrich layers, *Paleoceanography*, *16*(3), 240–259, doi:10.1029/2000PA000559.
Gudlaugsson, E., A. Humbert, M. Winsborrow, and K. Andreassen (2013), Subglacial roughness of the former Barents Sea ice sheet, *J. Geophys. Res. Earth Surf.*, *118*, 2546–2556, doi:10.1002/2013JF002714.
Gudmundsson, G. H., J. Krug, G. Durand, L. Favier, and O. Gagliardini (2012), The stability of grounding lines on retrograde slopes, *Cryosphere*, *6*(6), 1497–1505, doi:10.5194/tc-6-1497-2012.
Gyllencreutz, R., J. Mangerud, J. I. Svendsen, and Ø. S. Lohne (2007), DATED—A dating database and GIS-based reconstruction of the Eurasian deglaciation, *Geol. Surv. Finl. Spec. Pap.*, *46*, 113–120.
Hahne, J., and M. Melles (1997), Late- and post-glacial vegetation and climate history of the south-western Taymyr Peninsula, central Siberia, as revealed by pollen analysis of a core from Lake Lama, *Veg. Hist. Archaeobot.*, *6*(1), 1–8, doi:10.1007/BF01145880.
Hald, M., J. Sættem, and E. Nesse (1990), Middle and Late Weichselian stratigraphy in shallow drillings from the southwestern Barents Sea: Foraminiferal, amino acid and radiocarbon evidence, *Nor. Geogr. Tidsskr.*, *70*, 241–257.
Hättestrand, C., and C. D. Clark (2006), The glacial geomorphology of Kola Peninsula and adjacent areas in the Murmansk Region, Russia, *J. Maps*, *2*(1), 30–42, doi:10.4113/jom.2006.41.
Hebbeln, D. (1992), Weichselian glacial history of the Svalbard area: Correlating the marine and terrestrial records, *Boreas*, *21*(3), 295–302, doi:10.1111/j.1502-3885.1992.tb00035.x.
Hebbeln, D., T. Dokken, E. S. Andersen, M. Hald, and A. Elverhøi (1994), Moisture supply for northern ice-sheet growth during the Last Glacial Maximum, *Nature*, *370*(6488), 357–360, doi:10.1038/370357a0.
Helmens, K. (2000), The Last Interglacial-Glacial cycle in NE Fennoscandia: A nearly continuous record from Sokli (Finnish Lapland), *Quat. Sci. Rev.*, *19*(16), 1605–1623, doi:10.1016/S0277-3791(00)00004-4.
Helmens, K. F., and S. Engels (2010), Ice-free conditions in eastern Fennoscandia during early Marine Isotope Stage 3: Lacustrine records, *Boreas*, *39*(2), 399–409, doi:10.1111/j.1502-3885.2010.00142.x.

Helsen, M. M., M. R. van den Broeke, R. S. W. van de Wal, W. J. van de Berg, E. van Meijgaard, C. H. Davis, Y. Li, and I. Goodwin (2008), Elevation changes in Antarctica mainly determined by accumulation variability, *Science*, *320*(5883), 1626–1629, doi:10.1126/science.1153894.

Henriksen, M., H. Alexanderson, J. Y. Landvik, H. Linge, and G. Peterson (2014), Dynamics and retreat of the Late Weichselian Kongsfjorden ice stream, NW Svalbard, *Quat. Sci. Rev.*, *92*, 235–245, doi:10.1016/j.quascirev.2013.10.035.

Hindmarsh, R. C. A. (1993), Modeling the dynamics of ice sheets, *Prog. Phys. Geogr.*, *17*(4), 391–412.

Hiscott, R. N., and A. E. Aksu (1996), Quaternary sedimentary processes and budgets in Orphan Basin, southwestern Labrador Sea, *Quat. Res.*, *45*(2), 160–175, doi:10.1006/qres.1996.0017.

Hogan, K. A., J. A. Dowdeswell, R. Noormets, J. Evans, and C. Ó. Cofaigh (2010a), Evidence for full-glacial flow and retreat of the Late Weichselian Ice Sheet from the waters around Kong Karls Land, eastern Svalbard, *Quat. Sci. Rev.*, *29*(25–26), 3563–3582, doi:10.1016/j.quascirev.2010.05.026.

Hogan, K. A., J. A. Dowdeswell, R. Noormets, J. Evans, C. Ó. Cofaigh, and M. Jakobsson (2010b), Submarine landforms and ice-sheet flow in the Kvitøya Trough, northwestern Barents Sea, *Quat. Sci. Rev.*, *29*(25–26), 3545–3562, doi:10.1016/j.quascirev.2010.08.015.

Holland, D. M., R. H. Thomas, B. de Young, M. H. Ribergaard, and B. Lyberth (2008), Acceleration of Jakobshavn Isbræ triggered by warm subsurface ocean waters, *Nat. Geosci.*, *1*(10), 659–664, doi:10.1038/ngeo316.

Hormes, A., N. Akçar, and P. W. Kubik (2011), Cosmogenic radionuclide dating indicates ice-sheet configuration during MIS 2 on Nordaustlandet, Svalbard, *Boreas*, *40*(4), 636–649, doi:10.1111/j.1502-3885.2011.00215.x.

Hormes, A., E. F. Gjermundsen, and T. L. Rasmussen (2013), From mountain top to the deep sea—Deglaciation in 4D of the northwestern Barents Sea ice sheet, *Quat. Sci. Rev.*, *75*, 78–99, doi:10.1016/j.quascirev.2013.04.009.

Hostetler, S., P. Bartlein, P. Clark, E. Small, and A. Solomon (2000), Stimulated influences of Lake Agassiz on the climate of central North America 11,000 years ago, *Nature*, *405*(6784), 334–337, doi:10.1038/35012581.

Howat, I. M., and A. Eddy (2011), Multi-decadal retreat of Greenland's marine-terminating glaciers, *J. Glaciol.*, *57*(203), 389–396, doi:10.3189/002214311796905631.

Howell, D., M. J. Siegert, and J. A. Dowdeswell (2000), Modelling the influence of glacial isostasy on Late Weichselian ice-sheet growth in the Barents Sea, *J. Quat. Sci.*, *15*(5), 475–486.

Hubbard, A., T. Bradwell, N. Golledge, A. Hall, H. Patton, D. Sugden, R. Cooper, and M. Stoker (2009), Dynamic cycles, ice streams and their impact on the extent, chronology and deglaciation of the British–Irish ice sheet, *Quat. Sci. Rev.*, *28*(7–8), 758–776, doi:10.1016/j.quascirev.2008.12.026.

Hubbard, B., M. J. Siegert, and D. McCarroll (2000), Spectral roughness of glaciated bedrock geomorphic surfaces: Implications for glacier sliding, *J. Geophys. Res.*, *105*(B9), 21,295–21,303, doi:10.1029/2000JB900162.

Hubberten, H. W., et al. (2004), The periglacial climate and environment in northern Eurasia during the Last Glaciation, *Quat. Sci. Rev.*, *23*(11–13), 1333–1357, doi:10.1016/j.quascirev.2003.12.012.

Hughes, A. L. C., R. Gyllencreutz, Ø. S. Lohne, J. Mangerud, and J. I. Svendsen (2015), The last Eurasian Ice Sheets—A chronological database and time-slice reconstruction, DATED-1, *Boreas*, doi:10.1111/bor.12142, in press.

Hughes, T. (1987), The marine ice transgression hypothesis, *Geogr. Ann. Ser. A*, *69*, 237–250.

Hughes, T. (2011), A simple holistic hypothesis for the self-destruction of ice sheets, *Quat. Sci. Rev.*, *30*(15–16), 1829–1845, doi:10.1016/j.quascirev.2011.04.004.

Hughes, T., G. H. Denton, and M. G. Grosswald (1977), Was there a late-Würm Arctic Ice Sheet?, *Nature*, *266*(5603), 596–602, doi:10.1038/266596a0.

Hulton, N. R. J., and M. J. Mineter (2000), Modelling self-organization in ice streams, *Ann. Glaciol.*, *30*(1), 127–136, doi:10.3189/172756400781820561.

Ingólfsson, Ó., and J. Y. Landvik (2013), The Svalbard–Barents Sea ice-sheet—Historical, current and future perspectives, *Quat. Sci. Rev.*, *64*, 33–60, doi:10.1016/j.quascirev.2012.11.034.

Ingólfsson, Ó., F. Rögnvaldsson, H. Bergsten, L. Hedenäs, G. Lemdahl, J. M. Lirio, and H. P. Sejrup (1995), Late Quaternary glacial and environmental history of Kongsøya, Svalbard, *Polar Res.*, *14*(2), 123–139, doi:10.3402/polar.v14i2.6659.

Ingólfsson, Ó., P. Möller, and H. Lokrantz (2008), Late Quaternary marine-based Kara Sea ice sheets: A review of terrestrial stratigraphic data highlighting their formation, *Polar Res.*, *27*(2), 152–161, doi:10.1111/j.1751-8369.2008.00060.x.

Intergovernmental Panel on Climate Change (IPCC) (2013), Summary for Policymakers, in *Climate Change 2013: The Physical Science Basis. Contribution of Working Group 1 to the Fifth Assessment Report of the Intergovernmental Panel on Climate Change*, edited by T. F. Stocker et al., Cambridge Univ. Press, Cambridge.

Ivy-Ochs, S., H. Kerschner, M. Maisch, M. Christl, P. W. Kubik, and C. Schlüchter (2009), Latest Pleistocene and Holocene glacier variations in the European Alps, *Quat. Sci. Rev.*, *28*(21–22), 2137–2149, doi:10.1016/j.quascirev.2009.03.009.

Jakobsson, M., et al. (2011), Geological record of ice shelf break-up and grounding line retreat, Pine Island Bay, West Antarctica, *Geology*, *39*(7), 691–694, doi:10.1130/G32153.1.

Jakobsson, M., J. B. Anderson, F. O. Nitsche, R. Gyllencreutz, A. E. Kirshner, N. Kirchner, M. O'Regan, R. Mohammad, and B. Eriksson (2012a), Ice sheet retreat dynamics inferred from glacial morphology of the central Pine Island Bay Trough, West Antarctica, *Quat. Sci. Rev.*, *38*, 1–10, doi:10.1016/j.quascirev.2011.12.017.

Jakobsson, M., et al. (2012b), The International Bathymetric Chart of the Arctic Ocean (IBCAO) version 3.0, *Geophys. Res. Lett.*, *39*, L12609, doi:10.1029/2012GL052219.

Jakobsson, M., et al. (2014a), Arctic Ocean glacial history, *Quat. Sci. Rev.*, *92*, 40–67, doi:10.1016/j.quascirev.2013.07.033.

Jakobsson, M., Ó. Ingólfsson, A. J. Long, and R. F. Spielhagen (2014b), The dynamic Arctic, *Quat. Sci. Rev.*, *92*, 1–8, doi:10.1016/j.quascirev.2014.03.022.

Jamieson, S. S. R., A. Vieli, C. Ó. Cofaigh, C. R. Stokes, S. J. Livingstone, and C.-D. Hillenbrand (2014), Understanding controls on rapid ice-stream retreat during the last deglaciation of Marguerite Bay, Antarctica, using a numerical model, *J. Geophys. Res. Earth Surf.*, *119*, 247–263, doi:10.1002/2013JF002934.

Jansen, E., T. Fronval, F. Rack, and J. E. T. Channell (2000), Pliocene-Pleistocene ice rafting history and cyclicity in the Nordic Seas during the last 3.5 Myr, *Paleoceanography*, *15*(6), 709–721, doi:10.1029/1999PA000435.

Jessen, S. P., T. L. Rasmussen, T. Nielsen, and A. Solheim (2010), A new Late Weichselian and Holocene marine chronology for the western Svalbard slope 30,000–0 cal years BP, *Quat. Sci. Rev.*, *29*(9–10), 1301–1312, doi:10.1016/j.quascirev.2010.02.020.

Jones, G. A., and L. D. Keigwin (1988), Evidence from Fram Strait (78°N) for early deglaciation, *Nature*, *336*(6194), 56–59, doi:10.1038/336056a0.

Joughin, I., and R. B. Alley (2011), Stability of the West Antarctic ice sheet in a warming world, *Nat. Geosci.*, *4*(8), 506–513, doi:10.1038/ngeo1194.

Junttila, J., S. Aagaard-Sørensen, K. Husum, and M. Hald (2010), Late Glacial–Holocene clay minerals elucidating glacial history in the SW Barents Sea, *Mar. Geol.*, *276*(1–4), 71–85, doi:10.1016/j.margeo.2010.07.009.
Kirchner, N., K. Hutter, M. Jakobsson, and R. Gyllencreutz (2011), Capabilities and limitations of numerical ice sheet models: A discussion for Earth-scientists and modelers, *Quat. Sci. Rev.*, *30*(25–26), 3691–3704, doi:10.1016/j.quascirev.2011.09.012.
Kjær, K., E. Larsen, S. Funder, I. Demidov, M. Jensen, L. Håkansson, and A. Murray (2006), Eurasian ice-sheet interaction in northwestern Russia throughout the late Quaternary, *Boreas*, *35*(3), 444–475, doi:10.1080/03009480600781891.
Kjær, K. H., I. N. Demidov, E. Larsen, A. Murray, and J. K. Nielsen (2003), Mezen Bay—A key area for understanding Weichselian glaciations in northern Russia, *J. Quat. Sci.*, *18*(1), 73–93, doi:10.1002/jqs.700.
Kjær, K. H., et al. (2012), Aerial photographs reveal late-20th-century dynamic ice loss in northwestern Greenland, *Science*, *337*(6094), 569–573, doi:10.1126/science.1220614.
Kleiber, H. P., J. Knies, and F. Niessen (2000), The Late Weichselian glaciation of the Franz Victoria Trough, northern Barents Sea: Ice sheet extent and timing, *Mar. Geol.*, *168*(1–4), 25–44, doi:10.1016/S0025-3227(00)00047-5.
Kleman, J. (1992), The palimpsest glacial landscape in northwestern Sweden. Late Weichselian deglaciation landforms and traces of older west-centered ice sheets, *Geogr. Ann. Ser. A*, *74*(4), 305–325.
Kleman, J. (1994), Preservation of landforms under ice sheets and ice caps, *Geomorphology*, *9*(1), 19–32, doi:10.1016/0169-555X(94)90028-0.
Kleman, J., and C. Hattestrand (1999), Frozen-bed Fennoscandian and Laurentide ice sheets during the Last Glacial Maximum, *Nature*, *402*(6757), 63–66, doi:10.1038/47005.
Knies, J., C. Vogt, and R. Stein (1999), Late Quaternary growth and decay of the Svalbard/Barents Sea ice sheet and paleoceanographic evolution in the adjacent Arctic Ocean, *Geo-Mar. Lett.*, *18*(3), 195–202, doi:10.1007/s003670050068.
Knies, J., N. Nowaczyk, C. Müller, C. Vogt, and R. Stein (2000), A multiproxy approach to reconstruct the environmental changes along the Eurasian continental margin over the last 150 000 years, *Mar. Geol.*, *163*(1–4), 317–344, doi:10.1016/S0025-3227(99)00106-1.
Knies, J., H.-P. Kleiber, J. Matthiessen, C. Müller, and N. Nowaczyk (2001), Marine ice-rafted debris records constrain maximum extent of Saalian and Weichselian ice-sheets along the northern Eurasian margin, *Global Planet. Change*, *31*(1–4), 45–64, doi:10.1016/S0921-8181(01)00112-6.
Knies, J., J. Matthiessen, C. Vogt, J. S. Laberg, B. O. Hjelstuen, M. Smelror, E. Larsen, K. Andreassen, T. Eidvin, and T. O. Vorren (2009), The Plio-Pleistocene glaciation of the Barents Sea–Svalbard region: A new model based on revised chronostratigraphy, *Quat. Sci. Rev.*, *28*(9–10), 812–829, doi:10.1016/j.quascirev.2008.12.002.
Koç, N., D. Klitgaard-Kristensen, K. Hasle, C. F. Forsberg, and A. Solheim (2002), Late glacial palaeoceanography of Hinlopen Strait, northern Svalbard, *Polar Res.*, *21*(2), 307–314, doi:10.1111/j.1751-8369.2002.tb00085.x.
Krabill, W., et al. (2004), Greenland ice sheet: Increased coastal thinning, *Geophys. Res. Lett.*, *31*, L24402, doi:10.1029/2004GL021533.
Krinner, G., J. Mangerud, M. Jakobsson, M. Crucifix, C. Ritz, and J. I. Svendsen (2004), Enhanced ice sheet growth in Eurasia owing to adjacent ice-dammed lakes, *Nature*, *427*(6973), 429–432, doi:10.1038/nature02233.
Kristensen, D. K., T. L. Rasmussen, and N. Koç (2013), Palaeoceanographic changes in the northern Barents Sea during the last 16 000 years—New constraints on the last deglaciation of the Svalbard-Barents Sea ice sheet, *Boreas*, *42*(3), 798–813, doi:10.1111/j.1502-3885.2012.00307.x.
Kvasov, D. D. (1978), The Barents ice sheet as a relay regulator of glacial-interglacial alternation, *Quat. Res.*, *9*(3), 288–299, doi:10.1016/0033-5894(78)90034-0.
Laberg, J. S., and T. O. Vorren (1995), Late Weichselian submarine debris flow deposits on the Bear Island Trough Mouth Fan, *Mar. Geol.*, *127*(1–4), 45–72.
Laberg, J. S., and T. O. Vorren (1996a), The glacier-fed fan at the mouth of Storfjorden trough, western Barents Sea: A comparative study, *Geol. Rundschau*, *85*(2), 338–349, doi:10.1007/BF02422239.
Laberg, J. S., and T. O. Vorren (1996b), The Middle and Late Pleistocence evolution and the Bear Island Trough Mouth Fan, *Global Planet. Change*, *12*(1–4), 309–330, doi:10.1016/0921-8181(95)00026-7.
Laberg, J. S., K. Andreassen, J. Knies, T. O. Vorren, and M. Winsborrow (2010), Late Pliocene-Pleistocene development of the Barents Sea ice sheet, *Geology*, *38*(2), 107–110, doi:10.1130/G30193.1.
Laberg, J. S., K. Andreassen, and T. O. Vorren (2012), Late Cenozoic erosion of the high-latitude southwestern Barents Sea shelf revisited, *Geol. Soc. Am. Bull.*, *124*(1–2), 77–88, doi:10.1130/B30340.1.
Łącka, M., M. Zajączkowski, M. Forwick, and W. Szczuciński (2015), Late Weichselian and Holocene palaeoceanography of Storfjordrenna, southern Svalbard, *Clim. Past*, *11*(3), 587–603, doi:10.5194/cp-11-587-2015.
Lambeck, K. (1995), Constraints on the Late Weichselian ice sheet over the Barents Sea from observations of raised shorelines, *Quat. Sci. Rev.*, *14*(1), 1–16, doi:10.1016/0277-3791(94)00107-M.
Lambeck, K. (1996), Limits on the areal extent of the Barents Sea ice sheet in Late Weichselian time, *Global Planet. Change*, *12*(1–4), 41–51, doi:10.1016/0921-8181(95)00011-9.
Lambeck, K., A. Purcell, S. Funder, K. Kjær, E. Larsen, and P. Möller (2006), Constraints on the Late Saalian to early Middle Weichselian ice sheet of Eurasia from field data and rebound modelling, *Boreas*, *35*(3), 539–575, doi:10.1080/03009480600781875.
Lambeck, K., A. Purcell, J. Zhao, and N.-O. Svensson (2010), The Scandinavian Ice Sheet: From MIS 4 to the end of the Last Glacial Maximum, *Boreas*, *39*(2), 410–435, doi:10.1111/j.1502-3885.2010.00140.x.
Landvik, J. Y., A. Hansen, M. Kelly, O. Salvigsen, Ø. Slettemark, and O. P. Stubrup (1992), The last deglaciation and glacimarine/marine sedimentation on Barentsøya and Edgeøya, eastern Svalbard, *Lundqua Rep.*, *35*, 61–83.
Landvik, J. Y., S. Bondevik, A. Elverhøi, W. Fjeldskaar, J. Mangerud, O. Salvigsen, M. J. Siegert, J. I. Svendsen, and T. O. Vorren (1998), The Last Glacial Maximum of Svalbard and the Barents Sea Area: Ice sheet extent and configuration, *Quat. Sci. Rev.*, *17*(1–3), 43–75, doi:10.1016/S0277-3791(97)00066-8.
Landvik, J. Y., E. J. Brook, L. Gualtieri, G. Raisbeck, O. Salvigsen, and F. Yiou (2003), Northwest Svalbard during the last glaciation: Ice-free areas existed, *Geology*, *31*(10), 905–908, doi:10.1130/G19703.1.
Landvik, J. Y., Ó. Ingólfsson, J. Mienert, S. J. Lehman, A. Solheim, A. Elverhøi, and D. Ottesen (2005), Rethinking Late Weichselian ice-sheet dynamics in coastal NW Svalbard, *Boreas*, *34*(1), 7–24, doi:10.1111/j.1502-3885.2005.tb01001.x.
Landvik, J. Y., E. J. Brook, L. Gualtieri, H. Linge, G. Raisbeck, O. Salvigsen, and F. Yiou (2013), 10 Be exposure age constraints on the Late Weichselian ice-sheet geometry and dynamics in inter-ice-stream areas, western Svalbard, *Boreas*, *42*(1), 43–56, doi:10.1111/j.1502-3885.2012.00282.x.
Landvik, J. Y., H. Alexanderson, M. Henriksen, and Ó. Ingólfsson (2014), Landscape imprints of changing glacial regimes during ice-sheet build-up and decay: A conceptual model from Svalbard, *Quat. Sci. Rev.*, *92*, 258–268, doi:10.1016/j.quascirev.2013.11.023.
Larour, E., H. Seroussi, M. Morlighem, and E. Rignot (2012), Continental scale, high order, high spatial resolution, ice sheet modeling using the Ice Sheet System Model (ISSM), *J. Geophys. Res.*, *117*, F01022, doi:10.1029/2011JF002140.

Larsen, E., S. Funder, and J. Thiede (1999), Late Quaternary history of northern Russia and adjacent shelves—A synopsis, *Boreas*, *28*(1), 6–11, doi:10.1111/j.1502-3885.1999.tb00203.x.
Larsen, E., K. Kjær, I. Demidov, S. Funder, K. Grøsfjeld, M. Houmark-Nielsen, M. Jensen, H. Linge, and A. Lyså (2006), Late Pleistocene glacial and lake history of northwestern Russia, *Boreas*, *35*(3), 394–424, doi:10.1080/03009480600781958.
Lehman, S. J., and S. L. Forman (1992), Late Weichselian glacier retreat in Kongsfjorden, west Spitsbergen, Svalbard, *Quat. Res.*, *37*(2), 139–154, doi:10.1016/0033-5894(92)90078-W.
Li, Y., J. Napieralski, and J. Harbor (2008), A revised automated proximity and conformity analysis method to compare predicted and observed spatial boundaries of geologic phenomena, *Comput. Geosci.*, *34*(12), 1806–1814, doi:10.1016/j.cageo.2008.01.003.
Linge, H., E. Larsen, K. Kjær, I. Demidov, E. Brook, G. Raisbeck, and F. Yiou (2006), Cosmogenic 10Be exposure age dating across Early to Late Weichselian ice-marginal zones in northwestern Russia, *Boreas*, *35*(3), 576–586, doi:10.1080/03009480600781909.
Lubinski, D. J., S. Korsun, L. Polyak, S. L. Forman, S. J. Lehman, F. A. Herlihy, and G. H. Miller (1996), The last deglaciation of the Franz Victoria Trough, northern Barents Sea, *Boreas*, *25*(2), 89–100, doi:10.1111/j.1502-3885.1996.tb00838.x.
Lubinski, D. J., S. L. Forman, and G. H. Miller (1999), Holocene glacier and climate fluctuations on Franz Josef Land, Arctic Russia, 80°N, *Quat. Sci. Rev.*, *18*(1), 85–108, doi:10.1016/S0277-3791(97)00105-4.
Lucchi, R. G., et al. (2013), Postglacial sedimentary processes on the Storfjorden and Kveithola trough mouth fans: Significance of extreme glacimarine sedimentation, *Global Planet. Change*, *111*, 309–326, doi:10.1016/j.gloplacha.2013.10.008.
Lundqvist, J. (2004), Glacial history of Sweden, in *Quaternary Glaciations—Extent and Chronology Part 1: Europe*, edited by J. Ehlers and P. L. Gibbard, pp. 401–412, Elsevier B.V, Amsterdam.
Mahaffy, M. W. (1976), A three-dimensional numerical-model of ice sheets: Tests on Barnes Ice Cap, Northwest Territories, *J. Geophys. Res.*, *81*(6), 1059–1066, doi:10.1029/JC081i006p01059.
Mangerud, J. (2004), Ice sheet limits in Norway and on the Norwegian continental shelf, in *Quaternary Glaciations—Extent and Chronology Part 1: Europe2*, edited by J. Ehlers and P. L. Gibbard, pp. 271–294, Elsevier B.V, Amsterdam.
Mangerud, J., and J. I. Svendsen (1990), Deglaciation chronology inferred from marine sediments in a proglacial lake basin, western Spitsbergen, Svalbard, *Boreas*, *19*(3), 249–272, doi:10.1111/j.1502-3885.1990.tb00450.x.
Mangerud, J., and J. I. Svendsen (1992), The last interglacial-glacial period on spitsbergen, Svalbard, *Quat. Sci. Rev.*, *11*(6), 633–664, doi:10.1016/0277-3791(92)90075-J.
Mangerud, J., and J. Y. Landvik (2007), Younger Dryas cirque glaciers in western Spitsbergen: Smaller than during the Little Ice Age, *Boreas*, *36*(3), 278–285, doi:10.1111/j.1502-3885.2007.tb01250.x.
Mangerud, J., M. Bolstad, A. Elgersma, D. Helliksen, J. Y. Landvik, I. Lønne, A. K. Lycke, O. Salvigsen, T. Sandahl, and J. I. Svendsen (1992), The Last Glacial Maximum on Spitsbergen, Svalbard, *Quat. Res.*, *38*(1), 1–31, doi:10.1016/0033-5894(92)90027-G.
Mangerud, J., T. Dokken, D. Hebbeln, B. Heggen, Ó. Ingólfsson, J. Y. Landvik, V. Mejdahl, J. I. Svendsen, and T. O. Vorren (1998), Fluctuations of the Svalbard-Barents sea ice sheet during the last 150 000 years, *Quat. Sci. Rev.*, *17*(1–3), 11–42, doi:10.1016/S0277-3791(97)00069-3.
Mangerud, J., J. I. Svendsen, and V. I. Astakhov (1999), Age and extent of the Barents and Kara ice sheets in Northern Russia, *Boreas*, *28*(1), 46–80, doi:10.1111/j.1502-3885.1999.tb00206.x.
Mangerud, J., V. Astakhov, M. Jakobsson, and J. I. Svendsen (2001a), Huge Ice-age lakes in Russia, *J. Quat. Sci.*, *16*(8), 773–777, doi:10.1002/jqs.661.
Mangerud, J., V. I. Astakhov, A. Murray, and J. I. Svendsen (2001b), The chronology of a large ice-dammed lake and the Barents–Kara Ice Sheet advances, Northern Russia, *Global Planet. Change*, *31*(1–4), 321–336, doi:10.1016/S0921-8181(01)00127-8.
Mangerud, J., V. Astakhov, and J.-I. Svendsen (2002), The extent of the Barents–Kara ice sheet during the Last Glacial Maximum, *Quat. Sci. Rev.*, *21*(1–3), 111–119, doi:10.1016/S0277-3791(01)00088-9.
Mangerud, J., et al. (2004), Ice-dammed lakes and rerouting of the drainage of northern Eurasia during the Last Glaciation, *Quat. Sci. Rev.*, *23*(11–13), 1313–1332, doi:10.1016/j.quascirev.2003.12.009.
Mangerud, J., S. Bondevik, S. Gulliksen, A. Karin Hufthammer, and T. Høisæter (2006), Marine 14C reservoir ages for 19th century whales and molluscs from the North Atlantic, *Quat. Sci. Rev.*, *25*(23–24), 3228–3245, doi:10.1016/j.quascirev.2006.03.010.
Mangerud, J., J. Gosse, A. Matiouchkov, and T. Dolvik (2008a), Glaciers in the Polar Urals, Russia, were not much larger during the Last Global Glacial Maximum than today, *Quat. Sci. Rev.*, *27*(9–10), 1047–1057, doi:10.1016/j.quascirev.2008.01.015.
Mangerud, J., D. Kaufman, J. Hansen, and J. I. Svendsen (2008b), Ice-free conditions in Novaya Zemlya 35 000–30 000 cal years B.P., as indicated by radiocarbon ages and amino acid racemization evidence from marine molluscs, *Polar Res.*, *27*(2), 187–208, doi:10.3402/polar.v27i2.6176.
Mann, D. H., R. S. Sletten, and F. C. Ugolini (1986), Soil development at Kongsfjorden, Spitsbergen, *Polar Res.*, *4*(1), 1–16, doi:10.1111/j.1751-8369.1986.tb00513.x.
Marsiat, I., and P. J. Valdes (2001), Sensitivity of the Northern Hemisphere climate of the Last Glacial Maximum to sea surface temperatures, *Clim. Dyn.*, *17*(2–3), 233–248, doi:10.1007/s003820000108.
Martrat, B., J. O. Grimalt, J. Villanueva, S. van Kreveld, and M. Sarnthein (2003), Climatic dependence of the organic matter contributions in the north eastern Norwegian Sea over the last 15,000 years, *Org. Geochem.*, *34*(8), 1057–1070, doi:10.1016/S0146-6380(03)00084-6.
Mattingsdal, R., J. Knies, K. Andreassen, K. Fabian, K. Husum, K. Grøsfjeld, and S. De Schepper (2014), A new 6 Myr stratigraphic framework for the Atlantic–Arctic Gateway, *Quat. Sci. Rev.*, *92*, 170–178, doi:10.1016/j.quascirev.2013.08.022.
Miller, G. H., H. P. Sejrup, S. J. Lehman, and S. L. Forman (1989), Glacial history and marine environmental change during the last interglacial-glacial cycle, western Spitsbergen, Svalbard, *Boreas*, *18*(3), 273–296.
Möller, P., et al. (2006), Severnaya Zemlya, Arctic Russia: A nucleation area for Kara Sea ice sheets during the Middle to Late Quaternary, *Quat. Sci. Rev.*, *25*(21–22), 2894–2936, doi:10.1016/j.quascirev.2006.02.016.
Möller, P., J. Anjar, and A. S. Murray (2013), An OSL-dated sediment sequence at Idre, west-central Sweden, indicates ice-free conditions in MIS 3, *Boreas*, *42*(1), 25–42, doi:10.1111/j.1502-3885.2012.00284.x.
Möller, P., H. Alexanderson, S. Funder, and C. Hjort (2015), The Taimyr Peninsula and the Severnaya Zemlya archipelago, Arctic Russia: A synthesis of glacial history and palaeo-environmental change during the Last Glacial cycle (MIS 5e–2), *Quat. Sci. Rev.*, *107*, 149–181, doi:10.1016/j.quascirev.2014.10.018.
Müller, J., and R. Stein (2014), High-resolution record of late glacial and deglacial sea ice changes in Fram Strait corroborates ice–ocean interactions during abrupt climate shifts, *Earth Planet. Sci. Lett.*, *403*, 446–455, doi:10.1016/j.epsl.2014.07.016.
Murton, J., M. Bateman, and S. Dallimore (2010), Identification of Younger Dryas outburst flood path from Lake Agassiz to the Arctic Ocean, *Nature*, *464*, 740–743, doi:10.1038/nature08954.
Napieralski, J., A. Hubbard, Y. Li, J. Harbor, A. P. Stroeven, J. Kleman, G. Alm, and K. N. Jansson (2007), Towards a GIS assessment of numerical ice-sheet model performance using geomorphological data, *J. Glaciol.*, *53*(180), 71–83, doi:10.3189/172756507781833884.
Nesje, A. (2009), Latest Pleistocene and Holocene alpine glacier fluctuations in Scandinavia, *Quat. Sci. Rev.*, *28*(21–22), 2119–2136, doi:10.1016/j.quascirev.2008.12.016.

Nygård, A., H. P. Sejrup, H. Haflidason, W. A. H. Lekens, C. D. Clark, and G. R. Bigg (2007), Extreme sediment and ice discharge from marine-based ice streams: New evidence from the North Sea, *Geology*, *35*(5), 395–398, doi:10.1130/G23364A.1.
Ó Cofaigh, C., J. Taylor, J. A. Dowdeswell, and C. J. Pudsey (2003), Palaeo-ice streams, trough mouth fans and high-latitude continental slope sedimentation, *Boreas*, *32*(1), 37–55.
Ó Cofaigh, C., J. A. Dowdeswell, J. Evans, and R. D. Larter (2008), Geological constraints on Antarctic palaeo-ice-stream retreat, *Earth Surf. Processes Landforms*, *33*(4), 513–525.
Ó Cofaigh, C., D. J. A. Evans, and I. R. Smith (2010), Large-scale reorganization and sedimentation of terrestrial ice streams during late Wisconsinan Laurentide Ice Sheet deglaciation, *Geol. Soc. Am. Bull.*, *122*(5–6), 743–756, doi:10.1130/B26476.1.
O'Regan, M., M. Jakobsson, and N. Kirchner (2010), Glacial geological implications of overconsolidated sediments on the Lomonosov Ridge and Yermak Plateau, *Quat. Sci. Rev.*, *29*(25–26), 3532–3544, doi:10.1016/j.quascirev.2010.09.009.
Olsen, L. (2010), A buried late MIS 3 shoreline in northern Norway—Implications for ice extent and volume, *Norges Geol. Undersøkelse Bull.*, *450*, 1–14.
Ottesen, D., and J. A. Dowdeswell (2009), An inter-ice-stream glaciated margin: Submarine landforms and a geomorphic model based on marine-geophysical data from Svalbard, *Geol. Soc. Am. Bull.*, *121*(11–12), 1647–1665, doi:10.1130/B26467.1.
Ottesen, D., J. A. Dowdeswell, L. Rise, K. Rokoengen, and S. Henriksen (2002), Large-scale morphological evidence for past ice-stream flow on the mid-Norwegian continental margin, *Geol. Soc. London, Spec. Publ.*, *203*(1), 245–258.
Ottesen, D., J. A. Dowdeswell, and L. Rise (2005), Submarine landforms and the reconstruction of fast-flowing ice streams within a large Quaternary ice sheet: The 2500-km-long Norwegian-Svalbard margin (57°–80°N), *Geol. Soc. Am. Bull.*, *117*(7), 1033–1050, doi:10.1130/B25577.1.
Ottesen, D., J. A. Dowdeswell, J. Y. Landvik, and J. Mienert (2007), Dynamics of the Late Weichselian ice sheet on Svalbard inferred from high-resolution sea-floor morphology, *Boreas*, *36*(3), 286–306.
Pattyn, F. (2003), A new three-dimensional higher-order thermomechanical ice sheet model: Basic sensitivity, ice stream development, and ice flow across subglacial lakes, *J. Geophys. Res.*, *108*(B8), 2382, doi:10.1029/2002JB002329.
Pattyn, F., A. Huyghe, S. De Brabander, and B. De Smedt (2006), Role of transition zones in marine ice sheet dynamics, *J. Geophys. Res.*, *111*, F02004, doi:10.1029/2005JF000394.
Pattyn, F., et al. (2008), Benchmark experiments for higher-order and full-Stokes ice sheet models (ISMIP–HOM), *Cryosphere*, *2*(2), 95–108, doi:10.5194/tc-2-95-2008.
Pattyn, F., et al. (2012), Results of the Marine Ice Sheet Model Intercomparison Project, MISMIP, *Cryosphere*, *6*(3), 573–588, doi:10.5194/tc-6-573-2012.
Pausata, F. S. R., C. Li, J. J. Wettstein, M. Kageyama, and K. H. Nisancioglu (2011), The key role of topography in altering North Atlantic atmospheric circulation during the last glacial period, *Clim. Past*, *7*(4), 1089–1101, doi:10.5194/cp-7-1089-2011.
Payne, A. J., and P. W. Dongelmans (1997), Self-organization in the thermomechanical flow of ice sheets, *J. Geophys. Res.*, *102*(B6), 12,219–12,233, doi:10.1029/97JB00513.
Peltier, W. R. (2004), Global glacial isostasy and the surface of the ice-age Earth: The ICE-5G (VM2) Model and GRACE, *Annu. Rev. Earth Planet. Sci.*, *32*(1), 111–149, doi:10.1146/annurev.earth.32.082503.144359.
Peltier, W. R., and R. G. Fairbanks (2006), Global glacial ice volume and Last Glacial Maximum duration from an extended Barbados sea level record, *Quat. Sci. Rev.*, *25*(23–24), 3322–3337, doi:10.1016/j.quascirev.2006.04.010.
Peltier, W. R., D. F. Argus, and R. Drummond (2015), Space geodesy constrains ice age terminal deglaciation: The global ICE-6G_C (VM5a) model, *J. Geophys. Res. Solid Earth*, *120*, 450–487, doi:10.1002/2014JB011176.
Peyaud, V., C. Ritz, and G. Krinner (2007), Modelling the Early Weichselian Eurasian Ice Sheets: Role of ice shelves and influence of ice-dammed lakes, *Clim. Past*, *3*, 375–386, doi:10.5194/cp-3-375-2007.
Polyak, L., and A. Solheim (1994), Late-and postglacial environments in the northern Barents Sea west of Franz Josef Land, *Polar Res.*, *13*(2), 197–207, doi:10.1111/j.1751-8369.1994.tb00449.x.
Polyak, L., S. J. Lehman, V. Gataullin, and A. J. Timothy Jull (1995), Two-step deglaciation of the southeastern Barents Sea, *Geology*, *23*(6), 567–571, doi:10.1130/0091-7613(1995)023.
Polyak, L., S. L. Forman, F. A. Herlihy, G. Ivanov, and P. Krinitsky (1997), Late Weichselian deglacial history of the Svyataya (Saint) Anna Trough, northern Kara Sea, Arctic Russia, *Mar. Geol.*, *143*(1–4), 169–188, doi:10.1016/S0025-3227(97)00096-0.
Polyak, L., V. Gataullin, O. Okuneva, and V. Stelle (2000), New constraints on the limits of the Barents-Kara ice sheet during the Last Glacial Maximum based on borehole stratigraphy from the Pechora Sea, *Geology*, *28*(7), 611–614, doi:10.1130/0091-7613(2000)28.
Polyak, L., M. H. Edwards, B. J. Coakley, and M. Jakobsson (2001), Ice shelves in the Pleistocene Arctic Ocean inferred from glaciogenic deep-sea bedforms, *Nature*, *410*(6827), 453–457, doi:10.1038/35068536.
Polyak, L., M. Levitan, T. Khusid, L. Merklin, and V. Mukhina (2002), Variations in the influence of riverine discharge on the Kara Sea during the last deglaciation and the Holocene, *Global Planet. Change*, *32*(4), 291–309, doi:10.1016/S0921-8181(02)00072-3.
Polyak, L., F. Niessen, V. Gataullin, and V. Gainanov (2008), The eastern extent of the Barents-Kara ice sheet during the Last Glacial Maximum based on seismic-reflection data from the eastern Kara Sea, *Polar Res.*, *27*(2), 162–174, doi:10.1111/j.1751-8369.2008.00061.x.
Pritchard, H. D., R. J. Arthern, D. G. Vaughan, and L. A. Edwards (2009), Extensive dynamic thinning on the margins of the Greenland and Antarctic ice sheets, *Nature*, *461*(7266), 971–975, doi:10.1038/nature08471.
Pritchard, H. D., S. R. M. Ligtenberg, H. A. Fricker, D. G. Vaughan, M. R. van den Broeke, and L. Padman (2012), Antarctic ice-sheet loss driven by basal melting of ice shelves, *Nature*, *484*(7395), 502–5, doi:10.1038/nature10968.
Raab, A. (2003), Non-glacial paleoenvironments and the extent of Weichselian ice sheets on Severnaya Zemlya, Russian High Arctic, *Quat. Sci. Rev.*, *22*(21–22), 2267–2283, doi:10.1016/S0277-3791(03)00139-2.
Rasmussen, T. L., and E. Thomsen (2008), Warm Atlantic surface water inflow to the Nordic seas 34–10 calibrated ka B.P, *Paleoceanography*, *23*, PA1201, doi:10.1029/2007PA001453.
Rasmussen, T. L., and E. Thomsen (2014), Brine formation in relation to climate changes and ice retreat during the last 15,000 years in Storfjorden, Svalbard, 76–78°N, *Paleoceanography*, *29*, 911–929, doi:10.1002/2014PA002643.
Rasmussen, T. L., E. Thomsen, M. A. Ślubowska, S. Jessen, A. Solheim, and N. Koç (2007), Paleoceanographic evolution of the SW Svalbard margin (76°N) since 20,000 14C yr BP, *Quat. Res.*, *67*(1), 100–114, doi:10.1016/j.yqres.2006.07.002.
Rasmussen, T. L., E. Thomsen, K. Skirbekk, M. Ślubowska-Woldengen, D. Klitgaard Kristensen, and N. Koç (2014), Spatial and temporal distribution of Holocene temperature maxima in the northern Nordic seas: Interplay of Atlantic-, Arctic- and polar water masses, *Quat. Sci. Rev.*, *92*, 280–291, doi:10.1016/j.quascirev.2013.10.034.
Rebesco, M., et al. (2011), Deglaciation of the western margin of the Barents Sea ice sheet—A swath bathymetric and sub-bottom seismic study from the Kveithola Trough, *Mar. Geol.*, *279*(1–4), 141–147, doi:10.1016/j.margeo.2010.10.018.

Rebesco, M., J. S. Laberg, M. T. Pedrosa, A. Camerlenghi, R. G. Lucchi, F. Zgur, and N. Wardell (2014), Onset and growth of trough-mouth fans on the North-Western Barents Sea margin—Implications for the evolution of the Barents Sea/Svalbard Ice Sheet, *Quat. Sci. Rev.*, *92*, 227–234, doi:10.1016/j.quascirev.2013.08.015.

Reeh, N., H. H. Thomsen, A. K. Higgins, and A. Weidick (2001), Sea ice and the stability of north and northeast Greenland floating glaciers, *Ann. Glaciol.*, *33*(1), 474–480, doi:10.3189/172756401781818554.

Reimer, P., et al. (2013), IntCal13 and Marine13 radiocarbon age calibration curves 0–50,000 years cal BP, *Radiocarbon*, *55*(4), 1869–1887, doi:10.2458/azu_js_rc.55.16947.

Renssen, H., R. F. B. Isarin, D. Jacob, R. Podzun, and J. Vandenberghe (2001), Simulation of the Younger Dryas climate in Europe using a regional climate model nested in an AGCM: Preliminary results, *Global Planet. Change*, *30*(1–2), 41–57, doi:10.1016/S0921-8181(01)00076-5.

Reusche, M., et al. (2014), ^{10}Be surface exposure ages on the late-Pleistocene and Holocene history of Linnébreen on Svalbard, *Quat. Sci. Rev.*, *89*, 5–12, doi:10.1016/j.quascirev.2014.01.017.

Rignot, E. (2008), Changes in West Antarctic ice stream dynamics observed with ALOS PALSAR data, *Geophys. Res. Lett.*, *35*, L12505, doi:10.1029/2008GL033365.

Rignot, E., D. G. Vaughan, M. Schmeltz, T. Dupont, and D. MacAyeal (2002), Acceleration of Pine Island and Thwaites Glaciers, West Antarctica, *Ann. Glaciol.*, *34*(1), 189–194, doi:10.3189/172756402781817950.

Rignot, E., I. Velicogna, M. R. van den Broeke, A. Monaghan, and J. Lenaerts (2011), Acceleration of the contribution of the Greenland and Antarctic ice sheets to sea level rise, *Geophys. Res. Lett.*, *38*, L05503, doi:10.1029/2011GL046583.

Rippin, D. M., D. G. Vaughan, and H. F. J. Corr (2011), The basal roughness of Pine Island Glacier, West Antarctica, *J. Glaciol.*, *57*(201), 67–76, doi:10.3189/002214311795306574.

Ritzmann, O., N. Maercklin, J. Inge Faleide, H. Bungum, W. D. Mooney, and S. T. Detweiler (2007), A three-dimensional geophysical model of the crust in the Barents Sea region: Model construction and basement characterization, *Geophys. J. Int.*, *170*(1), 417–435, doi:10.1111/j.1365-246X.2007.03337.x.

Rüther, D. C., R. Mattingsdal, K. Andreassen, M. Forwick, and K. Husum (2011), Seismic architecture and sedimentology of a major grounding zone system deposited by the Bjørnøyrenna Ice Stream during Late Weichselian deglaciation, *Quat. Sci. Rev.*, *30*(19–20), 2776–2792, doi:10.1016/j.quascirev.2011.06.011.

Rüther, D. C., L. R. Bjarnadóttir, J. Junttila, K. Husum, T. L. Rasmussen, R. G. Lucchi, and K. Andreassen (2012), Pattern and timing of the northwestern Barents Sea ice sheet deglaciation and indications of episodic Holocene deposition, *Boreas*, *41*(3), 494–512, doi:10.1111/j.1502-3885.2011.00244.x.

Rüther, D. C., K. Andreassen, and M. Spagnolo (2013), Aligned glaciotectonic rafts on the central Barents Sea seafloor revealing extensive glacitectonic erosion during the last deglaciation, *Geophys. Res. Lett.*, *40*, 6351–6355, doi:10.1002/2013GL058413.

Sættem, J., D. A. R. Poole, L. Ellingsen, and H. P. Sejrup (1992), Glacial geology of outer Bjørnøyrenna, southwestern Barents Sea, *Mar. Geol.*, *103*(1–3), 15–51, doi:10.1016/0025-3227(92)90007-5.

Salvigsen, O. (1977), *Radiocarbon Datings and the Extension of the Weichselian Ice-sheet in Svalbard*, Norsk Polarinstitutt Arbok, Oslo.

Salvigsen, O. (1979), The last deglaciation of Svalbard, *Boreas*, *8*, 229–231.

Salvigsen, O. (1981), Radiocarbon dated raised beaches in Kong Karls Land, Svalbard, and their consequences for the glacial history of the Barents Sea area, *Geogr. Ann. Ser. A*, *63*(3/4), 283–291.

Salvigsen, O., and J. Mangerud (1991), Holocene shoreline displacement at Agardhbukta, eastern Spitsbergen, Svalbard, *Polar Res.*, *9*(1), 1–7, doi:10.1111/j.1751-8369.1991.tb00398.x.

Salvigsen, O., L. Adrielsson, C. Hjort, M. Kelly, J. Y. Landvik, and L. Ronnert (1995), Dynamics of the last glaciation in eastern Svalbard as inferred from glacier-movement indicators, *Polar Res.*, *14*(2), 141–152, doi:10.1111/j.1751-8369.1995.tb00686.x.

Scambos, T. A., J. A. Bohlander, C. A. Shuman, and P. Skvarca (2004), Glacier acceleration and thinning after ice shelf collapse in the Larsen B embayment, Antarctica, *Geophys. Res. Lett.*, *31*, L18402, doi:10.1029/2004GL020670.

Scherer, R. P. (1998), Pleistocene collapse of the West Antarctic ice sheet, *Science*, *281*(5373), 82–85, doi:10.1126/science.281.5373.82.

Schoof, C. (2007), Ice sheet grounding line dynamics: Steady states, stability, and hysteresis, *J. Geophys. Res.*, *112*, F03S28, doi:10.1029/2006JF000664.

Schytt, V., G. Hoppe, W. Blake Jr., and M. G. Grosswald (1968), The extent of the Würm glaciation in the European Arctic: A preliminary report about the Stockholm University Svalbard Expedition 1966, International Association of Scientific Hydrology, General Assembly in Bern 1967, Publ. 79, pp. 207–216.

Scourse, J. D., A. I. Haapaniemi, E. Colmenero-Hidalgo, V. L. Peck, I. R. Hall, W. E. N. Austin, P. C. Knutz, and R. Zahn (2009), Growth, dynamics and deglaciation of the last British–Irish ice sheet: The deep-sea ice-rafted detritus record, *Quat. Sci. Rev.*, *28*(27–28), 3066–3084, doi:10.1016/j.quascirev.2009.08.009.

Sejrup, H. P., E. Larsen, J. Landvik, E. L. King, H. Haflidason, and A. Nesje (2000), Quaternary glaciations in southern Fennoscandia: Evidence from southwestern Norway and the northern North Sea region, *Quat. Sci. Rev.*, *19*(7), 667–685, doi:10.1016/S0277-3791(99)00016-5.

Serebryanny, L., A. Andreev, E. Malyasova, P. Tarasov, and F. Romanenko (1998), Lateglacial and early-Holocene environments of Novaya Zemlya and the Kara Sea Region of the Russian Arctic, *Holocene*, *8*(3), 323–330, doi:10.1191/095968398677085532.

Shakun, J. D., P. U. Clark, F. He, S. A. Marcott, A. C. Mix, Z. Liu, B. Otto-Bliesner, A. Schmittner, and E. Bard (2012), Global warming preceded by increasing carbon dioxide concentrations during the last deglaciation, *Nature*, *484*(7392), 49–54, doi:10.1038/nature10915.

Shaw, J., D. J. W. Piper, G. B. J. Fader, E. L. King, B. J. Todd, T. Bell, M. J. Batterson, and D. G. E. Liverman (2006), A conceptual model of the deglaciation of Atlantic Canada, *Quat. Sci. Rev.*, *25*(17–18), 2059–2081, doi:10.1016/j.quascirev.2006.03.002.

Shepherd, A., D. J. Wingham, and J. A. D. Mansley (2002), Inland thinning of the Amundsen Sea sector, West Antarctica, *Geophys. Res. Lett.*, *29*(10), 1364, doi:10.1029/2001GL014183.

Shepherd, A., D. Wingham, and E. Rignot (2004), Warm ocean is eroding West Antarctic Ice Sheet, *Geophys. Res. Lett.*, *31*, L23402, doi:10.1029/2004GL021106.

Siegert, M. J., and I. Marsiat (2001), Numerical reconstructions of LGM climate across the Eurasian Arctic, *Quat. Sci. Rev.*, *20*(15), 1595–1605, doi:10.1016/S0277-3791(01)00017-8.

Siegert, M. J., and J. A. Dowdeswell (1996), Topographic control on the dynamics of the Svalbard-Barents Sea ice sheet, *Global Planet. Change*, *12*(1–4), 27–39, doi:10.1016/0921-8181(95)00010-0.

Siegert, M. J., and J. A. Dowdeswell (2002), Late Weichselian iceberg, surface-melt and sediment production from the Eurasian Ice Sheet: Results from numerical ice-sheet modelling, *Mar. Geol.*, *188*(1–2), 109–127.

Siegert, M. J., and J. A. Dowdeswell (2004), Numerical reconstructions of the Eurasian Ice Sheet and climate during the Late Weichselian, *Quat. Sci. Rev.*, *23*(11–13), 1273–1283, doi:10.1016/j.quascirev.2003.12.010.

Siegert, M. J., J. A. Dowdeswell, and M. Melles (1999), Late Weichselian Glaciation of the Russian High Arctic, *Quat. Res.*, *52*(3), 273–285, doi:10.1006/qres.1999.2082.
Siegert, M. J., J. A. Dowdeswell, M. Hald, and J.-I. Svendsen (2001), Modelling the Eurasian Ice Sheet through a full (Weichselian) glacial cycle, *Global Planet. Change*, *31*(1–4), 367–385, doi:10.1016/S0921-8181(01)00130-8.
Skirbekk, K., D. K. Kristensen, T. L. Rasmussen, N. Koc, and M. Forwick (2010), Holocene climate variations at the entrance to a warm Arctic fjord: Evidence from Kongsfjorden trough, Svalbard, *Geol. Soc. London, Spec. Publ.*, *344*(1), 289–304, doi:10.1144/SP344.20.
Ślubowska, M. A., N. Koç, T. L. Rasmussen, and D. Klitgaard-Kristensen (2005), Changes in the flow of Atlantic water into the Arctic Ocean since the last deglaciation: Evidence from the northern Svalbard continental margin, 80°N, *Paleoceanography*, *20*, PA4014, doi:10.1029/2005PA001141.
Ślubowska-Woldengen, M., T. L. Rasmussen, N. Koç, D. Klitgaard-Kristensen, F. Nilsen, and A. Solheim (2007), Advection of Atlantic Water to the western and northern Svalbard shelf since 17,500 cal yr BP, *Quat. Sci. Rev.*, *26*(3–4), 463–478, doi:10.1016/j.quascirev.2006.09.009.
Snyder, J. A., S. L. Forman, W. N. Mode, and G. A. Tarasov (1997), Postglacial relative sea-level history: Sediment and diatom records of emerged coastal lakes, north-central Kola Peninsula, Russia, *Boreas*, *26*(4), 329–346, doi:10.1111/j.1502-3885.1997.tb00859.x.
Solheim, A., and A. Elverhøi (1993), Gas-related sea floor craters in the Barents Sea, *Geo-Mar. Lett.*, *13*(4), 235–243, doi:10.1007/BF01207753.
Solheim, A., L. Russwurm, A. Elverhøi, and M. Nyland-Berg (1990), Glacial geomorphic features in the northern Barents Sea: Direct evidence for grounded ice and implications for the pattern of deglaciation and late glacial sedimentation, in *Glacimarine Environments: Processes and Sediments*, edited by J. A. Dowdeswell and J. D. Scourse, pp. 253–268, Geol. Soc., London.
Sollid, J. L., S. Andersen, N. Hamre, O. Kjeldsen, O. Salvigsen, S. Sturød, T. Tveitå, and A. Wilhelmsen (1973), Deglaciation of Finnmark, North Norway, *Nor. Geogr. Tidsskr. - Nor. J. Geogr.*, *27*(4), 233–325, doi:10.1080/00291951.1973.9728306.
Stein, R., B. Boucsein, K. Fahl, T. Garcia de Oteyza, J. Knies, and F. Niessen (2001), Accumulation of particulate organic carbon at the Eurasian continental margin during late Quaternary times: Controlling mechanisms and paleoenvironmental significance, *Global Planet. Change*, *31*(1–4), 87–104, doi:10.1016/S0921-8181(01)00114-X.
Stein, R., F. Niessen, K. Dittmers, M. Levitan, F. Schoster, J. Simstich, T. Steinke, and O. V. Stepanets (2002), Siberian river run-off and late Quaternary glaciation in the southern Kara Sea, Arctic Ocean: Preliminary results, *Polar Res.*, *21*(2), 315–322, doi:10.1111/j.1751-8369.2002.tb00086.x.
Stokes, C. R., and C. D. Clark (2002), Are long subglacial bedforms indicative of fast ice flow?, *Boreas*, *31*(3), 239–249, doi:10.1111/j.1502-3885.2002.tb01070.x.
Stokes, C. R., G. D. Corner, M. C. M. Winsborrow, K. Husum, and K. Andreassen (2014), Asynchronous response of marine-terminating outlet glaciers during deglaciation of the Fennoscandian Ice Sheet, *Geology*, *42*(5), 455–458, doi:10.1130/G35299.1.
Stokes, C. R., et al. (2015), On the reconstruction of palaeo-ice sheets: Recent advances and future challenges, *Quat. Sci. Rev.*, *125*, 15–49, doi:10.1016/j.quascirev.2015.07.016.
Stokes, C., C. Clark, and R. Storrar (2009), Major changes in ice stream dynamics during deglaciation of the north-western margin of the Laurentide Ice Sheet, *Quat. Sci. Rev.*, *28*(7–8), 721–738, doi:10.1016/j.quascirev.2008.07.019.
Stuiver, M., and P. Reimer (1993), Extended ^{14}C data base and revised Calib 3.0 ^{14}C age calibration program, *Radiocarbon*, *35*(1), 215–230.
Svendsen, J. I., and J. Mangerud (1992), Paleoclimatic inferences from glacial fluctuations on Svalbard during the last 20 000 years, *Clim. Dyn.*, *6*(3), 213–220, doi:10.1007/BF00193533.
Svendsen, J. I., J. Mangerud, A. Elverhøi, A. Solheim, and R. T. Schüttenhelm (1992), The Late Weichselian glacial maximum on western Spitsbergen inferred from offshore sediment cores, *Mar. Geol.*, *104*(1–4), 1–17, doi:10.1016/0025-3227(92)90081-R.
Svendsen, J. I., et al. (1999), Maximum extent of the Eurasian ice sheets in the Barents and Kara Sea region during the Weichselian, *Boreas*, *28*(1), 234–242, doi:10.1111/j.1502-3885.1999.tb00217.x.
Svendsen, J. I., et al. (2004a), Late Quaternary ice sheet history of northern Eurasia, *Quat. Sci. Rev.*, *23*(11–13), 1229–1271, doi:10.1016/j.quascirev.2003.12.008.
Svendsen, J. I., V. Gataullin, J. Mangerud, and L. Polyak (2004b), The glacial history of the Barents and Kara Sea region, in *Quaternary Glaciations—Extent and Chronology Part 1: Europe*, edited by J. Ehlers and P. L. Gibbard, Elsevier B.V., Amsterdam.
Svendsen, J. I., L. C. Krüger, J. Mangerud, V. I. Astakhov, A. Paus, D. Nazarov, and A. Murray (2014), Glacial and vegetation history of the Polar Ural Mountains in northern Russia during the Last Ice Age, Marine Isotope Stages 5–2, *Quat. Sci. Rev.*, *92*, 409–428, doi:10.1016/j.quascirev.2013.10.008.
Tarasov, L., A. S. Dyke, R. M. Neal, and W. R. Peltier (2012), A data-calibrated distribution of deglacial chronologies for the North American ice complex from glaciological modeling, *Earth Planet. Sci. Lett.*, *315–316*, 30–40, doi:10.1016/j.epsl.2011.09.010.
Tarasov, P. E., O. Peyron, J. Guiot, S. Brewer, V. S. Volkova, L. G. Bezusko, N. I. Dorofeyuk, E. V. Kvavadze, I. M. Osipova, and N. K. Panova (1999), Last Glacial Maximum climate of the former Soviet Union and Mongolia reconstructed from pollen and plant macrofossil data, *Clim. Dyn.*, *15*(3), 227–240, doi:10.1007/s003820050278.
Thiede, J., et al. (2004), What was QUEEN? Its history and international framework—An introduction to its final synthesis issue, *Quat. Sci. Rev.*, *23*(11–13), 1225–1227, doi:10.1016/j.quascirev.2003.12.006.
Thomas, R. H., and C. R. Bentley (1978), Model for Holocene retreat of West Antarctic ice sheet, *Quat. Res.*, *10*(2), 150–170.
Thomas, R. H., W. Abdalati, E. Frederick, W. B. Krabill, S. Manizade, and K. Steffen (2003), Investigation of surface melting and dynamic thinning on Jakobshavn Isbrae, Greenland, *J. Glaciol.*, *49*(165), 231–239, doi:10.3189/172756503781830764.
Thomas, R., E. Frederick, W. Krabill, S. Manizade, and C. Martin (2009), Recent changes on Greenland outlet glaciers, *J. Glaciol.*, *55*(189), 147–162, doi:10.3189/002214309788608958.
Truffer, M., and K. A. Echelmeyer (2003), Of Isbræ and ice streams, *Ann. Glaciol.*, *36*, 66–72.
Ukkonen, P., J. P. Lunkka, H. Jungner, and J. Donner (1999), New radiocarbon dates from Finnish mammoths indicating large ice-free areas in Fennoscandia during the Middle Weichselian, *J. Quat. Sci.*, *14*(7), 711–714.
Ukkonen, P., L. Arppe, M. Houmark-Nielsen, K. H. Kjær, and J. A. Karhu (2007), MIS 3 mammoth remains from Sweden—Implications for faunal history, palaeoclimate and glaciation chronology, *Quat. Sci. Rev.*, *26*(25–28), 3081–3098, doi:10.1016/j.quascirev.2007.06.021.
Vasil'chuk, Y., J.-M. Punning, and A. Vasil'chuk (1997), Radiocarbon ages of mammoths in northern Eurasia: Implications for population development and late Quaternary environment, *Radiocarbon*, *39*(1), 1–18.
Vaughan, D. G. (2008), West Antarctic Ice Sheet collapse—The fall and rise of a paradigm, *Clim. Change*, *91*(1–2), 65–79, doi:10.1007/s10584-008-9448-3.
Vaughan, D. G., H. F. J. Corr, A. M. Smith, H. D. Pritchard, and A. Shepherd (2008), Flow-switching and water piracy between Rutford Ice Stream and Carlson Inlet, West Antarctica, *J. Glaciol.*, *54*(184), 41–48, doi:10.3189/002214308784409125.
Velichko, A. A., Y. M. Kononov, and M. A. Faustova (1997), The last glaciation of earth: Size and volume of ice-sheets, *Quat. Int.*, *41–42*, 43–51, doi:10.1016/S1040-6182(96)00035-3.
Vogt, C., J. Knies, R. F. Spielhagen, and R. Stein (2001), Detailed mineralogical evidence for two nearly identical glacial/deglacial cycles and Atlantic water advection to the Arctic Ocean during the last 90,000 years, *Global Planet. Change*, *31*(1–4), 23–44, doi:10.1016/S0921-8181(01)00111-4.

Vogt, P. R., K. Crane, and E. Sundvor (1994), Deep Pleistocene iceberg plowmarks on the Yermak Plateau: Sidescan and 3.5 kHz evidence for thick calving ice fronts and a possible marine ice sheet in the Arctic Ocean, *Geology*, *22*(5), 403–406, doi:10.1130/0091-7613(1994)022.

Vorren, T. O., and J. S. Laberg (1997), Trough mouth fans—Palaeoclimate and ice-sheet monitors, *Quat. Sci. Rev.*, *16*(8), 865–881, doi:10.1016/S0277-3791(97)00003-6.

Vorren, T. O., and L. Plassen (2002), Deglaciation and palaeoclimate of the Andfjord-Vågsfjord area, North Norway, *Boreas*, *31*(2), 97–125, doi:10.1111/j.1502-3885.2002.tb01060.x.

Vorren, T. O., I. F. Strass, and O. W. Lind-Hansen (1978), Late Quaternary sediments and stratigraphy on the continental shelf off Troms and west Finnmark, northern Norway, *Quat. Res.*, *10*(3), 340–365, doi:10.1016/0033-5894(78)90026-1.

Vorren, T. O., M. Hald, and E. Thomsen (1984), Quaternary sediments and environments on the continental shelf off northern Norway, *Mar. Geol.*, *57*(1–4), 229–257, doi:10.1016/0025-3227(84)90201-9.

Vorren, T. O., E. Lebesbye, K. Andreassen, and K.-B. Larsen (1989), Glacigenic sediments on a passive continental margin as exemplified by the Barents Sea, *Mar. Geol.*, *85*(2–4), 251–272, doi:10.1016/0025-3227(89)90156-4.

Vorren, T. O., G. Richardsen, S.-M. Knutsen, and E. Henriksen (1991), Cenozoic erosion and sedimentation in the western Barents Sea, *Mar. Pet. Geol.*, *8*(3), 317–340, doi:10.1016/0264-8172(91)90086-G.

Vorren, T. O., J. S. Laberg, F. Blaume, J. A. Dowdeswell, N. H. Kenyon, J. Mienert, J. Rumohr, and F. Werner (1998), The Norwegian-Greenland Sea continental margins: Morphology and late Quaternary sedimentary processes and environment, *Quat. Sci. Rev.*, *17*(1–3), 273–302.

Wadham, J. L., et al. (2012), Potential methane reservoirs beneath Antarctica, *Nature*, *488*(7413), 633–637, doi:10.1038/nature11374.

Walker, D. P., M. A. Brandon, A. Jenkins, J. T. Allen, J. A. Dowdeswell, and J. Evans (2007), Oceanic heat transport onto the Amundsen Sea shelf through a submarine glacial trough, *Geophys. Res. Lett.*, *34*, L02602, doi:10.1029/2006GL028154.

Weertman, J. (1974), Stability of the junction of an ice sheet and ice shelf, *J. Glaciol.*, *13*, 3–11.

Wingham, D. J., A. J. Ridout, R. Scharroo, R. J. Arthern, and C. K. Shum (1998), Antarctic elevation change from 1992 to 1996, *Science*, *282*(5388), 456–458, doi:10.1126/science.282.5388.456.

Winkelmann, D., C. Schäfer, R. Stein, and A. Mackensen (2008), Terrigenous events and climate history of the Sophia Basin, Arctic Ocean, *Geochem. Geophys. Geosyst.*, *9*, Q07023, doi:10.1029/2008GC002038.

Winsborrow, M. C. M., K. Andreassen, G. D. Corner, and J. S. Laberg (2010), Deglaciation of a marine-based ice sheet: Late Weichselian palaeo-ice dynamics and retreat in the southern Barents Sea reconstructed from onshore and offshore glacial geomorphology, *Quat. Sci. Rev.*, *29*(3–4), 424–442, doi:10.1016/j.quascirev.2009.10.001.

Winsborrow, M. C. M., C. R. Stokes, and K. Andreassen (2012), Ice-stream flow switching during deglaciation of the southwestern Barents Sea, *Geol. Soc. Am. Bull.*, *124*(3–4), 275–290, doi:10.1130/B30416.1.

Zeeberg, J., D. J. Lubinski, and S. L. Forman (2001), Holocene relative sea-level history of Novaya Zemlya, Russia, and implications for late Weichselian ice-sheet loading, *Quat. Res.*, *56*(2), 218–230, doi:10.1006/qres.2001.2256.

Zeeberg, J., D. J. Lubinski, and S. L. Forman (2002), Size and extent of the last ice sheets in the Barents Sea: Evidence from Novaya Zemlya and Vaygach, in *Climate and Glacial History of the Novaya Zemlya Archipelago, Russian Arctic*, pp. 49–60, Rozenberg Publishers, Amsterdam.

Zweck, C., and P. Huybrechts (2005), Modeling of the northern hemisphere ice sheets during the last glacial cycle and glaciological sensitivity, *J. Geophys. Res.*, *110*(D7), D07103, doi:10.1029/2004JD005489.